AN IMPROVED ALGORITHM FOR SATELLITE ORBIT DECAY AND RE-ENTRY PREDICTION

by

JON D. STRIZZI
B.S., Aeronautical and Astronautical Engineering,
Massachusetts Institute of Technology
(1992)

Submitted to the Department of Aeronautics and Astronautics
In Partial Fulfillment of the Requirements for the Degree of

MASTER OF SCIENCE IN AERONAUTICS AND ASTRONAUTICS
at the
MASSACHUSETTS INSTITUTE OF TECHNOLOGY
June, 1993

Signature of Author.....
Department of Aeronautics and Astronautics
7 May 1993

Certified by.....
Professor Walter M. Hollister
Thesis Supervisor

Certified by.....
Dr. C.C. (George) Chao
The Aerospace Corporation
Company Supervisor

Accepted by.....
Professor Harold Y. Wachman
Chairman, Department Graduate Committee

An Improved Algorithm for Satellite Orbit Decay and Re-entry Prediction

by

Jon D. Strizzi

Submitted to the Department of Aeronautics and Astronautics
on 7 May 1993 in partial fulfillment of the requirements for the degree of
Master of Science in Aeronautics and Astronautics

ABSTRACT

A study to improve the accuracy and capabilities of an existing algorithm for satellite orbit decay and debris impact prediction has been completed. The existing algorithm, program LIFETIME 3.0, was developed by The Aerospace Corporation to predict satellite orbital lifetimes. Although its accuracy is quite good (~ 10% error), the algorithm's semi-analytic method does not account for the intrack motion of the satellite. Additionally, the program's propagation routine limits the minimum step size and causes some uncertainty in impact time prediction. Furthermore, no geographical impact location is computed. This study sought to correct these deficiencies and to perform a sensitivity study on factors affecting impact prediction accuracy.

Using NORAD data of actual decayed objects, inaccuracies in satellite period calculation by the existing algorithm as well as inconsistancies in the data conversion method were discovered. These were corrected using a new method of period calculation and an improved data conversion routine. A numerical integration scheme was developed to calculate the final portion of the satellite's decay. Improved output capabilities included groundtrack and debris impact area plots on a world map and an altitude decay history. These major changes and upgrades formed a new program version, LIFETIME 4.0.

Comparisons between version 3.0 and 4.0 were made using four actual decayed objects. Results show that version 4.0 is significantly more accurate than version 3.0 during decay curve fitting. Comparison of impact prediction shows some increase in accuracy with version 4.0 for some cases. Generally, LIFETIME 4.0 is an improved algorithm with less uncertainty in impact prediction than LIFETIME 3.0, and it has enhanced output capabilities. The impact error sensitivity results indicate some improved accuracy by using long data spans, short prediction spans, and estimated solar flux values equal to the value on the last day of data. These results are not definitive and further research is recommended.

Thesis Supervisor:
Dr. Walter Hollister
Professor of Aeronautics & Astronautics

Company Supervisor:
Dr. C.C. (George) Chao
Manager, Orbit Dynamics
The Aerospace Corporation

Acknowledgments

I would first like to express my deep appreciation for the advice and technical assistance I received from many members of The Aerospace Corporation during my two summer work sessions and long thesis research session at the company. Most notable is my thanks to Dr. C.C. (George) Chao, manager of the Orbit Dynamics Section of the Astrodynamics Department, without whom this research would never have even gotten off the ground. George, whose constant desire for improving computational methods and models through intense investigation motivated me through this project, was a never-ending source of knowledge, ideas, support, and guidance. My sincere thanks, George.

Three other Astrodynamics members deserve special thanks and recognition for their unique and important roles in the completion of this research. First, I thank Daniel Oltrogge for his expertise with numerical integration routines, knowledge of Macintosh computers, dedication to improving the accuracy and efficiency of any computer code, extensive library, stash of snacks, never-ending support, and lively sense of humor. Dan put in a lot of effort with the integration routine additions, algorithm testing, and Macintosh software packaging. Second, I thank Cassandra Johnson, without whose help the enhanced output plots of LIFETIME 4.0 would not have been possible. Cassandra is also the caretaker of the menu-driven version of LIFETIME, and she put in much effort in working with me to adapt LIFETIME 4.0 to the menu shell program. Last to thank is my office-mate for seven months, Matthew Hart. Matt's hard work ethic was an inspiration and his diverse interests helped make months of intense research almost enjoyable.

Some other members of the Astrodynamics Department also deserve mention here. Thanks go to: Hans Karrenberg, the reason I came to The Aerospace Corp.; Jimmy Miyamoto, patient teacher; Jim Gidney, mentor and friend; Karolyn Young, for support, comic relief, and reality check; and Brian von Kleek, for coffee. I also want to extend my appreciation to the rest of the members of the Astrodynamics Department and The Aerospace Corporation as a whole for all help, guidance, and support over the past three years.

A special note of thanks goes to Debbie Nerio of the Space Test Range, Sunnyvale, CA. Her interest and funding efforts both initiated this research and

supported it to its conclusion. Her office is entirely responsible for the financial support that made this thesis possible, and I offer my sincere appreciation.

Back at MIT, Professor Walter Hollister was a major inspiration on my approach to my graduate studies. Additionally, his support and critiques in the final phases of research and writing were helpful and insightful. Thank you so much, Professor.

Of final mention are those family and friends who have been of personal support and inspiration over my college career, especially through the trying times of this research. First and foremost I want to thank the brothers of the Alpha Tau Omega Fraternity for valuable lessons and experiences in friendship, love, and respect. These virtues leave an impression that is everlasting. In particular, thanks goes to Tyler Worden, fellow thesis workaholic, for his companionship and steadfast friendship. Thanks are also in order for Celia Liu, fellow internist at The Aerospace Corporation, confidant, matchmaker, and friend. I thank Melonie, who lent caring support and managed to make daily life as unpredictable as possible. My most sincere appreciation goes to Renée, whose beauty, intelligence, and outlook on life have been a source of happiness and firm support over this last year at MIT.

Final thanks, above all others, goes to my parents. Their love and guidance over the years have been a true inspiration. I can only hope that someday I can return to them a fraction of the love, support, and strength they have given to me.

This research and writing was conducted at The Aerospace Corporation, El Segundo, California, from June 1992 to January 1993, and at MIT from January to May 1993. It was financially supported by the Space Test Range through The Aerospace Corporation, along with an Aerospace Graduate Fellowship and cooperation with the MIT Engineering Internship Program.

This report was prepared on a Macintosh LC III computer using Microsoft Word 5.1a® as the text editor. Additional plots and figures were created using LIFETIME 4.0©, Cricket Graph®, and MacDraw II®.

Table of Contents

List of Figures

List of Tables

Chapter 1

Introduction

The continuing advances in space technology worldwide has led to a record number of countries with currently active or planned space programs. Additionally, ambitious telecommunications and Earth-imaging companies have put forth a multitude of plans for new low Earth orbit (LEO) satellite systems.[Ref. 1] These are sure signs of an increase in the number of artificial satellites to be launched over the next decade. As it is, current satellite launches both replace satellites whose operational lives have ended and place new operational systems in orbit. There are also many satellites that are launched into LEO for short duration missions only.

The result of this current and future satellite launch activity is an increase in the number of satellites in LEO. The question remains as to what happens to those satellites that have completed their missions, especially those launched for short-duration, low altitude missions. The answer is that an inoperative satellite in LEO experiences an orbit decay process that leads to the re-entry of the spacecraft through the Earth's atmosphere. Pieces of the satellite's structure or internal instruments may survive the strong heating and forces of the re-entry process and impact the Earth's surface.[Ref. 2]

Thus, it is highly desirable to be able to accurately predict the orbital motion and the decay of such LEO satellites. Additional information concerning the satellite's potential impact location and time would also aid in warning areas of the world affected by the re-entry and may allow for preventive action to be taken. The computer tool that is the subject for this study, program LIFETIME, was developed at The Aerospace Corporation to predict such LEO satellite decay and orbital lifetimes. The aim of this research was to increase the accuracy of this computer tool and expand its capabilities.

This chapter will focus on defining the satellite orbit decay and re-entry problem, as well as reviewing past and present areas of research and current

orbit decay prediction tools. An explanation of the LIFETIME program will be presented as well as the specific goals and objectives of this research.

1.1 Satellite Orbit Decay and Re-entry

1.1.1 The General Problem

A classical treatment of the general problem of an artificial satellite in orbit about the Earth was presented by Roy (1965). For almost all Earth satellites the major perturbations of the two-body Keplerian orbit are caused by the Earth's oblateness effects and atmospheric drag. This is especially true for satellites in LEO. Looking at gravity effects only, the study of a satellite's orbit about an oblate planet was classically treated by many authors, among them Kozai (1959), Brouwer (1959), Sterne (1958), and King-Hele (1958). Classical approaches to the atmospheric drag effects were presented by Sterne (1959), Roy (1963), King-Hele (1964), and Morando (1969). Specific treatments of the satellite re-entry problem were presented by Martin (1966), Carlson (1968), and Louis (1968). A more modern look at the dynamics of a re-entering vehicle can be found in Regan (1984).

Figure 1-1 shows the orbital elements used to define a satellite's orbit.

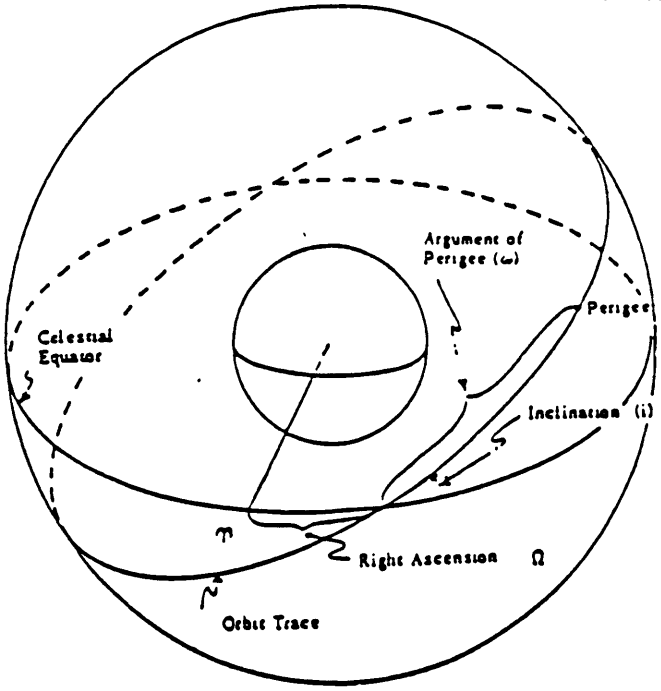

Figure 1-1 : Orbital Elements [Ref. 4]

A review of the orbital mechanics that form the background to the orbit decay and re-entry problem will not be discussed in this text. See Roy, Ref. 3.

The osculating orbit of a satellite is the instantaneous conic path associated with a time t_0.[Ref. 5] It is identified by the six orbital elements a, e, i, Ω, ω, and M where a is the semi-major axis, e is the eccentricity, i is the inclination of the orbital plane to the equator, Ω is the right ascension of the ascending node, ω is the argument of perigee, and M is the mean anomaly.[Ref. 3] The mean orbital elements are defined as the initial values from which periodic perturbations have been removed. In this paper, all discussions of a satellite's orbital elements refer to the mean elements and they will be presented in normal type. References to the osculating elements will use italic type.

The combined effects of the Earth's oblateness and atmosphere cause the satellite's orbit to deviate from the Keplerian two-body orbit. The true orbit contracts and the satellite eventually re-enters the Earth's atmosphere. Unless the eccentricity is very small, the apogee change is larger than the perigee change, over time, and the change in a satellite's orbit may be illustrated qualitatively, as in Figure 1-2.

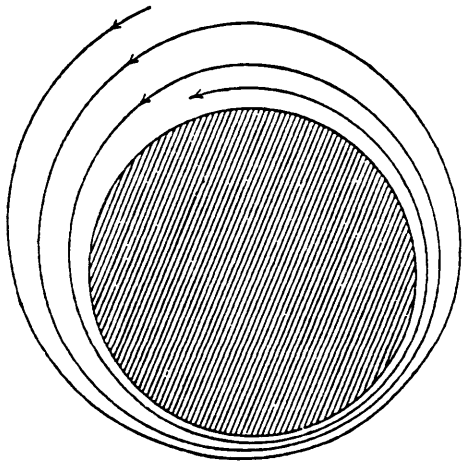

Figure 1-2 : General Satellite Orbit Decay [Ref. 3]

The challenge of representing this motion accurately comes from the fact that the oblateness and drag perturbation effects on the satellite's orbit are coupled. Drag affects mainly the semi-major axis and eccentricity, elements that are not changed secularly by the harmonics of the Earth's gravitational field. However, two separate theories (one for drag and one for gravitational perturbations) are not a solution to the problem.[Ref. 3] Research work over

the last fifteen years has led to a semi-analytic theory that embodies both drag and gravity perturbations. This theory formed the basis for the averaged equations of motion that are used in the LIFETIME algorithms.

1.1.2 Summary of Research

From the early 1960's onward, many researchers have further developed some of the classical work mentioned in Section 1.1.1, with the intent of developing accurate theories to describe the motion of a close-Earth artificial satellite with drag effects. Lane (1965) adapted methods of Brouwer and Hori (1961) with a power function density model to formulate a coupled solution to the orbital motion problem. More recently, Hoots (1979) combined Lane's work with Lyddane's modification for small eccentricities (1963) to derive a coupled analytic solution using a method of averaging. With another approach to the problem, Zee (1971) used the asymptotic method with an exponential density model to develop a closed-form solution in spherical coordinates. A short-coming of all the above theories is the use of a non-rotating, static, and spherical atmosphere density model. Chen (1974) improved upon these theories by using a modified exponential function with characteristics of atmospheric oblateness and diurnal bulge. Mueller (1977) developed an analytic density representation requiring series expansion and the periodic re-calibration of ten fitting parameters. Most of these analytic theories have some limitations on eccentricity or perigee height due to the use of series expansions. [Ref. 6]

Liu and Alford (1979) introduced the semi-analytic theory that has since been adapted within the LIFETIME program. Their alternative approach adopted a combination of general and special perturbation techniques (thus the term semi-analytic). The analytical method increased efficiency and sufficient numerical methods were included to allow the use of a high-accuracy atmospheric density model without series expansions. [Ref. 6] This original work, begun in the mid-1970's, was presented as a complete semi-analytic theory in 1980 and some advances were later presented by Liu (1983).

Other techniques for approaching the close-Earth artificial satellite problem can be classified as numerical and purely analytical. A numerical method applies numerical integration to an osculating state to obtain the state at a later time. These are often technically complicated to use and costly in computation time, yet have a high degree of accuracy. Many organizations have developed their own integration routines, and the notable ones experienced by this author include TRACE and SPIN, products of The Aerospace Corporation. A purely analytical satellite theory has been pursued by Hoots and France (1987). Their theory utilizes a totally analytical solution to the differential equations of motion, which can be useful for speedy analysis and program size limitations. A semi-analytic theory embodies the best of both methods, allowing a large step size integration of averaged equations of motion. These ideas will be developed further as the theory behind the LIFETIME program algorithm is introduced.

1.1.3 Notes on Solar Activity and Atmosphere Models

After establishing the accuracy of the equations of motion used to account for the variations in the Earth's gravity field, the two main factors that cause variations in the accuracy of an orbital lifetime prediction are: (1) the values for solar flux and magnetic index used; and (2) inaccuracies due to atmosphere model approximations. These factors have no relative importance; it is their deviations from predicted values that determine their effects on a lifetime prediction.[Ref. 7]

The most widely used measurement of solar activity is the solar flux, or received power per unit area at the Earth's surface at the 10.7 cm wavelength (for which the Earth's atmosphere is more or less transparent). The flux is often referred to as the $F_{10.7}$ solar index, in units of $10^{-22} \frac{W}{m^2}$ Hz; and in this report it will be written simply as F_{10}. For data measured since 1947, the sunspot number and F_{10} value have a strong correlation (0.95 correlation coefficient) with a relationship given by the following equation:

$$F_{10} = 62.58 + 0.815n + 4.06 \times 10^{-4} n^2 \qquad (1.1)$$

where n is the sunspot number.[Ref. 8] Observations of monthly mean values of both sunspots and F_{10} have revealed the well-known cycle that averages about 11.5 years in duration. Further trends with periods of 155 days, 22 years, and 100 years have been proposed.

An additional measurement of solar activity comes in the form of the planetary geomagnetic index, referred to as a_p. Both the F_{10} and a_p values are used as numerical inputs into most atmosphere models, including the ones used with the LIFETIME program. The more dominant driver has been the solar flux, which affects upper atmosphere density directly through heating and indirectly through geomagnetic activity. Even though its cyclic nature has been observed, there is no true understanding of the sometimes chaotic forces that seem to drive solar activity. Recent attempts, such as Williams (1991), have used neural networks to model and predict the sun's behavior, with further research pending. This inability to predict solar flux values with reasonable accuracy has and will continue to be a common source of error for all orbital lifetime predictions.

As an example of the effects of the solar flux value F_{10}, Figure 1-3 is presented. It is the altitude predictions over time of the Hubble Space Telescope (HST) for various assumed values of F_{10}. A sample of F_{10} and a_p recorded values and predicted estimates from a database of The Aerospace Corporation is presented as Figure 1-4.

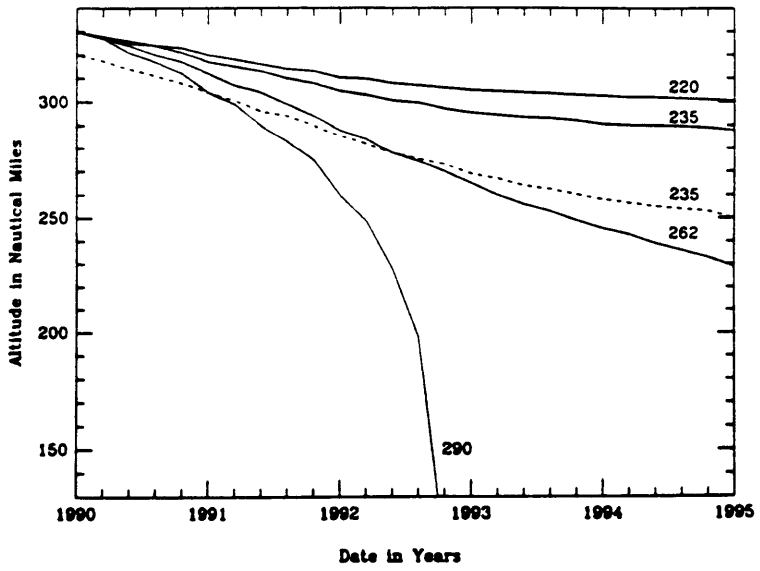

Figure 1-3 : Altitude of HST for Different Maximum F_{10} Levels [Ref. 9]

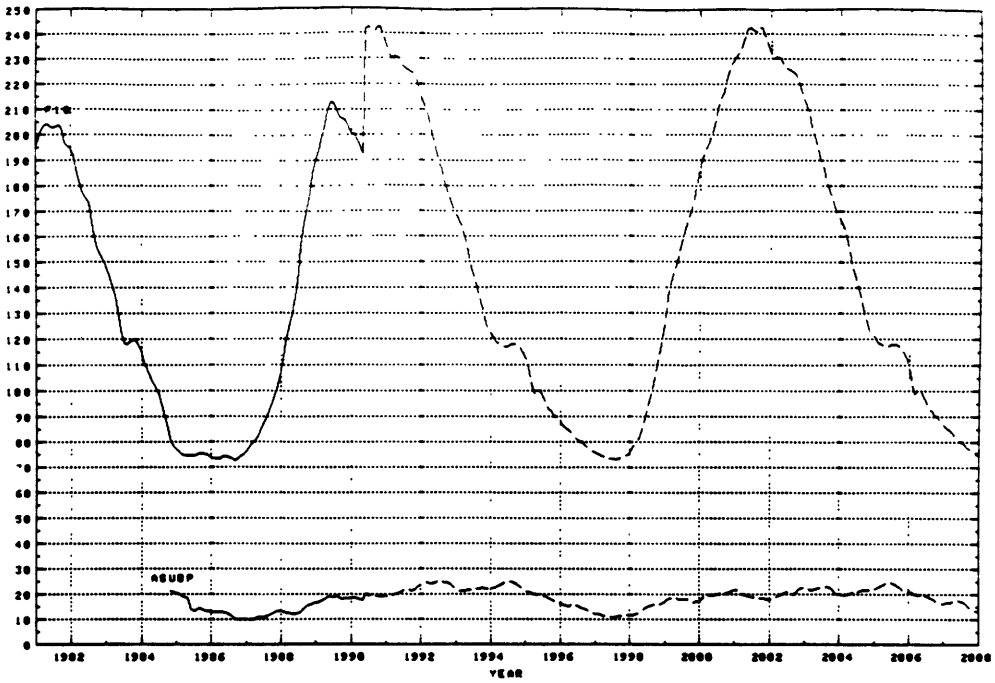

Figure 1-4 : Long Range Statistical Estimates of F_{10} and a_p [Ref. 10]

The solar flux and magnetic index values are used as inputs to atmosphere models used to determine atmospheric density at a given altitude. These models thus used by orbit theories for LEO satellites to determine the amount of drag and drag force encountered by a satellite. It is the drag that causes the rapid orbital decay and re-entry of the satellite at the end of its lifetime.

Of course, none of the existing atmosphere models are perfect; and a recent study by Marcos (1987) evaluated the accuracy of a wide range of models. He found that a typical accuracy figure for the most accurate atmosphere models was between 10% and 15%. The most accurate were determined to be the MSIS86 (Mass Spectrometer Incoherent Scatter model) and Jacchia 1971 models, with both having comparable errors.[Ref. 11] This would suggest that a satellite's lifetime could thus be estimated with no greater than a 15% accuracy, on the average. Current expectations for the United States Air Force for re-entry predictions are around 20% accuracy.[Ref. 4]

1.1.4 Current Tools for Orbit Decay and Re-entry Prediction

In the public domain, there have been many individuals and teams who have developed analytic and semi-analytic theories to calculate and predict the motion of an artificial satellite around the Earth, as evidenced by the

information in the proceeding section. In some cases, these theories have led to computer tools used for satellite orbit decay prediction: Liu (1975) and Hoots & France (1987). Other tools have been developed in the private sector and not published; and in some cases they are program-specific and therefore perhaps not generally applicable to the orbit decay prediction problem on a large scale.

The United States Space Command (USSPACECOM) utilizes a general-purpose computer tool for real-time orbit decay prediction on a large scale. This is the Tracking and Impact Prediction (TIP) process used by the USAF at its Space Surveillance Center (SSC) at Cheyenne Mountain Air Force Base, Colorado. A mission of the SSC is to use TIP processing to support USSPACECOM efforts in identifying possible re-entering space objects and their potential to impact the Earth. The TIP process uses special perturbation theory for its most accurate decay and impact predictions, which is fundamentally a numerical integration method. Possible re-entering objects considered by the process include payloads, rocket bodies, platforms, and debris.[Ref. 4]

The TIP process is not a simple one and multiple TIP runs are required for an accurate presentation of the decay picture. This is not an inexpensive process. Thus, it is not surprising that the USAF would be interested in a semi-analytical type orbit decay prediction tool with improved accuracy and efficiency, such as one based on some of the theories already presented. It was such an interest that inspired the work of Dr. C.C. Chao of The Aerospace Corporation in the development of the LIFETIME program.

1.2 Program LIFETIME

The computer tool LIFETIME is copyrighted by The Aerospace Corporation, El Segundo, CA. It was developed by Dr. Chao in support of various USAF programs. This section contains general information on the development and utility of LIFETIME, and is derived from a presentation by Chao, "LIFETIME: Past, Present, and Future" (1992).[Ref. 12]

1.2.1 Conceptualization and Initial Development

LIFETIME was conceptualized in the early 1980's. In the performance of mission trade studies for various Air Force programs it had become apparent that a fast yet efficient computer tool for orbital lifetime estimation was needed. Of further interest was the necessity to estimate the stationkeeping fuel requirements for a satellite to maintain a constant orbital altitude. The first version of this program was thus developed by Chao on an IBM/PC using a simplified perturbation theory and crude atmosphere model. The program could estimate the lifetime of a decaying satellite or estimate the amount of propellant needed to maintain a specified altitude.

Interest grew in the program and its potential as a fast and efficient computer tool. The program was set in its baseline configuration in 1985 with refinements in the method of averaging and the semi-analytic orbit theory of Liu & Alford (this will be presented in detail). The Walker representation of the Jacchia 1964 dynamic atmosphere model was added, completing LIFETIME as a software package to be used as a mission analysis tool. A number of low altitude space mission programs were immediately interested in its use. Among these were: Space Station, SDI, Space Based Radar, and various Space Test Programs. These missions required either accurate predictions of orbital lifetimes or estimates of orbit sustenance propellant requirements.

1.2.2 Version Upgrades

The first major upgrade to the LIFETIME program came in 1987. The need for another option for atmosphere modeling led to the addition of the Jacchia 1971 dynamic model. This is an extensive tabular model that has been shown over time to be one of the most accurate in use.[Ref. 11]

As interest in LIFETIME grew, The Aerospace Corporation provided the support for a major upgrade effort, also in 1987. This led to the refinement of the entire program, most notable in the areas of differential corrections of a satellite's ballistic coefficient (this will also be presented in detail here) and the

modeling of a satellite's solar panels tracking the sun. The differential correction process compares predicted orbital decay with NORAD tracking data and corrects the satellite's ballistic coefficient to allow a "best fit" of the predicted decay with the observed motion.

The years 1990 and 1991 saw the extensive testing of the program against a catalogue of NORAD decayed and re-entered objects. This led to the presentation of the LIFETIME program and its impressive performance at the AIAA/AAS Spaceflight Mechanics Meeting in Houston, Texas.[Ref. 7] The study of 15 decayed objects led to the results displayed in Table 1-1. The percent error in prediction was determined by dividing the amount of error in lifetime prediction by the length of the prediction period.

Table 1-1 : LIFETIME Estimates and Errors for NORAD Objects [Ref. 7]

Case No.	Initial F_{10}	Interval of Fit to Data (days)	Error/Prediction Period (days)	% Error
1	217.5	43	1.5 / 90	1.7
2	200.0	25	6.5 / 180	3.6
3	225.5	24	17 / 100	17.0
4	220.0	25	4 / 53	7.5
5	222.2	34	12 / 117	9.2
6	222.0	20	3 / 36	8.3
7	181.6	29	0.8 / 63	1.3
8	178.2	3	1.5 / 22	6.8
9	116.5	31	1 / 105	1.0
10	111.1	4	0.4 / 11	3.6
11	109.9	10	4 / 47	8.5
12	113.4	45	3.6 / 250	1.4
13	108.3	34	9.3 / 250	3.7
14	143.3	2	1.5 / 10	15.0
15	149.1	6	7 / 36	19.4

As can be seen from the table, accuracy in the range of 1% to 9.2% was achieved for 12 of 15 cases. Atmosphere models themselves have an accuracy in the 10% to 15% range. [Ref. 11] The differential correction process absorbs some of this inaccuracy in the LIFETIME program [Ref. 7] Additionally, it should be noted that the SSC sets an accuracy of ± 20% for its TIP runs as the acceptable error level.[Ref. 4] This performance of LIFETIME thus indicated its ability as an accurate and efficient PC-based tool.

Additional events surrounding the LIFETIME program in these years was its integration into the IMPACT program, used by the USAF for orbital debris lifetime studies, and its conversion into a format that could be run on Macintosh computers.

LIFETIME was used for the first real time re-entry prediction of a space object during the 1991 re-entry of the Soviet Salyut 7 spacecraft. Subsequently, in 1992 it was used for real time re-entry predictions of the LOSAT-X and Relay Mirror Satellite (RME) spacecraft. The program's potential as a highly accurate real time re-entry prediction tool was noted at this time, and the study that led to this research was initiated.

1.2.3 Current Program Status and Users

The current version of the LIFETIME program (at the start of this study) is designated LIFETIME 3.0. Its primary uses are for orbit decay prediction and orbit sustenance propellant estimation. It allows for differential corrections of the satellite's ballistic coefficient using observed orbit decay data and for solar array tracking of the sun (which gives accurate cross-sectional area computation). High quality plots of perigee and apogee decay histories are produced for each run. An example of such an output is shown as Figure 1-5.

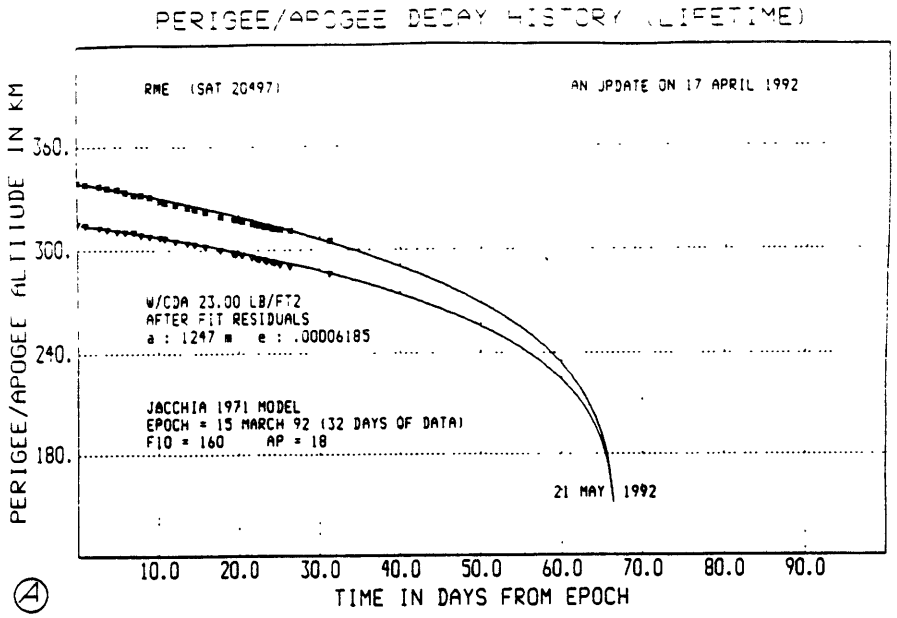

Figure 1-5 : Sample Perigee/Apogee Decay Plot from LIFETIME 3.0 [Ref. 7]

Various solar data (F_{10} and a_p) input options are also available. These are: (1) 11 year solar cycle values, which can be biased by day and value, (2) user-inputted values for the epoch time, which can remain constant or can change at a constant rate, or (3) user-inputted values for each day.

A chart depicting the current uses and users of LIFETIME has been reproduced as Figure 1-6.

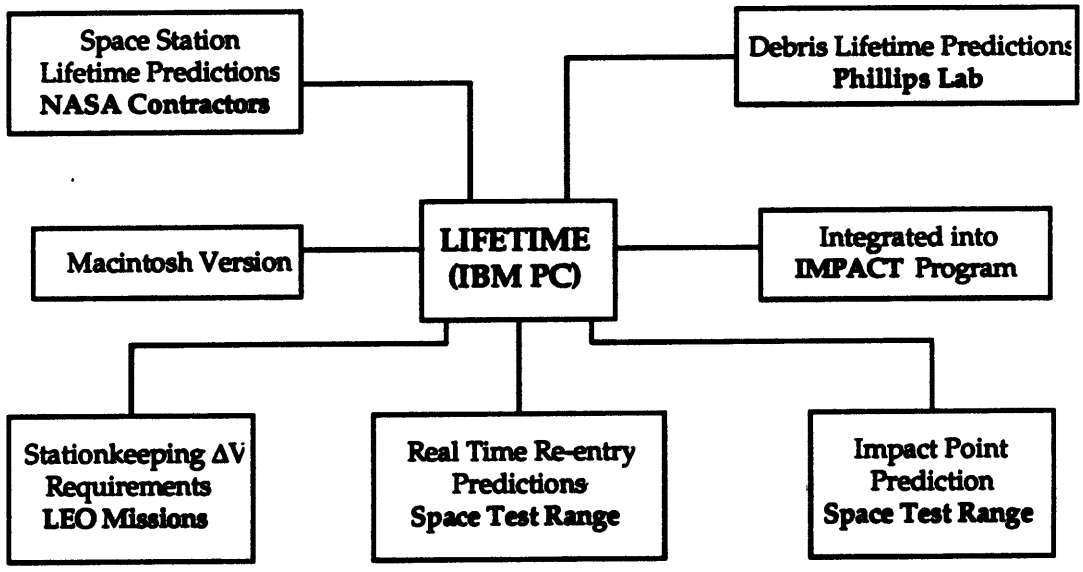

Figure 1-6 : LIFETIME Applications and Customers [from Ref. 12]

1.3 The Need for an Improved Algorithm

If the LIFETIME program has such efficient and accurate performance then why is there the need for an improved algorithm? Even though the accuracy was already good, by SSC standards, some deficiencies had been noted throughout the program's extensive use, possibly in the way the program accounted for the passage of time (which is in multiples of the satellite's orbital period). Because of the program's popularity with its customers and its potential for even more widespread use it seemed prudent to pursue its improvement as a scientific tool.

In addition to the potential building-up of time errors, it was also noted that the main propagation method using averaged equations of motion was limited by a minimum step size of one revolution. This caused a built-in uncertainty in Earth impact time prediction of at least one revolution. This is illustrated qualitatively in the relatively simple representation in Figure 1-7.

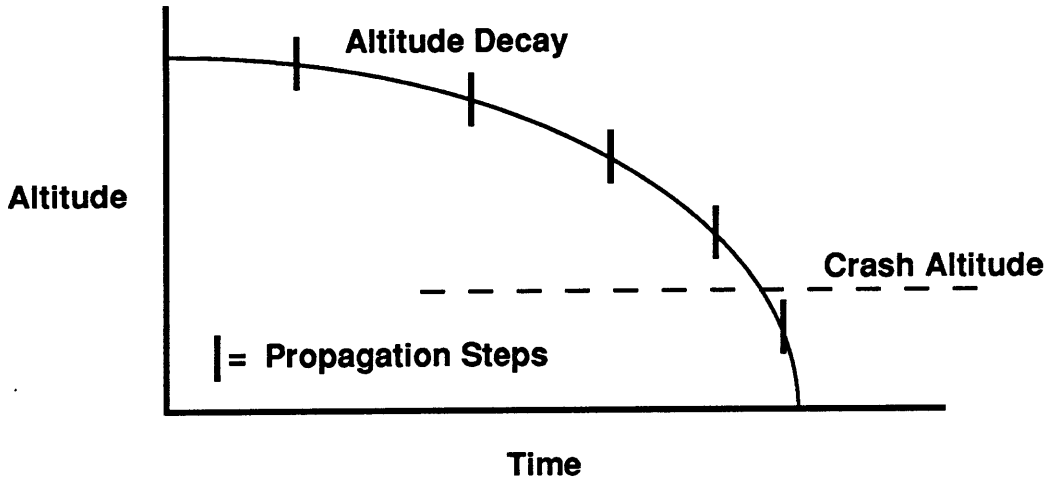

Figure 1-7 : Simple Illustration of Impact Point Prediction Uncertainty

As the program steps along at a minimum step size of one revolution, an impact flag is triggered at the end of a revolution that crosses a user-specified "crash altitude". The impact date and time is recorded as the time of that last revolution. Since there is no method within the algorithm to account for the

intrack motion of the vehicle, there is no way to determine exactly when the satellite impacted.

Additionally, one of the primary customers who use the LIFETIME program, the Space Test Range of the USAF, expressed an interest in improving both the accuracy, if possible, and the output capabilities. The Space Test Range wanted to be able to use LIFETIME regularly as a real time re-entry prediction program for decaying objects. This would provide a fast and efficient method for impact prediction that would not require the time or expense required for other prediction programs that depended on numerical integration techniques. Enhanced output that included a plot of the decayed object's last revolution and impact area on a world map was desired.

1.4 Goals and Objectives of the Study

The desire to improve the current algorithm led to the formulation of the following goals and objectives for this study.

(1) Improve upon the accuracy of the current LIFETIME algorithm, LIFETIME 3.0. The NORAD tracking data sets for decaying satellites contain intrack motion information that could aid in this improvement.

(2) Either adjust the current algorithm or develop a new one to decrease the uncertainty associated with the prediction of the impact time.

(3) Enhance the output capabilities of the program. Develop plots of the final revolution's altitude decay history and world-wide groundtrack with impact area.

(4) Package the completed software package as LIFETIME 4.0 in a variety of forms:

- IBM PC with NAMELIST input format
- IBM PC with a user-friendly menu-driven shell program to run it
- Macintosh version with NAMELIST input format

(5) Initiate an accuracy sensitivity study, looking at the sensitivity of the program's impact prediction accuracy to:

- The amount of NORAD data used for the differential correction fit
- The length of prediction, from the last data point to actual impact
- The inputted solar flux (F_{10}) values used for the prediction

Each of these objectives were attempted and met, in turn, and that is the information presented in the remainder of this report. Chapter 2 deals with the specific theoretical background of the LIFETIME 3.0 algorithm and the experimental background that confirmed the existing deficiencies in the program. Chapter 3 develops the theoretical improvements made to the LIFETIME 3.0 algorithm and compares the former and improved versions. Chapter 4 examines the problem of accurate re-entry and impact prediction and introduces the method developed to deal with this special topic and complete the formulation of LIFETIME 4.0. A final comparison between the 3.0 and 4.0 versions is presented in Chapter 5. Chapter 6 deals with the accuracy sensitivity studies; and conclusions and recommendations are made in Chapter 7.

Chapter 2

Theoretical & Experimental Background

This chapter presents the theories and algorithms that are the foundation of the LIFETIME program. Deficiencies in the period calculation method are then proposed and shown by experimental results from four satellite cases.

2.1 LIFETIME 3.0

This section will discuss in detail the three major theoretical and algorithmic features of LIFETIME: (1) semi-analytic satellite theory; (2) method of gaussian quadrature; and (3) differential corrections of the ballistic coefficient. Much of this material can be found in its original form in Ref. 7; and it is represented here to provide a clear understanding of the theories within the LIFETIME program.

2.1.1 Semi-Analytic Satellite Theory: Method of Averaging

The semi-analytic orbit theory presented by Liu & Alford (1979) is simplified into the averaged equations of motion that follow. These mean orbital element equations are integrated with a step size of one orbit period or larger (with increments of multiples of the period). The equations are:

$$\frac{da}{dt} = -\frac{1}{2\pi}\int_0^{2\pi} B\,\rho\,V\left(\frac{a}{1-e^2}\right)\left[1 + e^2 + 2\,e\cos f - \omega_e \cos i\sqrt{\frac{a^3\,(1-e^2)^3}{\mu}}\right] dM$$

$$\frac{de}{dt} = -\frac{1}{2\pi}\int_0^{2\pi} B\,\rho\,V\left[e + \cos f - \frac{r^2\,\omega_e \cos i}{2\sqrt{\mu\,a\,(1-e)^2}}\left[2\,(e+\cos f) - e\sin^2 f\right]\right] dM$$
$$-\frac{3}{8}\,n\,J_3\left(\frac{R_E}{p}\right)^3 \sin i\,(4 - 5\sin^2 i)\,(1-e^2)\cos\omega$$

$$\frac{di}{dt} = 0 \tag{2.1}$$

$$\frac{d\Omega}{dt} = -\frac{3}{2}\, n\, J2 \left(\frac{R_E}{p}\right)^2 \cos i$$

$$\frac{d\omega}{dt} = -\frac{3}{2}\, n\, J_2 \left(\frac{R_E}{p}\right)^2 (4 - 5\sin^2 i) + \frac{3}{8}\, n\, J_3 \left(\frac{R_E}{p}\right)^3 \left[(4 - 5\sin^2 i)\, \frac{\sin^2 i - e^2 \cos^2 i}{e \sin i} + 2 \sin i\, (13 - 15 \sin^2 i)\, e \right] \sin \omega$$

where

- B = inverse ballistic coefficient of satellite
- ρ = atmosphere density at current altitude
- V = satellite velocity relative to the atmosphere
- μ = Earth gravitational constant
- R_E = Earth equatorial radius
- ω_e = Earth rotation rate
- a = semi-major axis
- e = eccentricity
- i = inclination
- Ω = right ascension of ascending node
- ω = argument of perigee
- p = $a(1 - e^2)$
- n = satellite mean motion
- f = true anomaly
- M = mean anomaly
- J_2, J_3 = constants; gravity harmonics of the Earth's field

The inverse ballistic coefficient is defined as

$$B = \frac{C_D A}{M_s} \tag{2.2}$$

where

C_D = coefficient of drag
A = satellite cross-sectional area
M_s = satellite mass

The satellite's relative velocity is

$$V = \left[\frac{\mu}{p} (1 + e^2 + 2 e \cos f) \right]^{1/2} \left[1 - \frac{(\sqrt{1 - e^2})^3}{1 + e^2 + 2 e \cos f} \frac{\omega_e}{n} \cos i \right] \tag{2.3}$$

The results of evaluating the equations in (2.1) over multiples of one orbit period are the averaged gravity and drag effects on the orbital elements over the time step size. Accuracy in the drag effects due to atmospheric density comes from the fact that the $\dot{a}$ and $\dot{e}$ integrations are carried out quickly over each orbit using the gaussian quadrature method discussed in the next section.

2.1.2 Gaussian Quadrature

The gaussian quadrature method of integration requires a minimum step size of one orbit revolution. The integrations, in this case for semi-major axis and eccentricity, are computed for specific intervals around the orbit, arriving back at the original argument of latitude. For the case of orbit decay predictions using NORAD data, this location in the orbit is the ascending node. Using gaussian quadrature, the atmospheric density for the integrations of semi-major axis and eccentricity from equations (2.1) can be computed quickly around an entire orbit revolution.

The density is computed directly within the chosen atmosphere model: the Jacchia-Walker 1964 analytical or Jacchia 1971 tabular models. For either

selection, once the satellite's altitude falls below 90 km the LIFETIME program refers to the US Standard 1962 atmosphere model. The density is determined through the general relation

$$\rho = \rho (h, \phi, t_L , F_{10}, a_p) \tag{2.4}$$

where

- h = $r - R$
- r = satellite geocentric radius
- R = geocentric radius of oblate Earth surface at satellite geocentric subpoint
- ϕ = satellite geocentric latitude
- t_L = satellite local time
- F_{10} = solar flux index
- a_p = magnetic index

The satellite geocentric radius, r, is the sum of the mean orbital radius and the short-period variation due to J_2.

2.1.3 Differential Corrections of the Ballistic Coefficient

The option of using the differential correction process to estimate the satellite's effective ballistic coefficient is unique to the LIFETIME program and is a primary factor in its effectiveness and accuracy as an orbit decay prediction tool. This technique uses the semi-major axis and eccentricity as observed orbit parameters that can be compared against values predicted by the program itself. Through least squares procedures, the following equation for differentially correcting the inverse ballistic coefficient, B, can be formulated:

$$\Delta B = \frac{\sum_{i}^{N} \left(\Delta \tilde{a}_i \frac{\partial \tilde{a}_i}{\partial B} + \Delta e_i \frac{\partial e_i}{\partial B} \right)}{\left[\sum_{i} \left(\frac{\partial \tilde{a}_i}{\partial B} \right)^2 + \sum_{i} \left(\frac{\partial e_i}{\partial B} \right)^2 \right]} \tag{2.5}$$

where

N = number of observations

$\tilde{a}_i = \frac{a_i}{a_o}$

a_o = semi-major axis at epoch

a_i = observed semi-major axis at time i

e_i = observed eccentricity at time i

The differential changes in semi-major axis and eccentricity, $\Delta \tilde{a}_i$ and Δe_i, over one orbital period can be found from (2.1). Factoring out the coefficient B allows for easy expression of the partial derivatives, $\frac{\partial \tilde{a}_i}{\partial B}$ and $\frac{\partial e_i}{\partial B}$.

From (2.1) it can be seen how the orbit decay in semi-major axis and eccentricity is directly proportional to the product of inverse ballistic coefficient and density, (B ρ). Because of this, the differential correction process allows for uncertainties in density determination to be absorbed in the converged ballistic coefficient that results from multiple iterations of (2.5). This is what enables LIFETIME to sometimes achieve an accuracy that is better than that of the atmosphere models it uses, as mentioned in Section 1.2.

2.2 Determining LIFETIME Computation Errors

This section discusses how NORAD tracking data required for the differential correction process is used to determine the computational errors present in LIFETIME 3.0.

2.2.1 The NORAD 2 - Card Element Set and INAE File

In using LIFETIME for real-time decay predictions, the user can receive computer records from NORAD containing the 2-card element sets for a desired satellite over a number of days. A 2-card element set is of the format shown in Figure 2-1.

Card 1	Sat. No.	Yr. Launch	Epoch(YrDay.)		Ndot	Nddot	Bstar	Eph. Type	El. No
Card 2	Sat. No.	i (°)	Ω (°)	e	ω (°)	M (°)	n (revs/day)	Rev. No	

Figure 2-1 : NORAD 2-Card Element Set Format [Ref. 13]

The observations by NORAD are made at the satellite's ascending nodal crossing, approximately. A sample computer file of a series of these elements for one satellite is given as Figure 2-2. Such a file would form the basis of the NORAD data to be used for differential corrections.

```
1 20497U 90 15   B 92142.53032979  .01392997  15080-4  42123-3 0   1369
2 20497   43.0800 121.1275 0004827 119.2962 241.1239 16.25941602128446

1 20497U 90 15   B 92142.34598882  .01352270  00000-0  42555-3 0   1369
2 20497   43.0802 122.3290 0005530 120.6212 239.5811 16.25411382128415

1 20497U 90 15   B 92141.73122054  .01258362  13203-4  45948-3 0   1353
2 20497   43.0794 126.3347 0005609 110.5832 249.5901 16.23726237128311

1 20497U 90 15   B 92141.11586495  .01148820  11928-4  47735-3 0   1342
2 20497   43.0798 130.3315 0006245  99.9140 260.3988 16.22149364128218

1 20497U 90 15   B 92140.56151786  .01027906  11072-4  47329-3 0   1330
2 20497   43.0796 133.9275 0006983  99.0008 261.2514 16.20859677128121
```

Figure 2-2 : Sample NORAD 2-Card Element Set File

In using LIFETIME 3.0, the element set file is processed by a subroutine called CONVNOR (CONVert NORad) to form an input file to LIFETIME called "INAE". This file contains the time, semi-major axis, and eccentricity for each NORAD observation, to allow easy use within the differential correction process. The earliest time point of NORAD data is taken as the epoch time and ephemeris. The subsequent time points are referenced as increments from that time. A sample INAE file is shown in Figure 2-3. The integer appearing on the first line indicates the number of lines of data to follow.

Time From Epoch (days)	Semi-Major Axis (m)	Eccentricity
24		
0.000000000E+00	0.664542148E+07	0.734406557E-03
0.934299910E+00	0.664375152E+07	0.139410792E-02
0.193041760E+01	0.664172311E+07	0.157276137E-02
0.267721348E+01	0.664018457E+07	0.167781072E-02
0.292608534E+01	0.663968147E+07	0.148965875E-02
0.448103803E+01	0.663702226E+07	0.179207357E-02
0.485406168E+01	0.663624620E+07	0.191951863E-02
0.541347096E+01	0.663512674E+07	0.182275308E-02
0.684209719E+01	0.663085944E+07	0.171329497E-02
0.715250646E+01	0.662940778E+07	0.202518680E-02
0.752491089E+01	0.662819544E+07	0.183015540E-02
0.789710642E+01	0.662681870E+07	0.180245531E-02
0.851732121E+01	0.662524750E+07	0.181723936E-02
0.882734074E+01	0.662430679E+07	0.179825360E-02
0.907529972E+01	0.662364932E+07	0.179380863E-02
0.938520822E+01	0.662288997E+07	0.178717529E-02
0.981899483E+01	0.662158507E+07	0.179764673E-02
0.100048553E+02	0.662107414E+07	0.179423203E-02
0.108099696E+02	0.661842135E+07	0.182874426E-02
0.111814421E+02	0.661719438E+07	0.176589002E-02
0.115527237E+02	0.661586123E+07	0.176359995E-02
0.118002052E+02	0.661501529E+07	0.172347064E-02
0.121094998E+02	0.661400388E+07	0.173079594E-02
0.127896772E+02	0.661144886E+07	0.168254808E-02

Figure 2-3 : Sample INAE File

2.2.2 Using the INAE File in the Differential Correction Process

LIFETIME integrates the averaged equations of motion of the satellite with a step size of multiples of the orbital period. The internal time from epoch variable is thus updated after each integration step with the specified time step size. The most accurate prediction mode for LIFETIME is with a step size of one orbit period. In this mode, the time is updated by one period each integration and compared to the "time from epoch" column in the INAE file. When these values are within half an orbital revolution from each other, a subroutine to compute the differences between the computed and observed semi-major axis and eccentricity values is activated. This time comparison and subsequent element comparison is done for the entire length of the prediction run, for as much data as is available in the INAE file. The partial derivatives from (2.5) are collected and used in the least squares method to compute a new inverse ballistic coefficient that would minimize the differences between the computed and observed semi-major axis and eccentricity values. This process is illustrated by the sample differential correction output shown in Figure 2-4.

```
IP,REV,DA,DE =   1    0   0.1647E-04  0.5430E-07
IP,REV,DA,DE =   2   15  -0.4684E-05 -0.1169E-03
IP,REV,DA,DE =   3   19  -0.1143E-04  0.2221E-04
IP,REV,DA,DE =   4   31  -0.4113E-04 -0.3359E-03
IP,REV,DA,DE =   5   35  -0.4498E-04 -0.1827E-03
IP,REV,DA,DE =   6   50  -0.1882E-04  0.3026E-04
IP,REV,DA,DE =   7   66  -0.4230E-04  0.8906E-04
IP,REV,DA,DE =   8   78  -0.6325E-04  0.8524E-04
IP,REV,DA,DE =   9   82  -0.6727E-04 -0.4591E-04
IP,REV,DA,DE =  10  107   0.7292E-04  0.1011E-03
IP,REV,DA,DE =  11  113   0.1002E-03  0.1646E-03
IP,REV,DA,DE =  12  122   0.1432E-03  0.9836E-04
IP,REV,DA,DE =  13  145   0.1099E-03 -0.1075E-03
IP,REV,DA,DE =  14  150   0.2823E-04  0.1446E-03
IP,REV,DA,DE =  15  156   0.5289E-05 -0.1247E-04
IP,REV,DA,DE =  16  162  -0.4443E-04 -0.6238E-04
IP,REV,DA,DE =  17  172  -0.1554E-04 -0.5665E-04
IP,REV,DA,DE =  18  177  -0.1706E-04 -0.1057E-03
IP,REV,DA,DE =  19  181   0.2153E-06 -0.1164E-03
IP,REV,DA,DE =  20  186   0.3604E-04 -0.1240E-03
IP,REV,DA,DE =  21  193   0.5287E-04 -0.1270E-03
IP,REV,DA,DE =  22  196   0.6718E-04 -0.1337E-03
IP,REV,DA,DE =  23  209   0.5415E-04 -0.1064E-03
IP,REV,DA,DE =  24  215   0.4950E-04 -0.1793E-03
IP,REV,DA,DE =  25  221   0.3313E-04 -0.1849E-03
IP,REV,DA,DE =  26  225   0.2991E-04 -0.2239E-03
IP,REV,DA,DE =  27  230   0.3402E-04 -0.2188E-03
IP,REV,DA,DE =  28  241  -0.1312E-05 -0.2596E-03
IP,REV,DA,DE =  29  251  -0.2132E-04 -0.2873E-03
IP,REV,DA,DE =  30  267  -0.3036E-04 -0.3126E-03
IP,REV,DA,DE =  31  275  -0.5884E-04 -0.3630E-03
IP,REV,DA,DE =  32  291  -0.7657E-04 -0.3712E-03

NEW ESTIMATE OF CDAM =  0.93118280E+02 CM2/KG =  0.45503131E-01 FT2/LB;
FIT RESIDUALS: A =  0.36013137E+03 METERS & ECC =  0.17960388E-03
```

Figure 2-4 : Sample Differential Correction Output

In Figure 2-4, **IP** is the index of the NORAD data point, **REV** is the revolution number from epoch, and the remaining terms are the collected components to be used in (2.5). After the last data point is compared, the final two lines of output are produced. These contain the newly computed inverse ballistic coefficient (**CDAM**) that minimizes the differences and the corresponding fit residuals for semi-major axis and eccentricity. The run is then repeated, using the new inverse ballistic coefficient to refine the decay calculations. This process is repeated until a converged value for B is reached.

2.2.3 Computing Time and Semi-major Axis Errors

As mentioned in Section 1.3, an area of investigation in accuracy improvements to LIFETIME involved errors in time accounting, which comes directly from the period calculations. The NORAD tracking data present in the INAE file could be used to show these errors in the following ways: (1) at each step in the differential correction process, when the computed time and observed time are compared, calculate the actual difference and note the pattern of error accumulation; (2) divide the time difference at each differential correction step by the number of orbit revolutions up to that point to note any relationship; and (3) note the difference between computed and observed semi-major axis values at the end of a run, since that is the primary orbital element in period computation.

To view these items of interest, the program was modified to produce the values desired during each differential correction comparison. A sample of this modified differential correction output is Figure 2-5. This is taken from an actual satellite case, the RME satellite.

```
                *** NOW BEGINNING ORBIT PROPAGATION ***
IP,REV,DT,DTPR,DA,DE =    1     0      0 0.0  0.1647E-04  0.5430E-07
IP,REV,DT,DTPR,DA,DE =    2    15    122 8.2 -0.4684E-05 -0.1169E-03
IP,REV,DT,DTPR,DA,DE =    3    19    154 8.1 -0.1143E-04  0.2221E-04
IP,REV,DT,DTPR,DA,DE =    4    31    250 8.1 -0.4113E-04 -0.3359E-03
IP,REV,DT,DTPR,DA,DE =    5    35    281 8.0 -0.4498E-04 -0.1827E-03
IP,REV,DT,DTPR,DA,DE =    6    50    403 8.1 -0.1882E-04  0.3026E-04
IP,REV,DT,DTPR,DA,DE =    7    66    528 8.0 -0.4230E-04  0.8906E-04
IP,REV,DT,DTPR,DA,DE =    8    78    620 8.0 -0.6325E-04  0.8524E-04
IP,REV,DT,DTPR,DA,DE =    9    82    651 7.9 -0.6727E-04 -0.4591E-04
IP,REV,DT,DTPR,DA,DE =   10   107    855 8.0  0.7292E-04  0.1011E-03
IP,REV,DT,DTPR,DA,DE =   11   113    907 8.0  0.1002E-03  0.1646E-03
IP,REV,DT,DTPR,DA,DE =   12   122    987 8.1  0.1432E-03  0.9836E-04
IP,REV,DT,DTPR,DA,DE =   13   145   1181 8.1  0.1099E-03 -0.1075E-03
IP,REV,DT,DTPR,DA,DE =   14   150   1225 8.2  0.2823E-04  0.1446E-03
IP,REV,DT,DTPR,DA,DE =   15   156   1277 8.2  0.5289E-05 -0.1247E-04
IP,REV,DT,DTPR,DA,DE =   16   162   1318 8.1 -0.4443E-04 -0.6238E-04
IP,REV,DT,DTPR,DA,DE =   17   172   1395 8.1 -0.1554E-04 -0.5665E-04
IP,REV,DT,DTPR,DA,DE =   18   177   1434 8.1 -0.1706E-04 -0.1057E-03
IP,REV,DT,DTPR,DA,DE =   19   181   1465 8.1  0.2153E-06 -0.1164E-03
IP,REV,DT,DTPR,DA,DE =   20   186   1505 8.1  0.3604E-04 -0.1240E-03
IP,REV,DT,DTPR,DA,DE =   21   193   1563 8.1  0.5287E-04 -0.1270E-03
IP,REV,DT,DTPR,DA,DE =   22   196   1588 8.1  0.6718E-04 -0.1337E-03
IP,REV,DT,DTPR,DA,DE =   23   209   1696 8.1  0.5415E-04 -0.1064E-03
IP,REV,DT,DTPR,DA,DE =   24   215   1749 8.1  0.4950E-04 -0.1793E-03
IP,REV,DT,DTPR,DA,DE =   25   221   1794 8.1  0.3313E-04 -0.1849E-03
IP,REV,DT,DTPR,DA,DE =   26   225   1826 8.1  0.2991E-04 -0.2239E-03
IP,REV,DT,DTPR,DA,DE =   27   230   1867 8.1  0.3402E-04 -0.2188E-03
IP,REV,DT,DTPR,DA,DE =   28   241   1955 8.1 -0.1312E-05 -0.2596E-03
IP,REV,DT,DTPR,DA,DE =   29   251   2031 8.1 -0.2132E-04 -0.2873E-03
IP,REV,DT,DTPR,DA,DE =   30   267   2150 8.1 -0.3036E-04 -0.3126E-03
IP,REV,DT,DTPR,DA,DE =   31   275   2214 8.1 -0.5884E-04 -0.3630E-03
IP,REV,DT,DTPR,DA,DE =   32   291   2323 8.0 -0.7657E-04 -0.3712E-03

NEW ESTIMATE OF CDAM =  0.93118280E+02 CM2/KG =  0.45503131E-01 FT2/LB;
FIT RESIDUALS: A =  0.36013137E+03 METERS & ECC =  0.17960388E-03
```

Figure 2-5 : Sample of Modified Output Showing Time Errors

The value **DT** in Figure 2-5 is the time difference between the observed and calculated nodal crossing times of the satellite, in seconds, computed as

$$DT = T_{(NORAD\ data)} - T_{(LIFETIME)} \tag{2.6}$$

The value **DTPR** is the estimate of time difference per satellite revolution, from

$$DTPR = \frac{DT}{REV} \tag{2.7}$$

This sample case was the first indication of the trends that were later evident in all cases studied: The LIFETIME period calculations were always less than the actual period as recorded in the NORAD data. The time errors accumulated as in Figure 2-5 to result in a final time and semi-major axis error at the end of the differential correction process. Furthermore, the **DTPR** values remained fairly constant over the entire run, indicating a possible deficiency in the actual method of period calculation within the LIFETIME 3.0 algorithm.

2.3 Confirmation of Errors by the SPIN Program

It is always prudent to search for the independent confirmation of observed trends. A compact, PC based numerical integration program called SPIN was chosen as a computational baseline to compare LIFETIME against in order to confirm the type of time errors seen in Section 2.2. This section describes the SPIN program and presents the confirmation of these errors.

2.3.1 The SPIN Program

The SPIN program is the **S**atellite **P**erturbations **IN**tegration program developed by D.L. Oltrogge at The Aerospace Corporation. It is a general-purpose high-accuracy orbital and attitude dynamics simulation program whose major capabilities of interest here are: (1) forward and backward orbit integration using a fourth-order Runge/Kutta startup for a tenth-order Gauss/Jackson scheme; (2) modeling of terrestrial orbit perturbations with an 18 x 18 spherical harmonics gravity field (WGS 84) Earth model; and (3) modeling of drag perturbations using the Jacchia 1971 atmosphere model. Its accuracy has been verified through comparisons to other large and established numerical integration programs, such as the TRACE program.[Ref. 14]

In order to make an accurate comparison with LIFETIME, the capability of SPIN was set to a similar level. That is, only the J_2 and J_3 gravity harmonics were included and the exact same orbital and solar conditions at epoch were used. A sample case was constructed for both a LIFETIME and SPIN propagation run. Of interest were the values returned by both programs for the satellite's nodal period, as a function of time.

2.3.2 Comparison of LIFETIME and SPIN Sample Case

The results of the nodal period computations for the sample case are presented in Figure 2-6. Only the first ten revolutions of propagation are shown, to indicate the trend that is apparent.

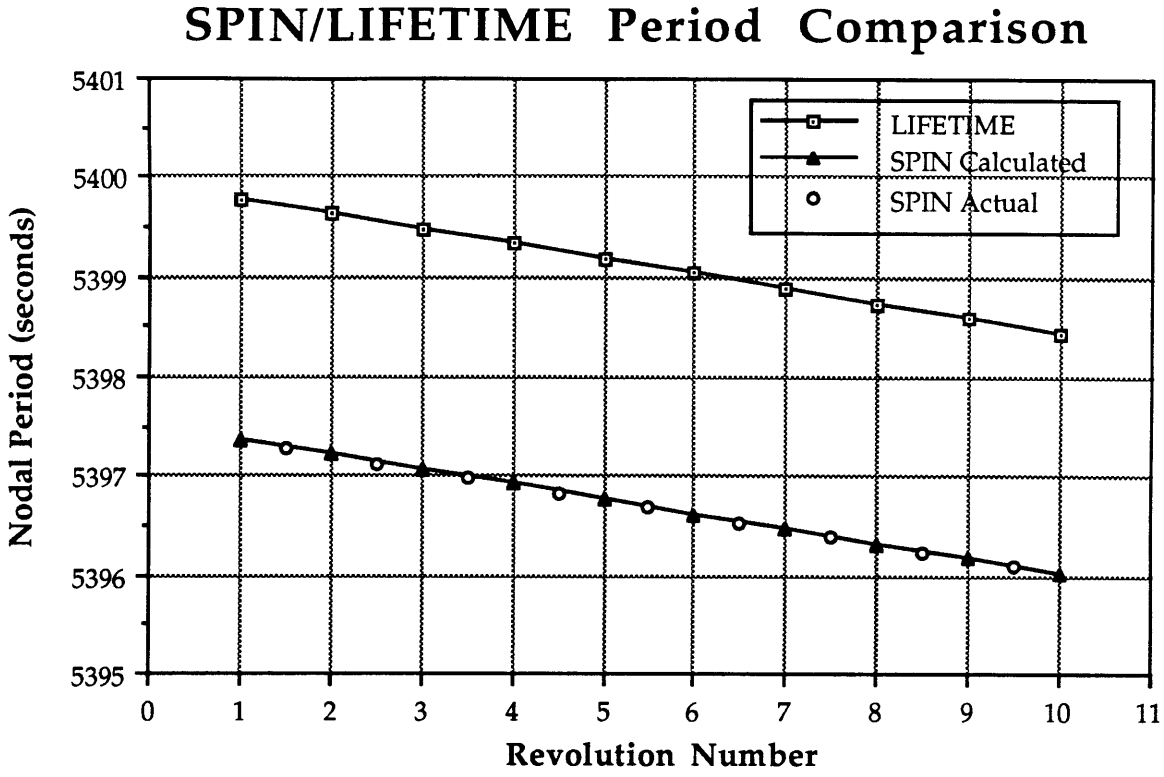

Figure 2-6 : Comparison of LIFETIME and SPIN Period Calculations

The "SPIN Calculated" values shown in the plot correspond to the nodal period calculations made by the program at the ascending node, the same location where LIFETIME's calculations occur. The "SPIN Actual" values are those determined solely from the actual propagation results, by looking at the amount of time it actually took the simulated satellite to complete one orbit, ascending node to ascending node.

Figure 2-6 indicates that some type of constant bias exists within the LIFETIME algorithm, assuming the SPIN program to be a "truth model" due to its high-accuracy integration methods. The result of this contrived sample case merely confirmed the existence of a potential algorithmic error and was not meant as a comparison to the real satellite case of Section 2.2 or to other cases presented later in this study.

2.4 Four Decayed Satellites as Case Studies

To determine the full range of time errors for the LIFETIME algorithm compared to actual decayed satellites, four cases were chosen. This section describes the four satellite cases and the values for F_{10} and a_p used.

2.4.1 The Satellite Cases

Table 2-1 contains the structure of the satellite cases used in this study. The RME satellite is the Relay Mirror Experiment satellite. LOSAT-X is an SDI experimental satellite. NORAD-1 and NORAD-2 refer to two other satellites for which a high volume of NORAD data was available for use with the LIFETIME program.

Table 2-1 : The Satellite Cases

Satellite Case	NORAD Data (days)	Epoch	Impact Day & Time (GMT)
RME - A	18	25 Apr 92	24 May 92 15:31
RME - B	18	1 May 92	24 May 92 15:31
RME - C	18	3 May 92	24 May 92 15:31
RME - D	18	11 May 92	24 May 92 15:31
LOSAT-X - A	7	29 Oct 91	15 Nov 91 16:06
LOSAT-X - B	12	29 Oct 91	15 Nov 91 16:06
LOSAT-X - C	14	29 Oct 91	15 Nov 91 16:06
LOSAT-X - D	17	29 Oct 91	15 Nov 91 16:06

NORAD-1 - A	20	11 Dec 92	10 Jan 93 12:50
NORAD-1 - B	20	16 Dec 92	10 Jan 93 12:50
NORAD-1 - C	20	18 Dec 92	10 Jan 93 12:50
NORAD-1 - D	20	21 Dec 92	10 Jan 93 12:50
NORAD-2 - A	8	25 Nov 92	14 Dec 92 01:57
NORAD-2 - B	13	25 Nov 92	14 Dec 92 01:57
NORAD-2 - C	15	25 Nov 92	14 Dec 92 01:57
NORAD-2 - D	18	25 Nov 92	14 Dec 92 01:57

Each satellite had a different amount of NORAD data associated with it. Thus, the prediction span from the last data point to impact was chosen as a controlled variable for determining the cases, identified with letters A, B, C, and D. These letters correspond to the prediction length according to Table 2-2.

Table 2-2 : Prediction Spans for the Satellite Cases

Case Letter	Prediction Span (days)
A	10
B	5
C	3
D	≤ 1

2.4.2 Solar Inputs for Satellite Cases

Plots of the F_{10} and a_p values used for each of the four satellites are presented in Figures 2-7, 2-8, 2-9, and 2-10. These values cover the span of days for the longest duration cases with the earliest epoch times (i.e. the "A" cases). The remaining cases for each satellite fall within this time span. The data terminates at the satellite's impact. These values are the daily values obtained from the USSPACECOM data center and the Threat Analysis Office of The Aerospace Corporation. Each of the four satellites thus become unique cases because each experiences varying levels of solar activity.

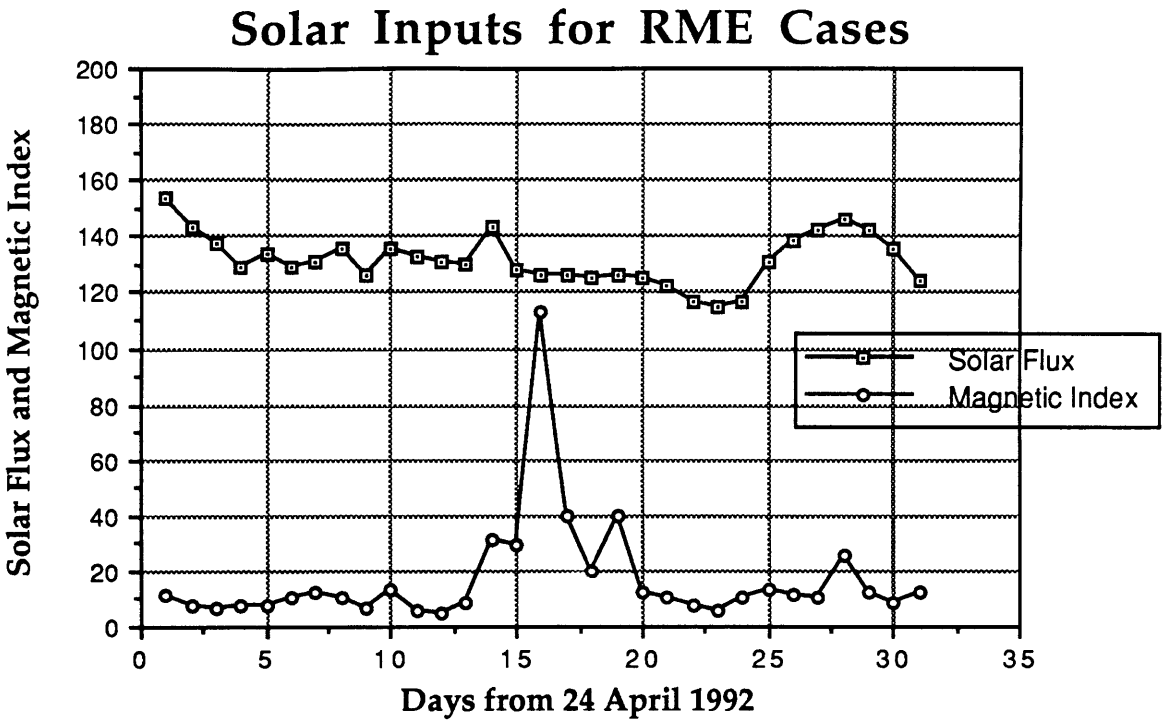

Figure 2-7 : F_{10} and a_p Values for the RME Satellite Cases

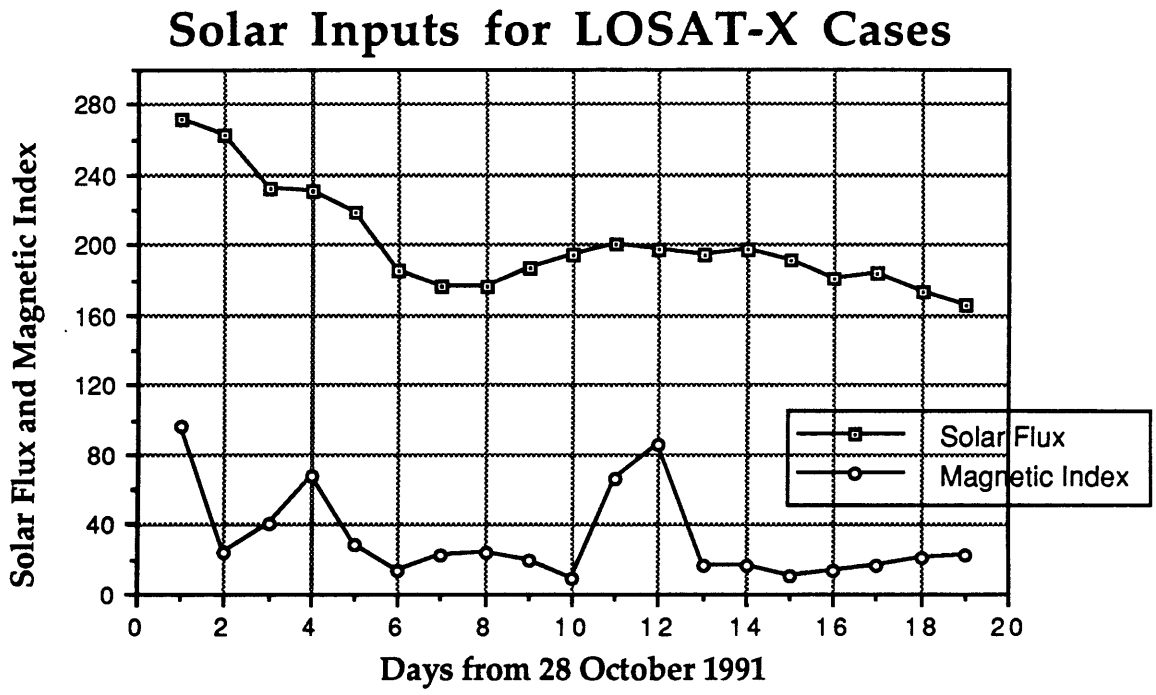

Figure 2-8 : F_{10} and a_p Values for the LOSAT-X Satellite Cases

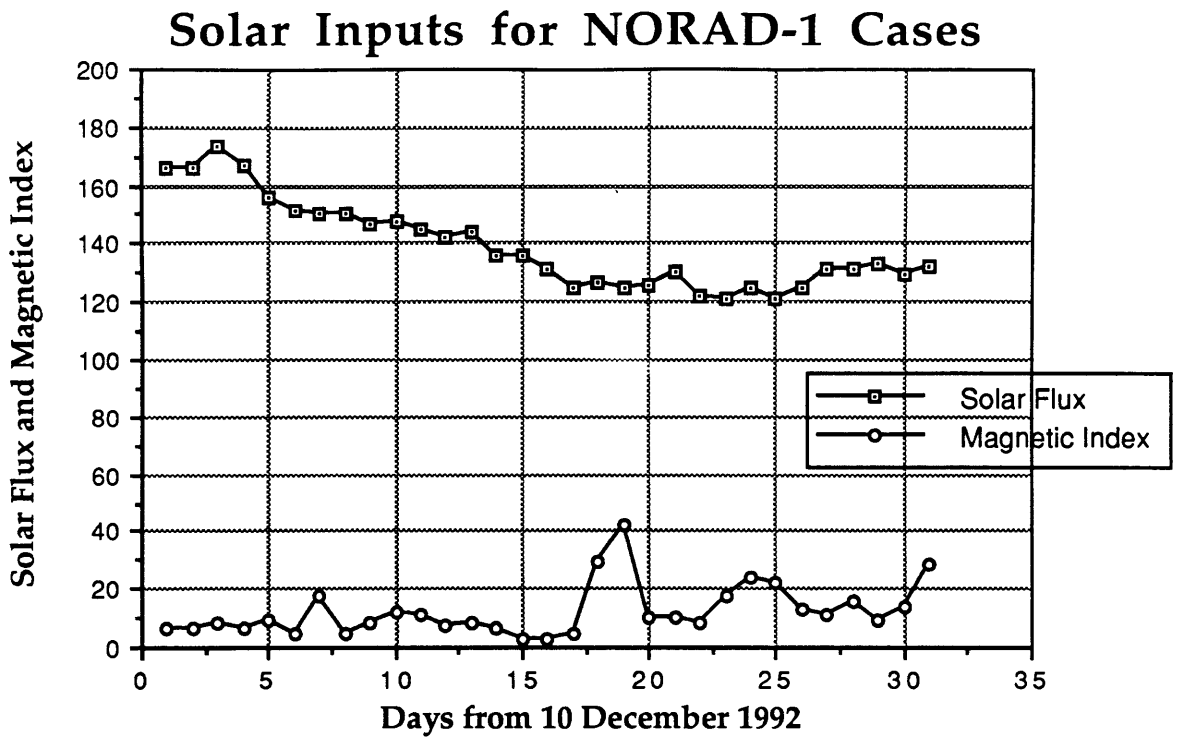

Figure 2-9 : F_{10} and a_p Values for the NORAD-1 Satellite Cases

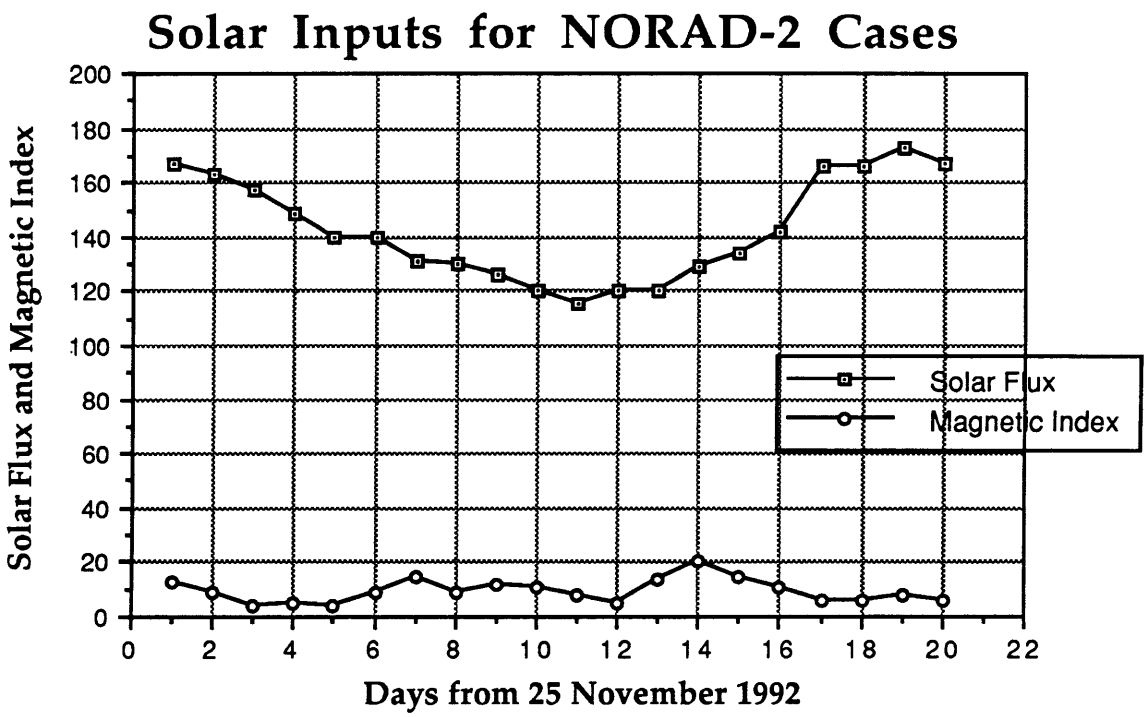

Figure 2-10 : F_{10} and a_p Values for the NORAD-2 Satellite Cases

2.5 Results of Case Studies: Time and Semi-Major Axis Errors

The four satellite case studies, each with the four prediction spans, were used as inputs for the LIFETIME 3.0 program. The NORAD data files for each case were processed by the program CONVNOR and the resulting INAE file used as LIFETIME input. The data of interest for these runs was the time from epoch errors and the semi-major axis errors present at the end of the data span used for the differential correction process. Once a converged value was reached for the inverse ballistic coefficient, the errors could be computed. The time, t, and semi-major axis, a, errors are defined through the following:

$$\text{Error}(t,a) = \text{LIFETIME}(t,a) - \text{NORAD}(t,a) \tag{2.8}$$

A table of these error values for all the cases is presented as Table 2-3.

Table 2-3 : Time and Semi-Major Axis Errors for Each Case

Satellite Case	NORAD Data (days)	Time Error (seconds)	Semi-Major Axis Error (meters)
RME - A	18	- 2177	- 833
RME - B	18	- 2322	+870
RME - C	18	- 2346	+865
RME - D	18	No Convergence	No Convergence
LOSAT-X - A	7	- 991	+1518
LOSAT-X - B	12	- 1708	+2600
LOSAT-X - C	14	- 1937	+1905
LOSAT-X - D	17	- 2291	+4371
NORAD-1 - A	20	- 2532	+2277
NORAD-1 - B	20	- 2165	- 1260
NORAD-1 - C	20	- 1582	+1177
NORAD-1 - D	20	- 1257	+634

NORAD-2 - A	8	- 1064	+1090
NORAD-2 - B	13	- 1868	+906
NORAD-2 - C	15	- 2035	- 1172
NORAD-2 - D	18	- 1912	- 14068

There was no convergence for the inverse ballistic coefficient for the RME - D case. The likely cause is the fact that the last few data points are so close to the impact that the algorithm cannot account for the fast rate of change of the orbital elements and still satisfy the least squares procedure that underlies the differential correction process.

A graphical representation of this data is shown in Figure 2-11. It plots the time and semi-major axis errors together, as single points.

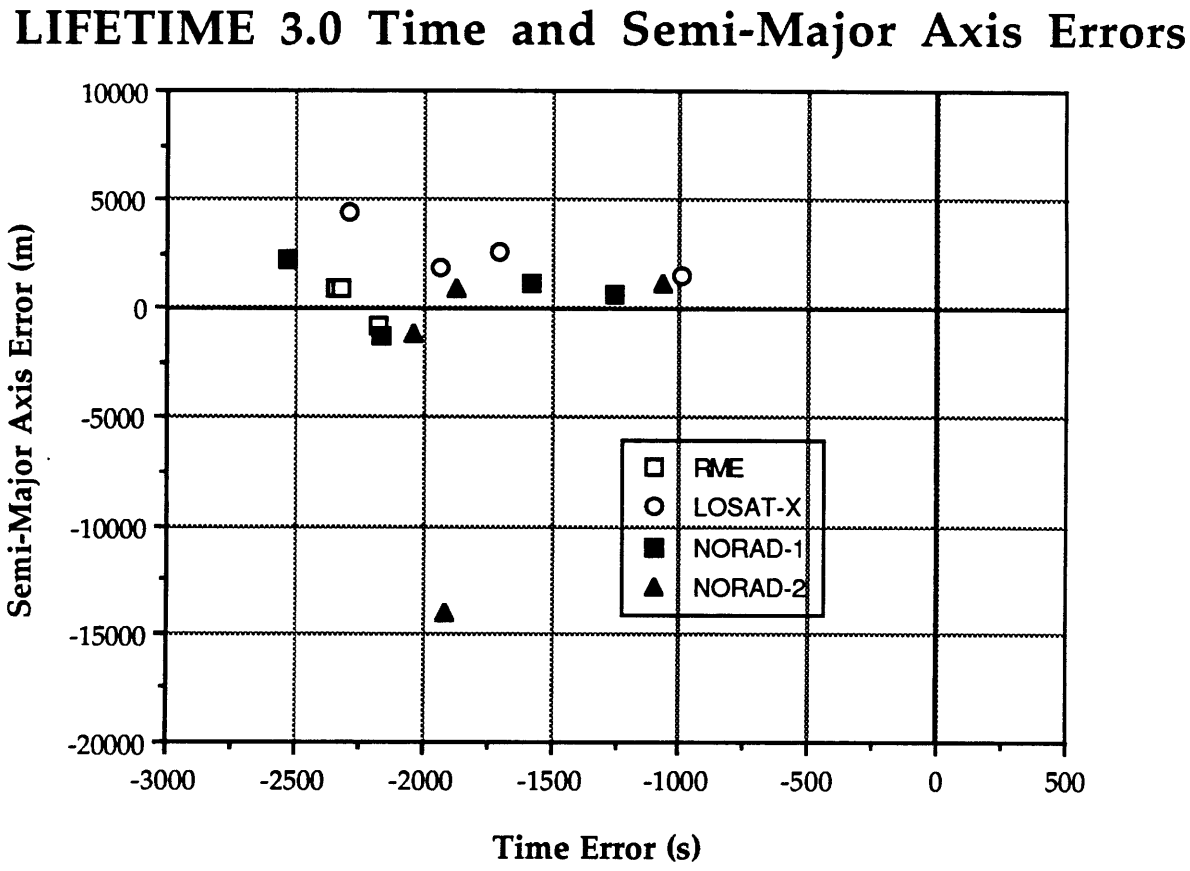

Figure 2-11 : Plot of LIFETIME 3.0 Time and Semi-Major Axis Errors

At this point, the data serve as background to the fact that there is deficiency in the LIFETIME 3.0 algorithm. The significant result is that consistent errors in updating the time from epoch counter accumulate to cause a substantial time error when the final NORAD data point and its closest computed value are compared. Since the time from epoch counter is updated by multiples of the orbit period, as specified by user input, the problem potentially lies within the method of orbit period calculation.

Chapter 3

Improving Program Accuracy

This chapter focuses on investigating the sources of error in the period calculation algorithm of LIFETIME 3.0. Improvements are proposed in the area of actual period calculation and in the method for converting NORAD data sets into the usable information of the INAE file. The improved algorithm is labeled LIFETIME 4.0 and is tested with the same satellite cases introduced in Chapter 2. The results are compared to the LIFETIME 3.0 results already presented.

3.1 Investigation of Sources of Period Calculation Errors

3.1.1 LIFETIME 3.0 Period Calculation Algorithm

The mean orbital elements inputted into LIFETIME 3.0 are contained in the element set **ORBIT**, defined as

$$\text{ORBIT} = a, e, i, \Omega, \omega \tag{3.1}$$

These elements correspond to the first NORAD data point. The true or mean anomaly is not a necessary input since the LIFETIME algorithm propagates with a step size of multiples of an orbit period. The intrack position at the completion of a propagation step is assumed to remain constant throughout an entire run.

In computing the orbital period, the algorithm first determines the satellite's mean motion, n, from

$$n = \sqrt{\frac{\mu}{a^3}} \tag{3.2}$$

The satellite's Keplerian period, P_o, can then be computed from

$$P_o = \frac{2\pi}{n} \tag{3.3}$$

The algorithm then uses the following equation [Ref. 15] to calculate the actual orbital period, P, to be used as the propagation step size:

$$P = P_o \left[1 - \frac{3}{2} J_2 \left(\frac{R_E}{a(1-e^2)} \right)^2 - \frac{3}{2} J_2 \left(\frac{R_E}{a(1-e^2)} \right)^2 \frac{(2 - \frac{5}{2}\sin^2 i)}{(1 + e\cos\omega)} \right] \tag{3.4}$$

The additional terms, to P_o, are used to arrive at the actual period by adjusting the Keplerian period by first order perturbation effects in terms of J_2, a, e, i, and ω.

3.1.2 Proposed Improvement in Period Calculation Method

Research into a more rigorously defined method of period calculation found the work of Claus & Lubowe (1966). They proposed a general equation for the "sidereal period", which represents the change in time, Δt, as the argument of latitude varies from u, its initial value, to $u + 2\pi$.[Ref. 16] This general equation is

$$\Delta t = P_o \left\{ 1 - \frac{3}{2} J_2 \frac{R_E^2 a}{r} \left[1 - 3\sin^2 i \sin^2 u + \frac{1}{2} \frac{(1-e^2)^{\frac{5}{2}} (4 - 5\sin^2 i)}{(1 + l\cos u + m\sin u)^5} \right] \right\} + O(J_2^2) \tag{3.5}$$

where

$l = e\cos w$

$m = e\sin w$

$r = \dfrac{a(1-e^2)}{1 + l\cos u + m\sin u}$

$O(J_2^2)$ = Second order correction to Δt, not considered here

As is noted through the notation, the orbital elements used in (3.5) are osculating.

For computing a nodal period from (3.5) the argument of latitude remains fixed at $u = 0$. This results in the equation for nodal period, P_N:

$$P_N = P_o \left\{ 1 - \frac{3}{2} J_2 \left(\frac{R_E}{a} \right)^2 \left(\frac{1 + e \cos w}{1 - e^2} \right)^3 \left[1 + \frac{1}{2} \frac{(1 - e^2)^{\frac{5}{2}} (4 - 5 \sin^2 i)}{(1 + e \cos u)^5} \right] \right\} \quad (3.6)$$

This method of nodal period calculation was added to the LIFETIME algorithm. In order to be used correctly, the osculating orbital elements had to be determined prior to their insertion into (3.6). This was done by using a subroutine to make the iteration conversion from mean to osculating classical orbital elements. The method used was adapted from an algorithm derived by C. Uphoff at the Jet Propulsion Laboratory (1987), which is based on a combination of Kozai's and Izsak's theories. The reader is referred to JPL EM 312/87-153 of 20 April 1987.

3.1.3 LIFETIME 3.0 NORAD Data Conversion Method

In using LIFETIME 3.0, the program CONVNOR is used to convert the NORAD 2-card element data file into the usable INAE file. A simple Keplerian transformation of the card element n, the mean motion, is used to compute the semi-major axis. The eccentricity is recorded directly from the 2-card element set. The semi-major axis is computed from

$$a^3 = \frac{\mu}{n^2} \quad (3.7)$$

Closer analysis of the NORAD 2-card format revealed that the transformation may have been over-simplified in the CONVNOR program. Referring back to Figure 2-1, there is an identifier on Card 1 that indicates the "ephemeris type". This refers to the type of propagation method used in the NORAD conversion of radar tracking data to the 2-card elements. An algorithm with

element variables defined in the same way as the original propagator type would have to be used for an accurate conversion of elements from the 2-card set to the INAE file. This realization led to the development of PRELIFE, a program run before LIFETIME to convert NORAD 2-card element sets.

3.1.4 Proposed Improved Conversion Scheme: Program PRELIFE

The program PRELIFE was constructed from existing software elements, including the actual propagator types employed by NORAD: SGP and SGP4. For details on these propagator models, the reader is referred to Space Track Report No. 3, December 1980.

The "ephemeris type" indicators on the 2-card element sets used in this study all indicated the use of the SGP4 model. However, PRELIFE was developed to handle the SGP model as well.

By using PRELIFE to convert the NORAD data sets into new INAE files for the cases studied in this report, different values for semi-major axis and eccentricity were indeed produced. Whether this change along with the period calculation change would result in improved accuracy was a matter of re-testing the satellite cases and comparing the time and semi-major axis errors.

3.2 Comparison of LIFETIME 4.0 and SPIN

As an outside source check on the new method of period calculation, the sample test case with the SPIN program presented in Section 2.3 was re-examined. The algorithm with the new nodal period equation derived from Claus & Lubowe was labeled LIFETIME 4.0. The results of the comparison of the sample case are presented in Figure 3-1.

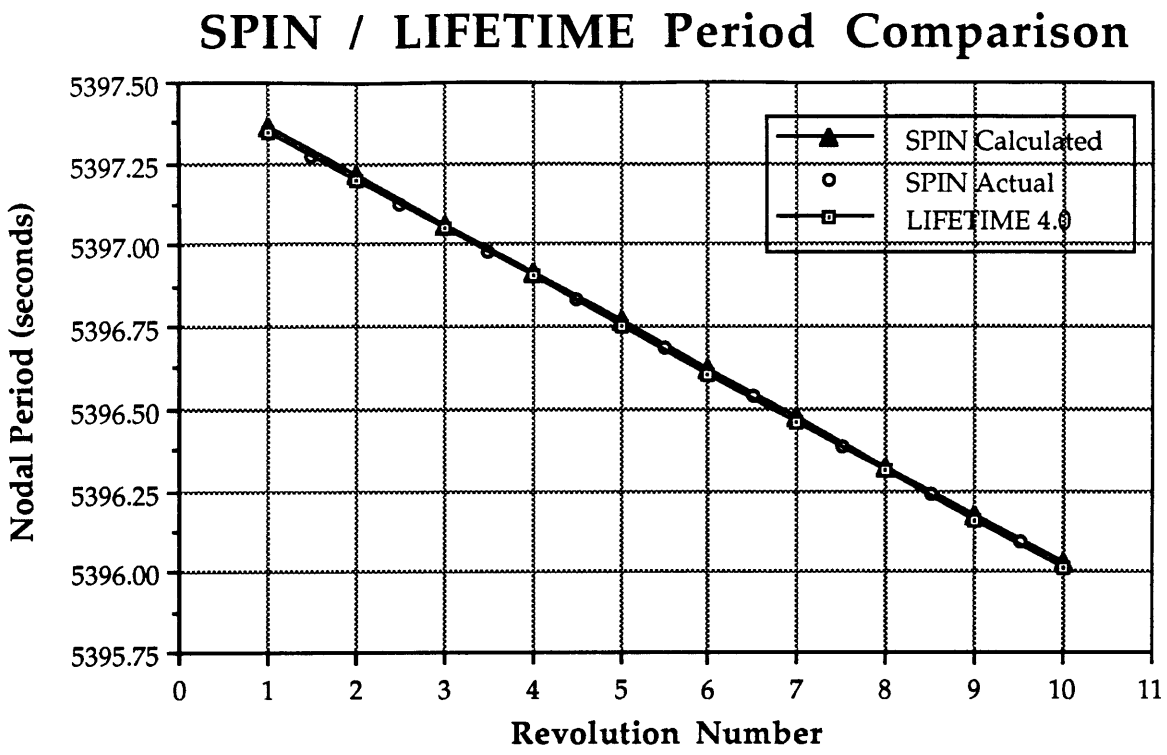

Figure 3-1 : Comparison of LIFETIME 4.0 and SPIN Period Calculations

The errors in period calculation seen previously in Figure 2-6 have mostly vanished. The actual difference in nodal period between LIFETIME 4.0 and SPIN for this sample case averages around 0.013 seconds.

3.3 Results of LIFETIME 4.0 Satellite Case Studies

Using PRELIFE as the NORAD conversion program to form the INAE files, LIFETIME 4.0 was used to re-visit the satellite cases previously examined with LIFETIME 3.0. An example of the screen output during the differential correction process for LIFETIME 4.0 is shown as Figure 3-2. Note how the **DT** values (time difference, in seconds) have been significantly reduced from those in Figure 2-5. The **DTPR** values have also been reduced.

```
                *** NOW BEGINNING ORBIT PROPAGATION ***
IPP,REV,DT,DA,DE =   2      15       -1    -0.1  0.2472E-03 -0.1005E-03
IPP,REV,DT,DA,DE =   3      19       -1    -0.1 -0.3034E-04 -0.2701E-03
IPP,REV,DT,DA,DE =   4      31        0     0.0 -0.6366E-04 -0.5479E-03
IPP,REV,DT,DA,DE =   5      35        2     0.1 -0.6874E-04 -0.5863E-03
IPP,REV,DT,DA,DE =   6      50        2     0.1 -0.4697E-04 -0.2045E-04
IPP,REV,DT,DA,DE =   7      66        7     0.1 -0.7547E-04  0.6234E-04
IPP,REV,DT,DA,DE =   8      78       13     0.2 -0.1021E-03  0.9976E-04
IPP,REV,DT,DA,DE =   9      82       16     0.2 -0.1081E-03 -0.1099E-03
IPP,REV,DT,DA,DE =  10     107       17     0.2  0.2580E-04  0.7736E-04
IPP,REV,DT,DA,DE =  11     113       15     0.1  0.5463E-04  0.1818E-03
IPP,REV,DT,DA,DE =  12     122        8     0.1  0.9961E-04  0.5303E-04
IPP,REV,DT,DA,DE =  13     145        0     0.0  0.8639E-04 -0.1148E-03
IPP,REV,DT,DA,DE =  14     150       -3     0.0  0.9436E-05  0.1876E-03
IPP,REV,DT,DA,DE =  15     156       -8    -0.1 -0.8943E-05 -0.1806E-04
IPP,REV,DT,DA,DE =  16     162       -2     0.0 -0.5584E-04 -0.5531E-04
IPP,REV,DT,DA,DE =  17     172        0     0.0 -0.2453E-04 -0.5310E-04
IPP,REV,DT,DA,DE =  18     177        0     0.0 -0.2441E-04 -0.7595E-04
IPP,REV,DT,DA,DE =  19     181        0     0.0 -0.5351E-05 -0.8226E-04
IPP,REV,DT,DA,DE =  20     186        0     0.0  0.3343E-04 -0.8971E-04
IPP,REV,DT,DA,DE =  21     193       -5     0.0  0.5507E-04 -0.7821E-04
IPP,REV,DT,DA,DE =  22     196       -6     0.0  0.7119E-04 -0.8059E-04
IPP,REV,DT,DA,DE =  23     209      -14    -0.1  0.6181E-04 -0.3874E-04
IPP,REV,DT,DA,DE =  24     215      -22    -0.1  0.5742E-04 -0.9577E-04
IPP,REV,DT,DA,DE =  25     221      -21    -0.1  0.4149E-04 -0.9023E-04
IPP,REV,DT,DA,DE =  26     225      -22    -0.1  0.3854E-04 -0.1242E-03
IPP,REV,DT,DA,DE =  27     230      -25    -0.1  0.4288E-04 -0.1080E-03
IPP,REV,DT,DA,DE =  28     241      -29    -0.1  0.7125E-05 -0.1328E-03
IPP,REV,DT,DA,DE =  29     251      -29    -0.1 -0.1492E-04 -0.1468E-03
IPP,REV,DT,DA,DE =  30     267      -26    -0.1 -0.2753E-04 -0.1346E-03
IPP,REV,DT,DA,DE =  31     275      -30    -0.1 -0.5698E-04 -0.1677E-03
IPP,REV,DT,DA,DE =  32     291      -19    -0.1 -0.7420E-04 -0.1357E-03

NEW ESTIMATE OF CDAM =  0.97187617E+02 CM2/KG =  0.47491651E-01 FT2/LB;
FIT RESIDUALS: A =  0.46658444E+03 METERS & ECC =  0.17964248E-03
```

Figure 3-2 : Sample of LIFETIME 4.0 Differential Correction Output

As explained in Section 2.5, the items of interest for all the case studies were the time and semi-major axis errors evident at the last data point of the differential correction process. Examination of all the cases yielded the results presented in Table 3-1.

Table 3-1 : Time and Semi-Major Axis Errors for Each Case

Satellite Case	NORAD Data (days)	Time Error (seconds)	Semi-Major Axis Error (meters)
RME - A	18	+138	- 1284
RME - B	18	- 19	+493
RME - C	18	- 77	+388
RME - D	18	- 5	- 729
LOSAT-X - A	7	- 97	+1302
LOSAT-X - B	12	- 290	+1979
LOSAT-X - C	14	- 344	+1249
LOSAT-X - D	17	- 447	+3508

NORAD-1 - A	20	- 1136	- 4524
NORAD-1 - B	20	- 243	- 1125
NORAD-1 - C	20	+206	+697
NORAD-1 - D	20	- 89	+272
NORAD-2 - A	8	- 47	+606
NORAD-2 - B	13	- 233	+573
NORAD-2 - C	15	- 197	- 1246
NORAD-2 - D	18	+126	- 12934

A plot all the data in Table 3-1 is shown in Figure 3-3.

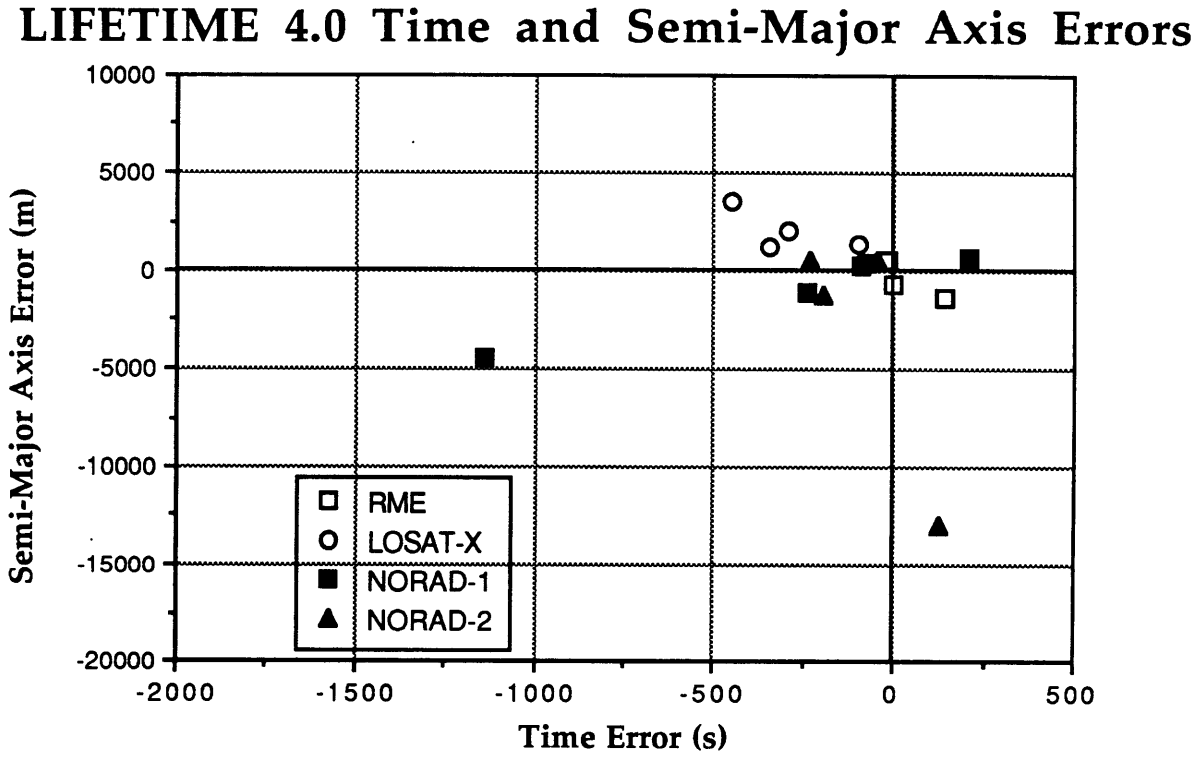

Figure 3-3 : Plot of LIFETIME 4.0 Time and Semi-Major Axis Errors

3.4 Comparison of LIFETIME 3.0 and LIFETIME 4.0

The full effects of the improvements made to the LIFETIME algorithm can best be viewed by comparing both the 3.0 and 4.0 versions directly regarding the time and semi-major axis errors at the end of the differential correction process. The results of the satellite case studies for both versions are thus plotted together in Figure 3-4.

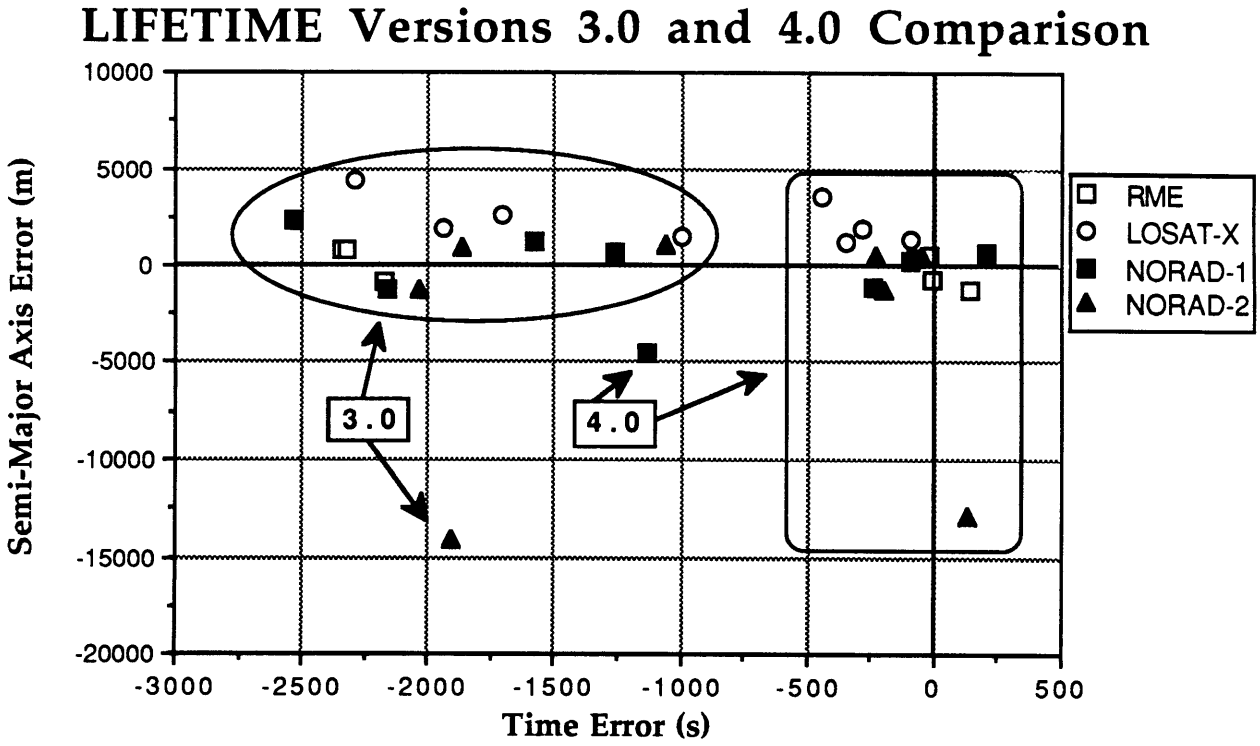

Figure 3-4 : Error Comparison of LIFETIME 3.0 and LIFETIME 4.0

Figure 3-4 clearly shows a significant reduction in the time errors of LIFETIME 4.0 as compared to LIFETIME 3.0 (at least an order of magnitude in most cases). Semi-major axis errors are relatively unaffected by the algorithm changes, although there is a small reduction in this error overall.

Of particular interest is the NORAD-2 data point with the large semi-major axis error (the NORAD-2 - D case). The last few observed data points for the differential correction span for this case occurred just prior to re-entry and the

high rate of change in semi-major axis probably was a major contributor to this error.

Another noted case would be the RME - D case, for which there was no convergence for LIFETIME 3.0. The LIFETIME 4.0 algorithm managed to produce a better decay curve fit during the differential corrections and converge to an effective ballistic coefficient.

Of general note is the LOSAT-X cases. As a group, they have the largest errors, especially in the LIFETIME 4.0 groupings. This would be expected, since the F_{10} and a_p values for this satellite were the highest and had the widest range of the four cases tested.(see Figure 2-8) Furthermore, the spacecraft was tumbling during the last segments of decay and re-entry. This would introduce some errors into the NORAD data.[Ref. 13]

At this stage in the research, the LIFETIME algorithm has been improved significantly by replacing the former method of period calculation with that introduced by Claus & Lubowe. Additionally, the method for converting NORAD 2-card element sets into the INAE file for use in the differential correction process has been revised to account for the NORAD propagator used in the actual formulation of the 2-card set. The result is the LIFETIME 4.0 program, which has shown a significant reduction in time errors exhibited by LIFETIME 3.0 for four satellite cases.

Chapter 4

Propagation Method for Impact Area Prediction

This chapter discusses the details of the satellite re-entry and breakup phenomenon. Options for the addition of a new propagation method into the LIFETIME 4.0 algorithm to deal with the problem are introduced and a scheme is proposed and implemented. Additionally, the enhanced output capabilities added to LIFETIME are discussed and examples are presented.

4.1 The Satellite Re-entry and Breakup Problem

A recent document by R. Stern, et al (1992) [Ref. 2] presented a review of orbital re-entry risk predictions for the Office of Commercial Space Transportation at the US Department of Transportation. This document contained, among other things, a fresh and detailed look at the re-entry process that accounted for recent USAF tests and empirical data analysis. It serves as the major reference for this section.

Essentially, the demise of a re-entering space vehicle (satellites and upper stages) occurs when it's outer structure achieves the melting temperature of the material. The maximum temperature experienced by the vehicle is determined by the peak heating rate, which in turn is governed by the object's ballistic coefficient. This assumption is justified because these re-entering objects have relatively thin outer skins with limited heat transfer paths to internal structures. Recent USAF re-entry breakup tests have also indicated that the classic convective heat transfer analysis to determine peak heating is in error. The actual flow conditions in the region of satellite breakup are in or approaching transition to continuum flow.[Ref 2]

USAF re-entry tests have shown that the survivability of an object is independent of its geometric configuration or orientation to the stagnation

point in the flow field. The initial breakup observed in all test cases occurred when the external structure of the vehicles melted simultaneously without regard to their orientation with respect to the incident velocity vector. The survival of an object or piece of debris to impact is assured if the radiation equilibrium temperature does not exceed the object's melting temperature.[Ref 2]

Thus, there are two main issues to be considered in dealing with the satellite re-entry, breakup, and impact problem. The first is to determine where the peak heating rate occurs (i.e. at what altitude) for a particular material type. This marks the catastrophic melting of the vehicle. Then the possibility of survival of debris to impact must be considered.

The altitude at which peak heating occurs is determined by two factors: material of the primary vehicle structure and the vehicle's ballistic coefficient. Figure 4-1 illustrates this effect of ballistic coefficient on peak heating rates. The region for which the heating would cause an aluminum or magnesium structure to melt is indicated in the figure. These materials are good assumptions to use in dealing with satellite structures.

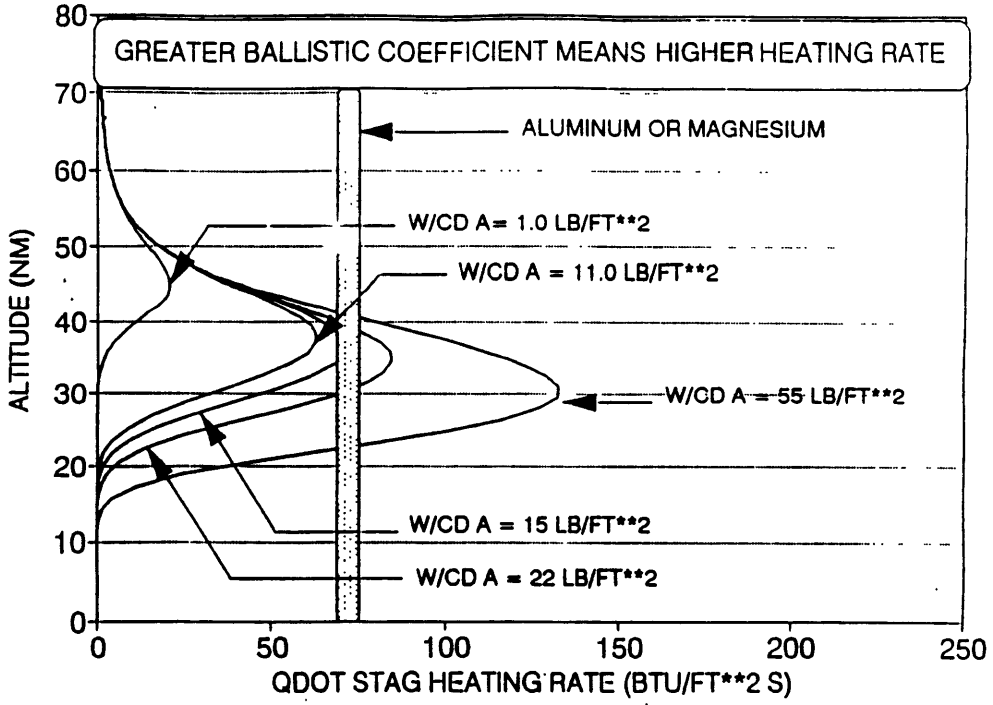

Figure 4-1: Heating Rate vs. Altitude for a Range of Ballistic Coefficients[Ref. 2]

The greatest ballistic coefficient possible before reaching the melting point of aluminum or magnesium is around 15 $\frac{lb}{ft^2}$. Thus for all objects with this ballistic coefficient or higher (assuming an aluminum or magnesium structure) melting will occur at the altitude indicated in Figure 4-1, which is around 42 nmi. Higher ballistic coefficient objects will survive if their material has a higher melting temperature. Overall, peak aerodynamic loading occurs about 10 nmi lower than peak heating, so some deformation would be noted in objects that survive the peak heating altitude.

Upon the breakup of the structure, two situations exist. One involves sub-components that may have ballistic coefficients low enough (high drag) to rapidly decelerate them through their peak heating and thus allow for their survival to impact. Surviving debris of this type generally show little evidence of re-entry heating.[Ref. 2] The second situation involves low drag (high ballistic coefficient) fragments that may continue their motion along the original trajectory and survive to impact. In looking at the impact of debris, both situations are considered.

The question remains as to how to use this information in the LIFETIME 4.0 program to model the re-entry process and attempt to eliminate the uncertainty in determining a satellite's re-entry during its final revolution. Thus, investigation into the probable propagation methods for this region began. Numerical integration methods are really the most efficient and accurate way to handle regions where a high rate of change in the equations of motion is prevalent.

4.2 Numerical Integration Schemes

This section discusses the integration scheme options available for development into a method of propagation for the re-entry portion of LIFETIME predictions. The main goal here was to investigate methods that would remove the uncertainty currently in LIFETIME but have little effect on the program's ease of use, compactness, or efficiency (speed of its running time).

4.2.1 Integration Options

It was desirable to use a "state of the art" integration routine that would yield the most accurate results. Three primary options seemed probable candidates, and each will be presented here.

The first option was the DASSL (Differential/Algebraic Systems Solver) program developed by L. Petzold of Sandia National Laboratories, Livermore CA. It uses the backward differentiation formulas of orders one through five to solve systems of the form

$$G(T, Y, Y') = 0 \tag{4.1}$$

This is a method employed to solve systems of stiff ordinary differential equations (ODE's). A formal definition of "stiff" ODE's is not easy to give, but they require extremely small step sizes in order to deal with numerical instabilities that are not actually connected with any instability of the problem itself.

The second option was the so-called "Shampine Integrator" developed by L. Shampine and M. Gordon of Sandia National Laboratories, Albuquerque NM. It solves initial value ODE's using an Adams-Bashforth-Moulton method. Specifically, the option that could be used in LIFETIME is a variable order (one through twelve) Adams code that is used to solve non-stiff or mildly-stiff ODE's when derivative evaluations are expensive, high accuracy is desired, or answers at many specific points are needed.

The third option was a Runge-Kutta 7(8) method as given by the Fehlberg Coefficients in NASA TR R-287. It is a variable-step size routine using a 7th order Runge-Kutta method with an 8th order error control mechanism.

Since a major decision driver in the selection of the integration option was simplicity and run time, as well as accuracy, the Runge-Kutta 7(8) method was chosen. The integration package itself was compact and already available on both the Macintosh and IBM PC and little or no modifications would have to be made to the core program to enable it to be used in LIFETIME.

Furthermore, the routine had been extensively tested and utilized in the programs RELMO (RELative MOtion) and SPIN and the high accuracy had been documented. The other two integration options were large, complicated, and expensive to run programs that would have to be adapted from mainframe versions. Their high accuracy has been established, but their effectiveness and compatibility with the LIFETIME algorithm was not certain.

4.2.2 The Runge-Kutta 7(8) Integration Scheme

The Runge-Kutta 7(8) integration scheme was packaged and inserted into LIFETIME for computation of the final part of orbit decay leading to and including re-entry and breakup. The idea was to transfer propagation of the satellite from the LIFETIME averaged equations of motion method to this method near the altitude of vehicle breakup. Thus, the satellite's motion could be numerically integrated during the last phase of orbit decay. The integration package consisted of three subroutines: RK78, RATES, and USEROP.

RK78 contains the actual Runge-Kutta 7(8) method using the Fehlberg Coefficients. The code is referenced from JPL EM 312/85.140 (1985).

The RATES subroutine, developed by D. Oltrogge of The Aerospace Corporation, is used to compute the time rates of change of the satellite's position and velocity states. This routine is called by RK78 to compute the rates needed for the integration process.

USEROP is a subroutine to allow variation in RK78 output and to present opportunities for controlling the integration. It is called by RK78 after each propagation step and was tailored to fit the needs of LIFETIME by D. Oltrogge and the author. This routine was developed to extract time, altitude, latitude, and longitude information from each propagation step to be used in plots at the end of a LIFETIME run. This routine also recorded the vehicle's passage of certain specified altitudes, such as a breakup altitude and crash altitude.

In general, the Runge-Kutta 7(8) integration package was installed as part of LIFETIME 4.0 to "take over" propagation of the satellite while it was still at an altitude greater than the breakup altitude described in Section 4.1. The output was designed to facilitate in expanding the output capabilities of LIFETIME 4.0 to include a groundtrack of the integration propagation and a plot of the altitude decay history.

4.3 LIFETIME 4.0 Integration Algorithm and Breakup Model

The satellite breakup model is adapted from Stern, et. al., as described in Section 4.1. Although a default breakup altitude of 42 nmi (about 78 km) is assumed for LIFETIME 4.0 computations, the user can adjust this number if a material other than aluminum or magnesium is to serve as the satellite's structure. It is desirable to have the numerical integration method take over the satellite's propagation before this breakup altitude is reached. Thus, the user must specify an altitude greater than 42 nmi (for the default case) to enable the program to integrate the satellite's position down to and through the breakup of the vehicle. Furthermore, an end-propagation altitude must be set to indicate the completion of propagation. The simple schematic of this process is illustrated in Figure 4-2.

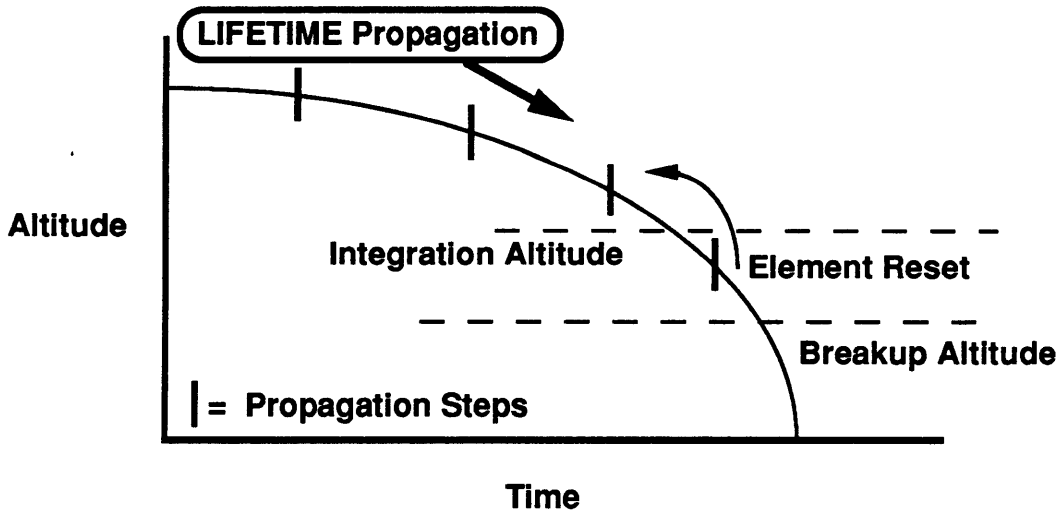

Figure 4-2 : Illustration of Integration and Breakup Model

As the LIFETIME algorithm steps along its propagation in multiples of the orbit period, it will reach a point, as indicated in Figure 4-2, when it completes a revolution and the satellite's altitude is below the integration altitude. At this point, the program essentially "backs up" one propagation step, resetting the orbital elements and the time counter to the previous step's values. Then the Runge-Kutta 7(8) integration routine takes over the propagation, numerically integrating the satellite's position and velocity down through the breakup altitude and to the crash altitude. Conversions from classical mean elements to classical osculating elements to Cartesian elements must occur when the integration routine takes over propagation.

The user-inputted altitude variables for integration, breakup, and vehicle crash are identified in Table 4-1.

Table 4-1 : User-Defined Altitude Variables for LIFETIME 4.0

Variable	Purpose	Default (km)	Remarks
RKALT	Altitude lower limit at which LIFETIME transitions to Cartesian numerical integration	0.000	Must be non-zero to turn integration option on. Most effective if > BRKALT
BRKALT	Altitude of vehicle breakup	77.784	Default value is for aluminum & magnesium structures
ENDALT	Perigee altitude lower limit at which LIFETIME ends propagation	10.000	This variable is invoked even when integration is turned off. When using integration should = 0.00 to model impact.

The subroutine USEROP was developed to allow the modeling of the approximate debris impact region following satellite breakup. At the point when the satellite reaches BRKALT, the latitude and longitude projection of the satellite is recorded. This marks the "debris heel point", or the first point along the groundtrack where debris could fall. Propagation continues until the satellite reaches ENDALT (which is 0.0 km for Earth impact). This latitude and longitude point is identified as the center of mass impact point.

The propagation method then resets the Cartesian elements to those at the BRKALT point, but the ballistic coefficient is changed to 60 $\frac{lb}{ft^2}$ and the propagation to ENDALT is repeated. This in effect computes a "debris toe point", or the point furthest along the groundtrack where satellite debris could fall. The hard-wired increase of the ballistic coefficient accounts for low-drag debris that may survive breakup and impact the Earth. 60 $\frac{lb}{ft^2}$ is in correlation with values identified in data collected by Stern, et al[Ref. 2] This "heel and toe" computation process can be simply illustrated in Figure 4-3.

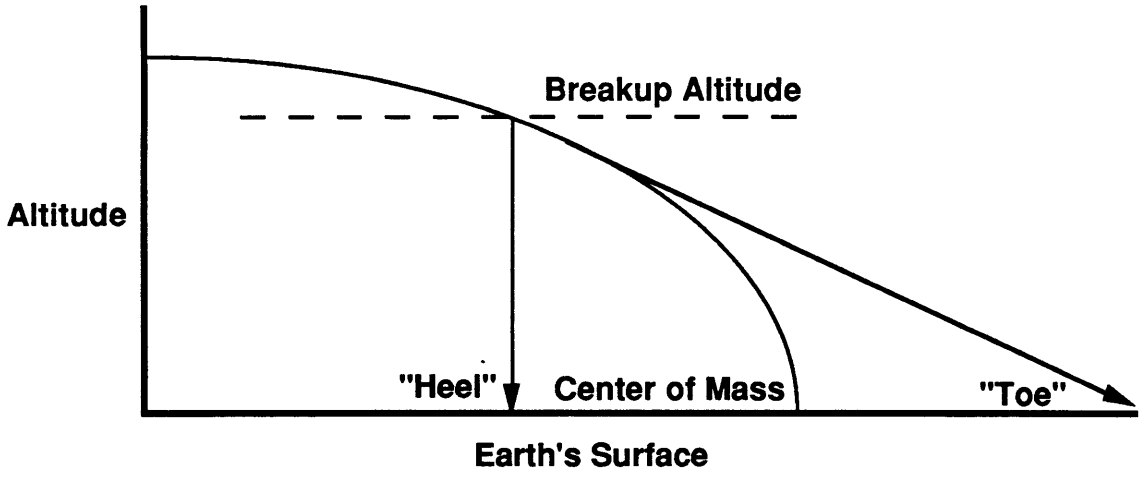

Figure 4-3 : Propagation Following Vehicle Breakup

The overall integration scheme just described can be viewed in a flowchart type format in Figures 4-4 and 4-5. The time, altitude, latitude, and longitude (TALL) data collected after each propagation step in the USEROP routine are used as inputs for the enhanced graphical outputs added to LIFETIME 4.0. These are described in the next section.

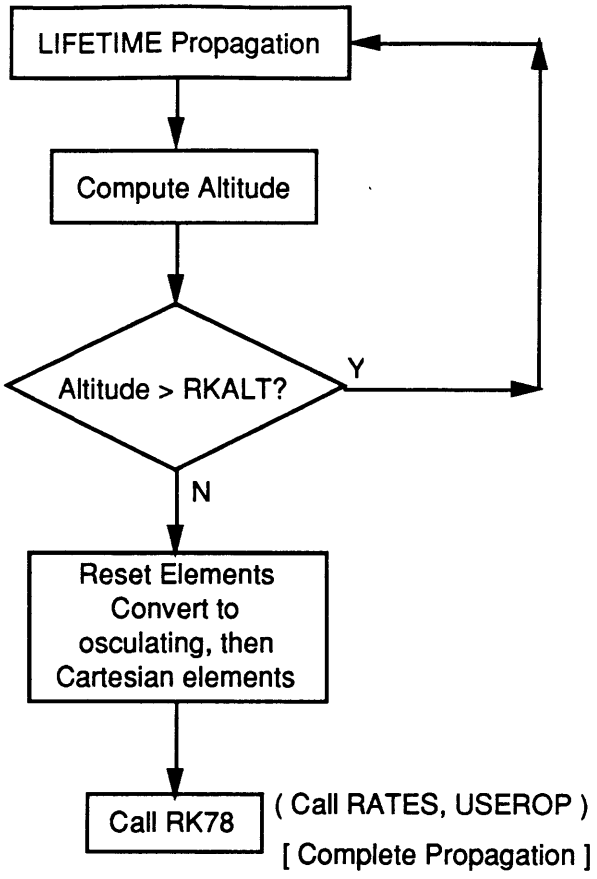

Figure 4-4 : Flowchart for Transition to Integration Scheme

Figure 4-5, on the following page, provides more detailed information on how the USEROP routine collects TALL information and handles the propagation of the satellite and its debris down to impact.

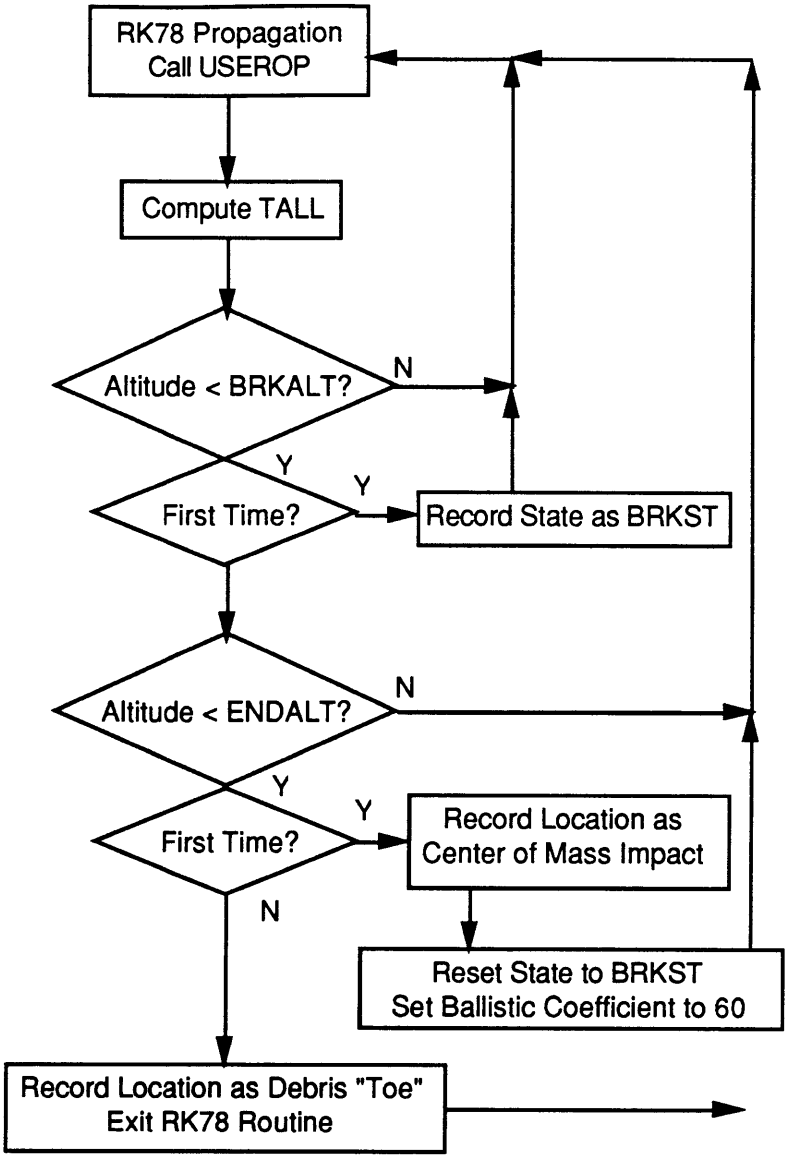

Figure 4-5 : Flowchart for USEROP Routine

4.4 LIFETIME 4.0 Output

The output capabilities of LIFETIME were enhanced to use the information generated by the integration routine to plot the satellite groundtrack and debris impact area on a world map. Additionally, an altitude decay history for the integration propagation was plotted. The "standard" perigee/apogee decay plots from LIFETIME 3.0 are still produced.

The plotting routines were written in C and produce plots for the IBM PC version of LIFETIME 4.0. C. Johnson of The Aerospace Corporation played a major role in implementing the plotting procedures. Plotting options for the Macintosh version of LIFETIME 4.0 are currently being pursued. Examples of the enhanced output capabilities are shown as Figures 4-6 and 4-7.

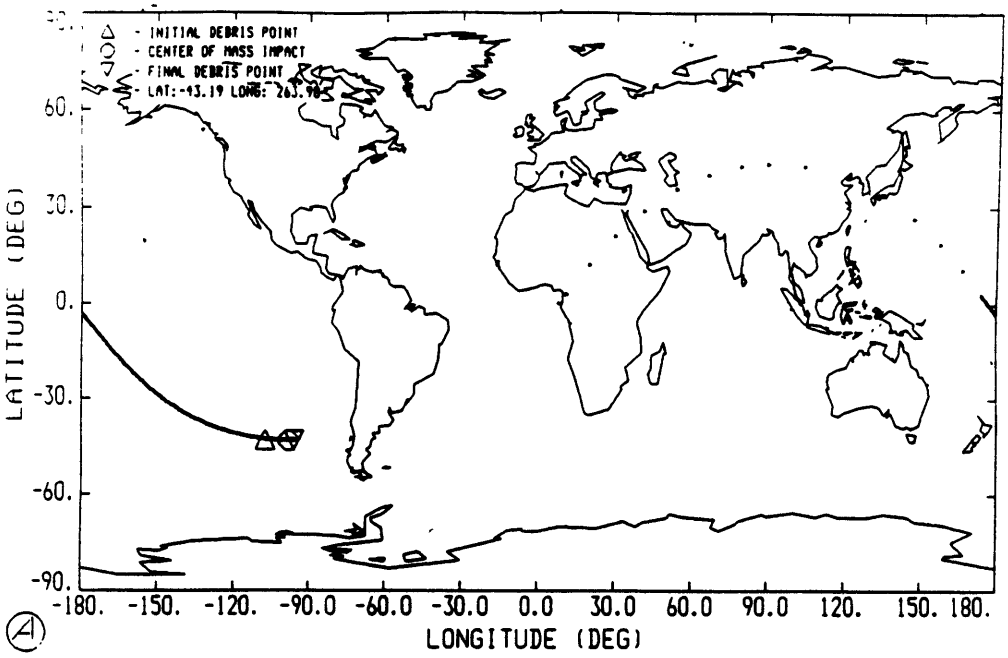

Figure 4-6: Sample Groundtrack and Impact Area Plot

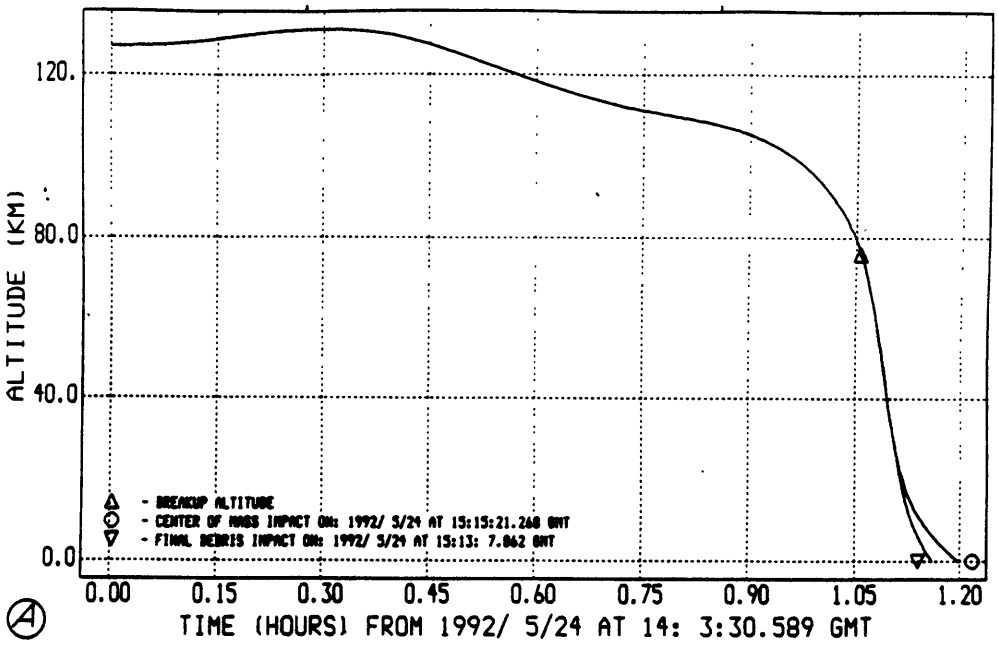

Figure 4-7: Sample Altitude Decay History

4.5 Overview of LIFETIME 4.0

At this stage in the development process, LIFETIME 4.0 can be defined as a completed software tool containing major upgrades in algorithm and output capabilities over its predecessor, LIFETIME 3.0. The author worked with C. Johnson to place LIFETIME 4.0 within a user-friendly shell program driven by menu screens on the IBM PC. This menu-driven version is a concise software package easily deliverable to the customer.

The remainder of this study involves using LIFETIME 4.0 to make actual impact predictions of the satellite cases examined earlier and compare the results to LIFETIME 3.0.

Chapter 5

LIFETIME Prediction Accuracy

This chapter will examine the accuracy of the LIFETIME program in predicting the impact time of a decaying satellite. The improved accuracy from the algorithm upgrades described in Chapter 3 was shown from comparisons of data from LIFETIME 3.0 and LIFETIME 4.0 at the last NORAD data point. Now the remainder of the process will be examined: the accuracy of predicting the actual impact.

5.1 Accuracy Comparison Using the Satellite Cases

The same satellite cases established in Table 2-1 were used in LIFETIME 3.0 and LIFETIME 4.0 for the prediction accuracy comparison. The actual recorded values of F_{10} and a_p presented in Figures 2-7 through 2-10 were used as solar inputs for the predictions. The percent error in prediction is calculated as

$$\% \text{ Error} = \frac{\text{Time Error in Prediction}}{\text{Length of Prediction Span}} \tag{5.1}$$

Recall that the letter with each case, A, B, C, or D, identifies the length of the prediction span.

Since prediction accuracy can be very sensitive to solar conditions and amount of NORAD data, which are unique to each satellite case, the results for each satellite are presented separately within this section and some analysis is offered. The next section will deal with a more general comparison and discussion of the results.

5.1.1 RME

Table 5-1 contains the impact prediction comparisons for the RME satellite cases. The actual impact was 24 May 15:31 GMT.

Table 5-1 : Impact Prediction Comparison for RME Cases

Satellite Case	Impact Prediction LIFETIME Version:		Percent Error LIFETIME Version:	
	3.0	4.0	3.0	4.0
RME - A	23 May 17:45	23 May 14:18	9.1	10.5
RME - B	24 May 12:30	24 May 12:26	2.5	2.4
RME - C	24 May 12:43	24 May 15:02	1.1	0.7
RME - D	---	24 May 15:13	---	1.1

Two things are immediately evident from Table 5-1. The first is that the order of magnitude improvement in period calculation for LIFETIME 4.0 observed in Chapter 3 is not obvious from the percent error values in the table. There is little or no difference between program versions, except for case D. That case showed no ballistic coefficient convergence for LIFETIME 3.0, yet it converged and resulted in a very good prediction for LIFETIME 4.0.

The second item of interest from Table 5-1 is the relationship between the prediction time and the percent error columns, especially for cases C and D. Even though the prediction accuracy improves in going from case C to case D, the percent error value indicates a slight loss of accuracy. This is because of the method used to compute percent error, which places "prediction span" in the denominator. Thus, as the last NORAD data point becomes closer in time to the actual impact, the "percent error" measure of accuracy seems to lose some of its meaning.

5.1.2 LOSAT-X

Table 5-2 contains the impact prediction comparisons for the LOSAT-X satellite cases. The actual impact was 15 Nov 16:06 GMT.

Table 5-2 : Impact Prediction Comparison for LOSAT-X Cases

Satellite Case	Impact Prediction LIFETIME Version:		Percent Error LIFETIME Version:	
	3.0	4.0	3.0	4.0
LOSAT-X - A	18 Nov 00:59	18 Nov 02:33	23	24
LOSAT-X - B	16 Nov 08:41	16 Nov 09:53	13	14
LOSAT-X - C	16 Nov 04:05	16 Nov 04:14	16	16
LOSAT-X - D	15 Nov 22:14	15 Nov 22:30	25	25

For this satellite the results for LIFETIME 3.0 and LIFETIME 4.0 are nearly identical. The generally high amount of error for this satellite can be attributed to the large range of solar activity during the prediction, the limited number of days of NORAD data available, and the fact that the satellite was tumbling during the re-entry process.

5.1.3 NORAD-1

Table 5-3 contains the impact prediction comparisons for the NORAD-1 satellite cases. The actual impact was 10 Jan 12:50 GMT.

Table 5-3 : Impact Prediction Comparison for NORAD-1 Cases

Satellite Case	Impact Prediction LIFETIME Version:		Percent Error LIFETIME Version:	
	3.0	4.0	3.0	4.0
NORAD-1 - A	11 Jan 01:14	8 Jan 14:40	5	19
NORAD-1 - B	9 Jan 20:55	10 Jan 10:50	13	2
NORAD-1 - C	10 Jan 10:38	10 Jan 14:26	3	2
NORAD-1 - D	10 Jan 10:16	10 Jan 13:02	11	1

Except for case A, the results for NORAD-1 indicate a substantial improvement in accuracy of LIFETIME 4.0 over LIFETIME 3.0. Fairly smooth solar activity and large number of NORAD data points for differential correction contributed to the overall lower percent error values for these cases.

5.1.4 NORAD-2

Table 5-4 contains the impact prediction comparisons for the NORAD-2 satellite cases. The actual impact was 14 Dec 01:57 GMT.

Table 5-4 : Impact Prediction Comparison for NORAD-2 Cases

Satellite Case	Impact Prediction LIFETIME Version:		Percent Error LIFETIME Version:	
	3.0	4.0	3.0	4.0
NORAD-2 - A	14 Dec 00:53	14 Dec 00:56	0.5	0.4
NORAD-2 - B	13 Dec 11:07	13 Dec 12:16	12.4	11.4
NORAD-2 - C	13 Dec 11:17	13 Dec 13:19	20.4	17.5
NORAD-2 - D	13 Dec 20:21	13 Dec 20:05	23	24

Again, the results are nearly identical for LIFETIME 3.0 and LIFETIME 4.0. However, there is a slight tendency of lower percent errors for LIFETIME 4.0. An increase in solar activity near the end of the prediction span attributed to the increase in error. Of separate note are the case D results, where the prediction for both versions is the closest to the actual, yet the percent error is the greatest.

5.2 Discussion of Comparison Results

While the "percent error" measurement breaks down as a statistical measure of specific accuracy for cases of short prediction span, it does serve well as an indicator of relative accuracy. The data for actual error in impact time

prediction is contained in the percent error value. In addition, it is the percent error measurement that allows comparison with other industry standards, such as the error requirements of USSPACECOM and the assumed error of atmosphere models.

Therefore, in order to look at the entire set of satellite case studies graphically, the percent errors from the previous section have been plotted in Figure 5-1.

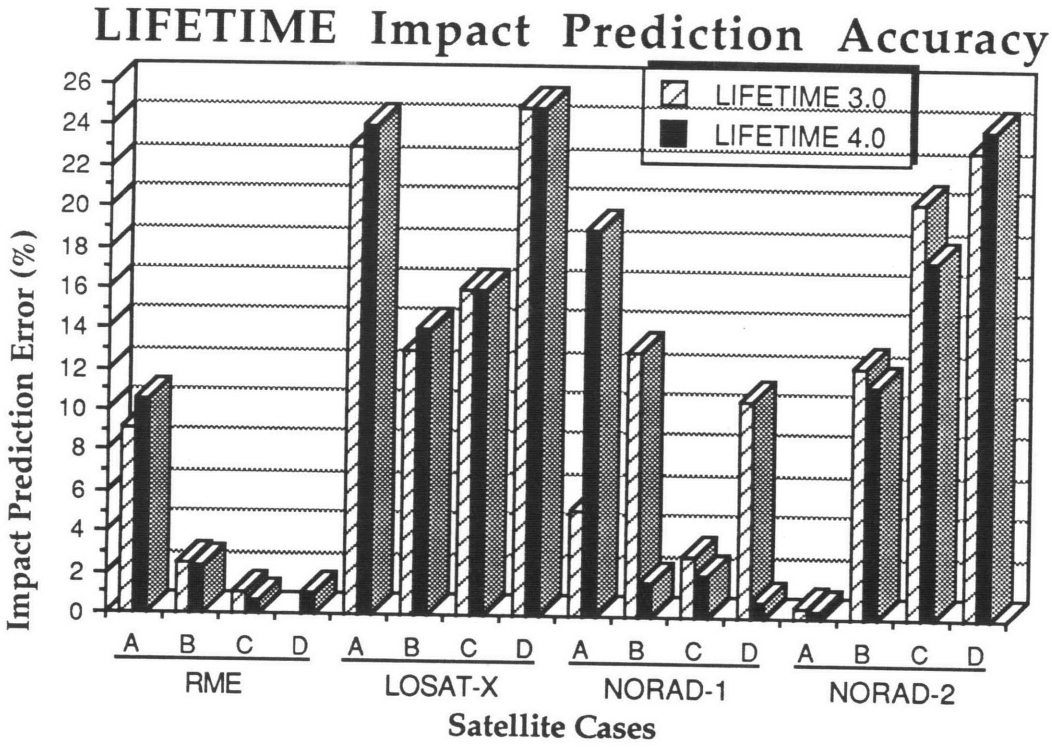

Figure 5-1 : Satellite Case Study Comparison of Impact Prediction Accuracy

Generally, the LIFETIME versions performed comparably. A specific exception would be the RME - D case, where there was no convergence for LIFETIME 3.0. The B, C, and D cases for NORAD-1 exhibit the most improvement for LIFETIME 4.0 over LIFETIME 3.0. It may help in the interpretation to present the comparison as in Table 5-5, where the versions are compared for relative percent error.

Table 5-5 : Relative Percent Error Comparison

Cases	No. Times 4.0 > 3.0	Sum When 4.0 > 3.0 (%)	No. Times 4.0 < 3.0	Sum When 4.0 < 3.0 (%)	No. Times 4.0 = 3.0
16	5	18.4	9	26.4	2

Table 5-5 shows that for a majority of the satellite cases the percent prediction error for LIFETIME 4.0 was less than LIFETIME 3.0. Furthermore, the sum of the percentage differences for the versions was almost twice as great when LIFETIME 4.0 had a lower percent error.

5.3 Conclusions

The results from the impact prediction accuracy comparisons of LIFETIME 3.0 and LIFETIME 4.0 do not definitively proclaim LIFETIME 4.0 as a major improvement over LIFETIME 3.0. However, the results as seen in Figure 5-1 and Table 5-5 indicate some notable improvement in accuracy for the new version of the program.

Furthermore, the algorithm improvements in LIFETIME 4.0 over LIFETIME 3.0 add a significant amount of confidence in the period calculations. Additionally, the addition of the Runge-Kutta integration routine to LIFETIME 4.0 for final impact propagation eliminates the uncertainty in impact prediction associated with LIFETIME 3.0. For instances where both versions would have similar predictions the LIFETIME 4.0 version could be said to have less uncertainty in its prediction.

The completion of this comparison establishes LIFETIME 4.0 as the new version of the program LIFETIME. In addition to the algorithm improvements and favorable comparison to the existing version, LIFETIME 4.0 includes enhanced output capabilities that increase its usefulness as an orbit decay and impact prediction tool. These capabilities are the integration groundtrack with debris impact area plot and the altitude decay history plot.

Chapter 6

Sensitivity Studies and Analysis

This chapter attempts to deal with some of the factors that contribute to the accuracy of orbital lifetime predictions. Comparisons between the two versions of LIFETIME will not be made. Rather, additional factors affecting accuracy will be discussed: (1) the amount and quality of NORAD data; (2) the length of prediction span from last NORAD point to impact; (3) solar conditions during the differential correction process; and (4) estimates in F_{10} values during the prediction period. These will each be discussed in turn and the LIFETIME 4.0 results from the previous case studies will be used for analysis.

6.1 Effects of NORAD Data Span on Program Accuracy

Since the NORAD data span is used during the differential correction process for the iterations to converge to a ballistic coefficient for the satellite, the amount and quality of the data should have an effect on prediction accuracy. The satellite cases previously introduced are used for this analysis and their NORAD data spans are reproduced below in Table 6-1.

Table 6-1 : NORAD Data Spans for Satellite Cases

Satellite Case	NORAD Data Span (days)	Satellite Case	NORAD Data Span (days)
RME - (All)	18	NORAD-1 (All)	20
LOSAT-X - A	7	NORAD-2 - A	8
LOSAT-X - B	12	NORAD-2 - B	13
LOSAT-X - C	14	NORAD-2 - C	15
LOSAT-X - D	17	NORAD-2 - D	18

Enough NORAD data was attainable for the RME and NORAD-1 satellites to make the data spans for each letter-designated case the same (as the letters progress, the span of data moves closer to the impact time). The LOSAT-X and NORAD-2 satellite's had limited NORAD data that had to be partitioned in order to form the cases of different prediction span.

For clear analysis, it is necessary to use categories of data span length. These are shown in Table 6-2.

Table 6-2 : Data Span Categories for Sensitivity Analysis

NORAD Data Span (days)	Category Designator
5 - 10	I
10 - 15	II
15 - 20	III

6.1.1 Period Calculation Accuracy

One observable effect of variations in NORAD data span is the accuracy in the period calculations of the LIFETIME program. The data for this analysis comes from the time error results recorded in Chapter 3. These are the time errors computed as the difference between calculated and observed times of the last NORAD data point, at the end of the differential correction process.

The time errors for all the cases, grouped by NORAD data span, are presented in Figure 6-1.

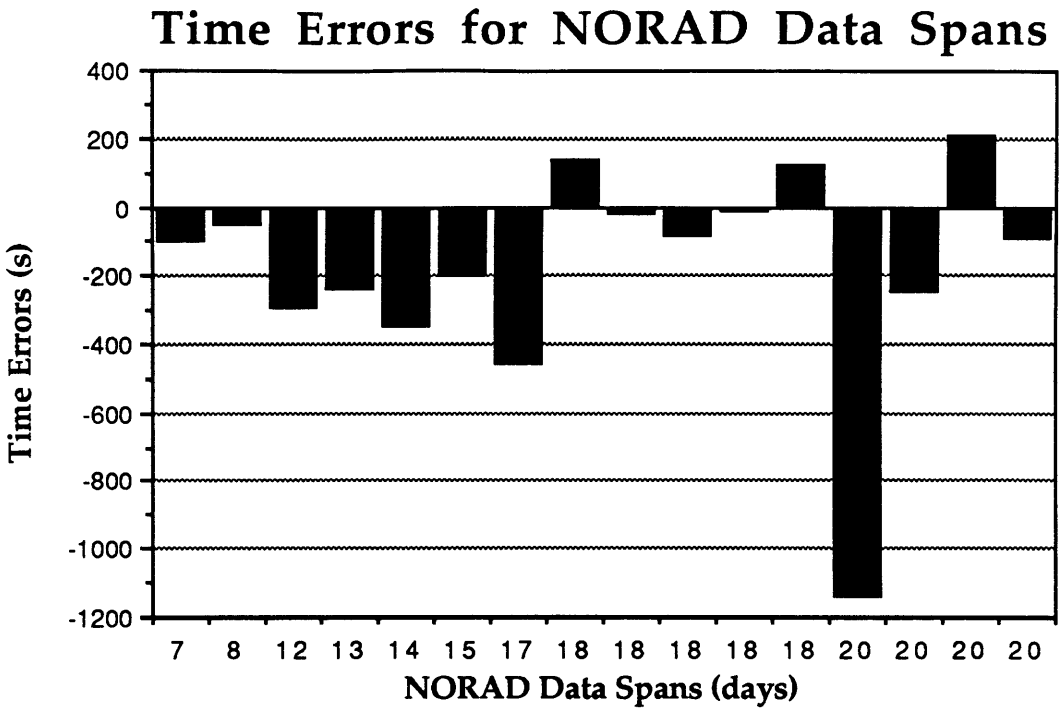

Figure 6-1 : Time Errors Grouped by NORAD Data Span

A clearer picture can be presented when the 18 and 20 day data spans are averaged, in Figure 6-2.

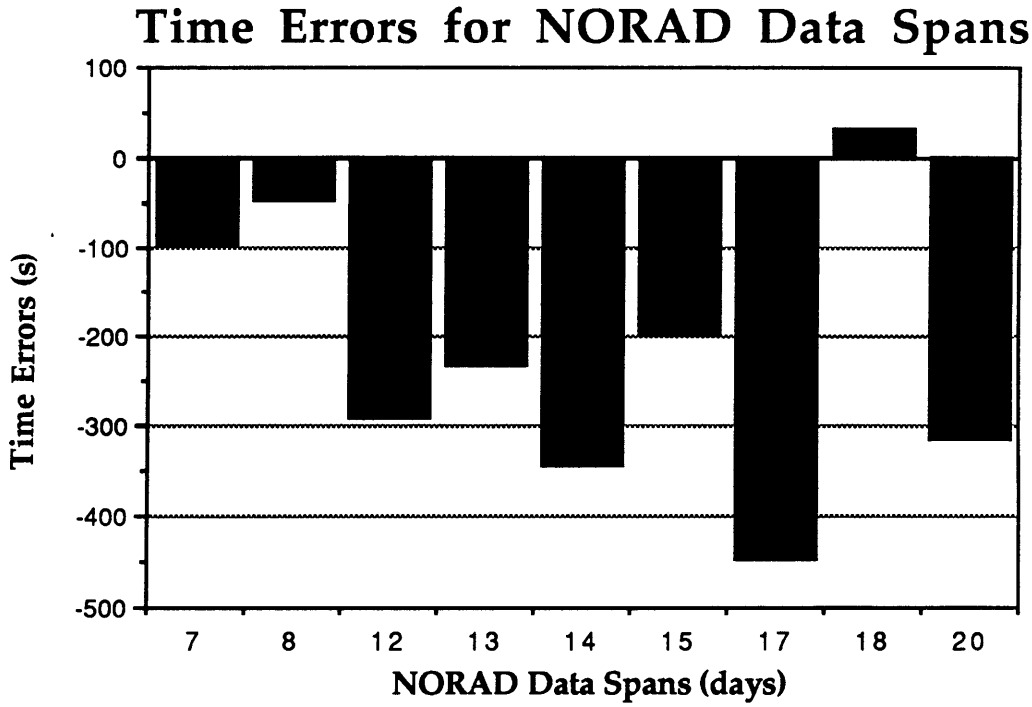

Figure 6-2 : Time Errors (Some Averaged Values)

Figure 6-2 does not establish a definite trend for time errors based on data span. However, there is a general trend for increased errors with longer data span. This intuitively makes sense, as more data points means more differences to minimize through the least squares differential correction process. A general increase in time errors should be expected. The 18-day span of data, with a surprisingly low time error, is from the RME satellite. This could be due to smooth solar activity and high-quality NORAD data (i.e., most or all data recorded very close to ascending node). The averaged time errors for each data span category are presented in Table 6-3.

Table 6-3 : Average Time Errors for Different NORAD Data Spans

Data Span Category	Average Time Error (s)
I	- 72
II	- 266
III	- 137

A Category I data span seems to offer significantly lower time errors. It should be noted that the shorter the data span, the less time there is for errors of each period calculation to accumulate. Additionally, the Category II spans come from the LOSAT-X and NORAD-2 satellites, exclusively. These satellites experienced the greatest amount of solar activity of all the cases; and these results may indicate the role solar activity on accuracy which will be explored in later section.

6.1.2 Impact Prediction Accuracy

An analysis of the effects of data span on overall prediction accuracy should give more insight into the true accuracy sensitivity. Since the percent error measurement is better suited for relevant error comparison, this analysis will use the magnitudes of the actual time errors in impact prediction that were

produced by the results of Chapter 5. These errors, categorized by NORAD data spans, are presented in Figure 6-3.

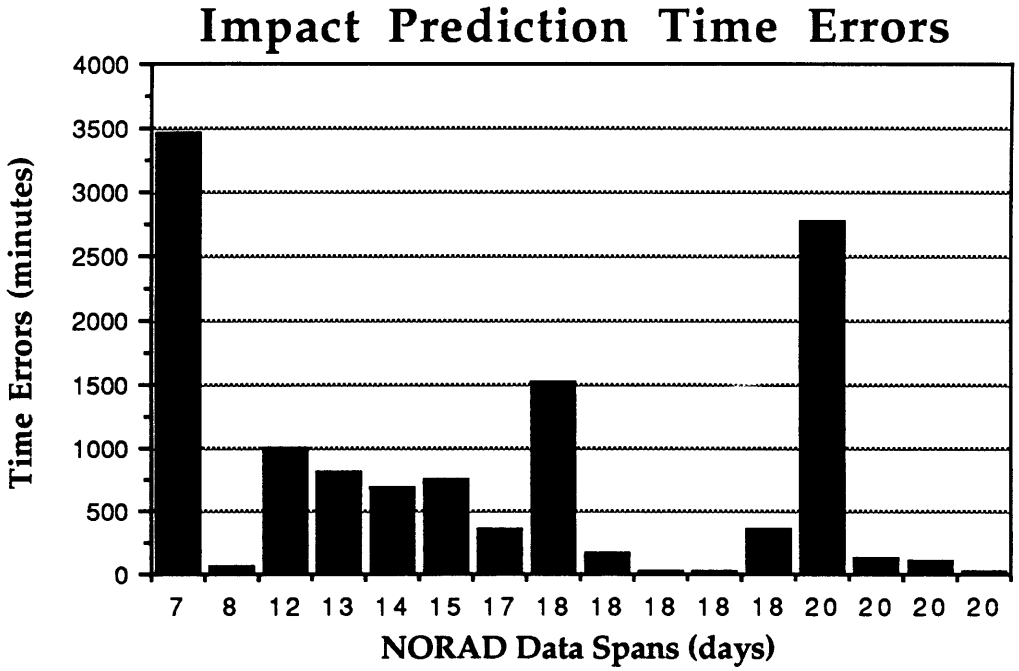

Figure 6-3 : Time Errors in Impact Predictions, by NORAD Data Spans

Averaging the values for repeated data spans produces Figure 6-4.

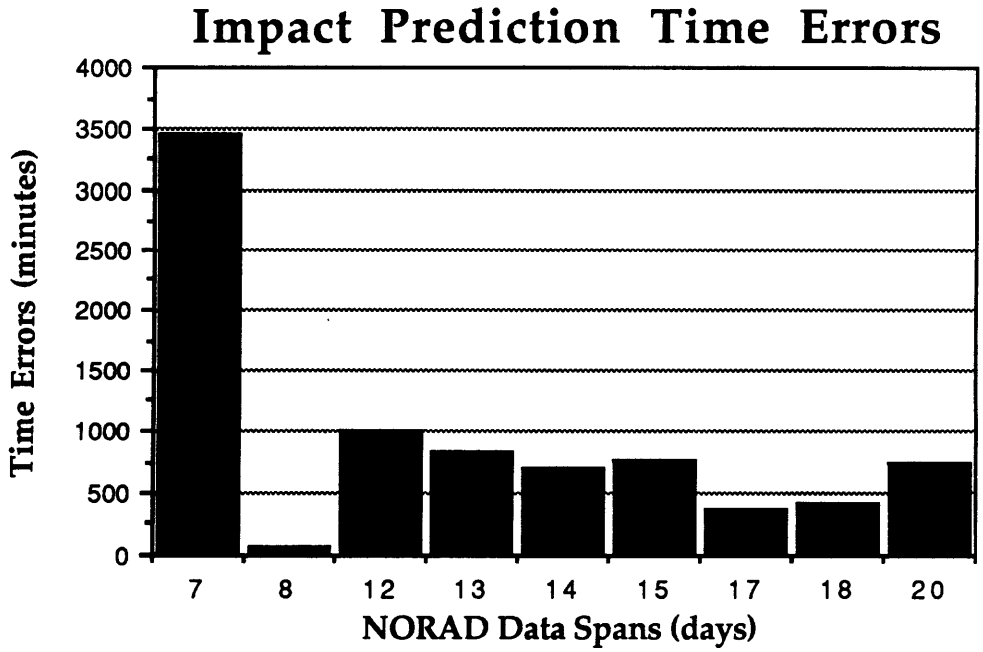

Figure 6-4 : Time Errors in Impact Predictions (Some Averaged Values)

Figure 6-4 indicates a slight tendency for longer data spans to yield more accurate impact predictions. The eight day span seems to be an exception to the pattern (its value represents only a single case). However, the trend is not well defined for this data set, and it is obvious that there are other effects that can play a part in the accuracy.

Table 6-4 contains the impact time errors by data span category.

Table 6-4 : Average Impact Time Errors for Different NORAD Data Spans

Data Span Category	Average Time Error (min.)
I	1759
II	819
III	544

Table 6-4 indicates a general trend of less impact prediction error as the data span increases. Considering only the effects of data span on impact accuracy, this trend seems intuitive. More data should yield a more accurate decay curve fit during differential corrections, and thus a more accurate impact prediction. Unfortunately, as this research is showing, it's not quite that simple for all cases.

6.2 Effects of Prediction Span on Program Accuracy

Thus far the sensitivity analysis has focused on NORAD data span. It is also necessary to consider the length of time following the last NORAD data point up to the impact time (the prediction span). The length of prediction span for each satellite case was designated by the letter (A, B, C, or D) in Table 2-2, reproduced below as Table 6-5.

Table 6-5 : Prediction Spans for the Satellite Cases

Case Letter	Prediction Span (days)
A	10
B	5
C	3
D	≤ 1

The impact time errors for all the satellite cases in terms of prediction span are presented in Figure 6-5.

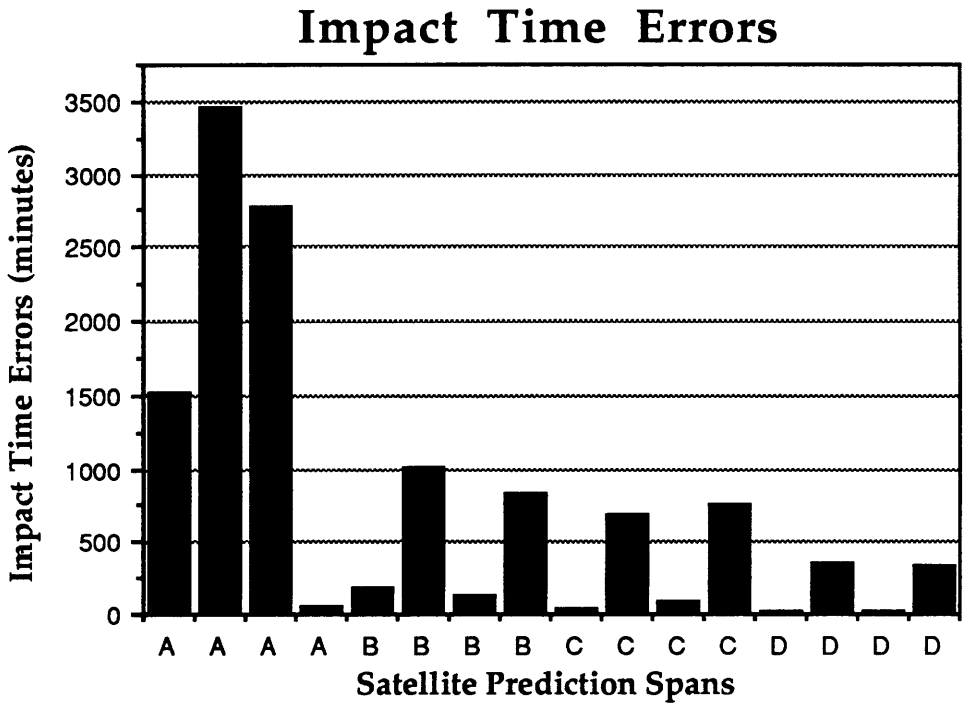

Figure 6-5 : Impact Time Errors for Different Prediction Spans

A trend is almost readily apparent, and even more clear when averaged values for each prediction span are plotted in Figure 6-6.

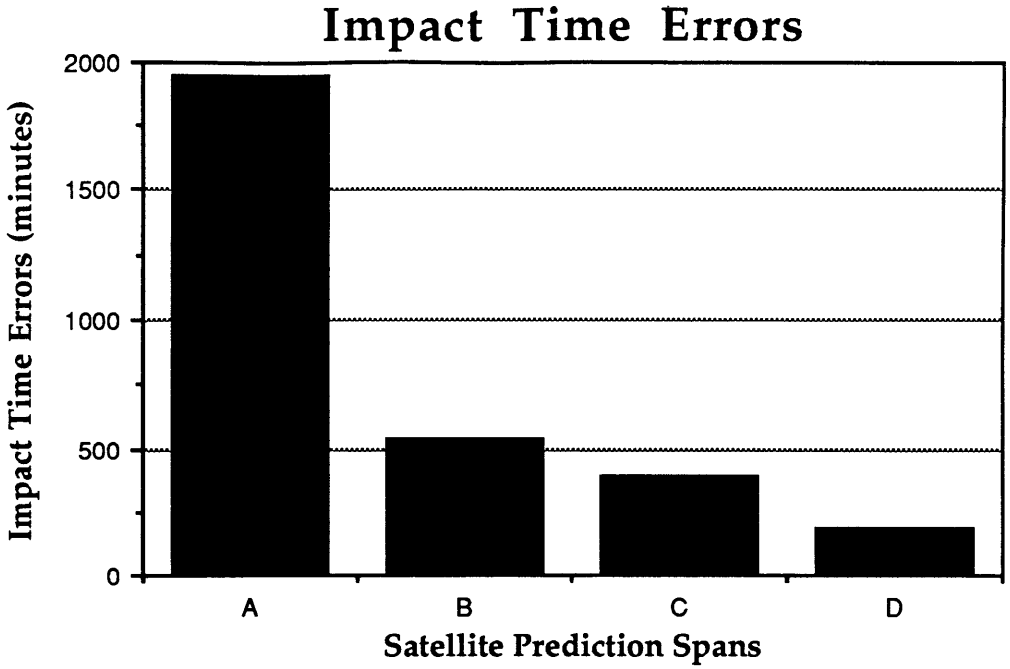

Figure 6-6 : Impact Time Errors (Averaged Values for Prediction Spans)

Figure 6-6 clearly shows the effect of prediction span on impact prediction accuracy, for the tested satellite cases. Since the prediction span is not the only variable at work here, this trend cannot be viewed as universal for all instances. A very short data span with a short prediction span, for instance, will probably not result in a great amount of accuracy. The shortest data span for a "D" case was 17 days (the longest overall was 20). However, this does indicate a general trend for increased accuracy with shorter prediction spans.

6.3 Effects of Solar Conditions During Differential Corrections

The sensitivity of prediction accuracy to solar activity has been mentioned as a major source of error many times in this report. There are two main regions of program operation where the solar data inputs take effect: the differential correction process and the prediction process after differential corrections.

Since LIFETIME uses the solar inputs (F_{10} and a_p), among other values, to determine the atmosphere density during each step of propagation (and differential correction) the most accurate mode of operation would be to use

the actual recorded solar data for all days covered by the NORAD data. This is what was done in this study. This is a practical mode of operation since the solar data is readily available. In this manner, the program computes orbit decay and differential correction with information based on the true atmospheric conditions at the time of the recorded NORAD data.

The ballistic coefficient that the program iterates to through the differential correction process thus represents the inputted solar conditions and their variations during the data span. If the solar activity after the data span follows a similar trend that existed within the data span, the ballistic coefficient computed should subsequently provide an accurate lifetime prediction as the satellite is propagated through the prediction span to impact. It is when the solar activity during the prediction span differs from the previous trend that inaccuracies can accumulate quickly. This has already been demonstrated in some previous studies.[Ref. 7]

In short, the solar activity during the differential correction process is absorbed in and characterized by the converged value of the ballistic coefficient that results from the process (when actual recorded solar data is used as input). It is the deviations from this established trend of solar data that can lead to errors in impact prediction. This area of sensitivity is treated in the next section.

6.4 Solar Flux Sensitivity Study

This section deals with the issue of solar data inputs during the prediction span. The first order effect is the measured F_{10} value, so that is the parameter of interest.

The main purpose behind the accuracy improvements and testing discussed so far in this report is to evolve LIFETIME into a highly effective orbital lifetime and impact prediction program. The mode of operation to yield the best results includes using the actual recorded values of solar flux for the differential correction process, and then making the best estimate of future solar conditions for the prediction span. A series of simple sensitivity tests

were designed to note the fluctuations in impact prediction accuracy based on differences in the F_{10} values used for the prediction. The results should give some insight in the accuracy sensitivity to predicted solar flux ranges.

6.4.1 Test Methodology

The sensitivity tests revisited the satellite cases already introduced. Only the A, B, and C cases were considered for this part of the study, since the prediction span for the D cases was too short to provide any clear sensitivity results. The uniqueness of the solar data for each satellite requires that each one be examined separately for the effects of the solar flux during the prediction span.

In trying to predict the solar flux activity following the last day of NORAD data, it may seem that estimating a constant-slope F_{10} following the previous trend should approximate the solar activity, at least for short term predictions. The danger in this is that if the actual solar activity is in a constant, opposite slope than the estimate, the resulting error in the F_{10} estimate could be twice as large than if simply a constant value is assumed. In fact, most previous studies in this area have relied on using constant F_{10} values. The fact that F_{10} activity is highly unpredictable and subject to rapid change in either direction supports the idea that it is better to err on the conservative side and assume some constant solar flux value.

Thus, a five-case test plan was developed to examine the effects of using five different constant F_{10} values during the prediction span for each satellite case. The testing steps were as follows:

(1) Use the actual solar data for the differential correction process
(2) Use the a_p value of the last day of data as a constant input for the prediction span (a_p has a second-order effect)
(3) The F_{10} value of the last day of data then becomes the adjustable parameter
(4) This constant F_{10} value is used for impact prediction and the results are compared to the actual impact time

(5) The constant F_{10} value is varied as +10%, -10%, +20%, and -20% of itself and each case is propagated to impact

The results could relay some insight in two areas: (1) the variation of impact prediction accuracy with errors in predicting the F_{10} values (since the actual values and impact accuracy are already known); and (2) the general impact prediction error ranges associated with percent ranges of change in F_{10} values.

To illustrate the test case structure described above, a sample case using the RME - A case will be shown here. Figure 6-7 illustrates the five solar flux inputs to this study and their relationship to the actual solar data. The RME - A case used 18 days of NORAD data with a prediction span of 10 days.

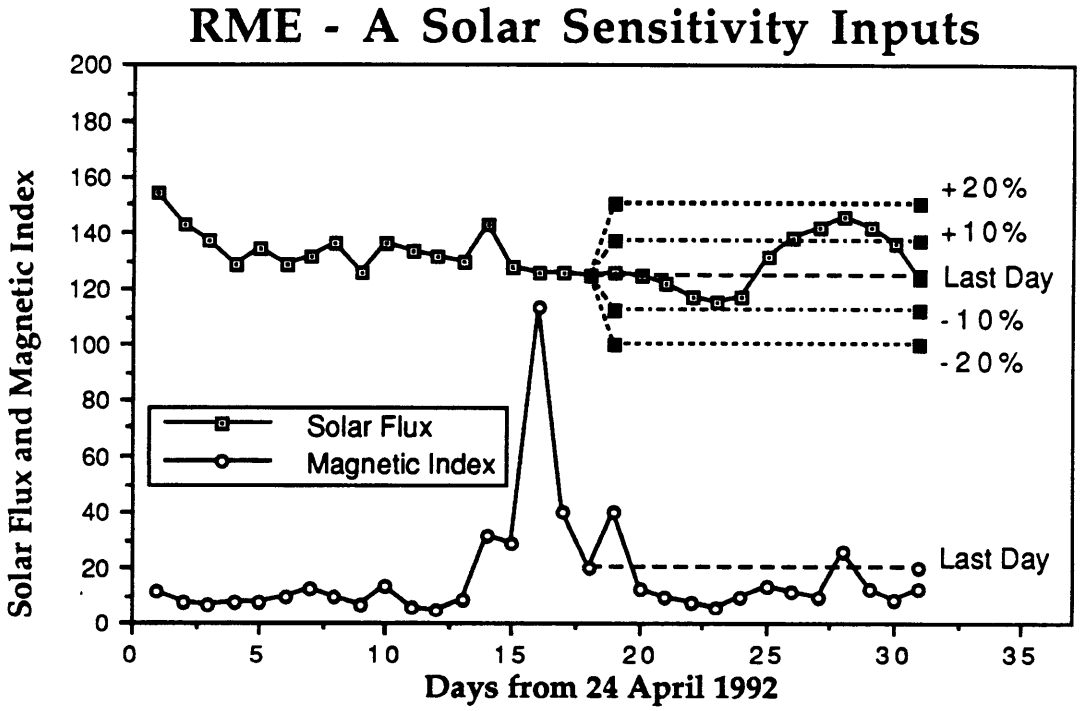

Figure 6-7 : Solar Data Inputs Used for RME - A Sensitivity Study

6.4.2 Test Results and Analysis

The results for each satellite will be presented and discussed in turn. A general analysis considering the entire range of satellite cases will follow. Within each satellite prediction span case, the actual time error of impact prediction will be used as a comparison value. A positive time error indicates

that the predicted impact time was greater than the actual (i.e., the satellite was calculated by LIFETIME to crash at a later time than it actually did).

Figure 6-8 shows the results for the RME satellite. The "0" F_{10} category represents the value for the last day of NORAD data held constant with no percent change.

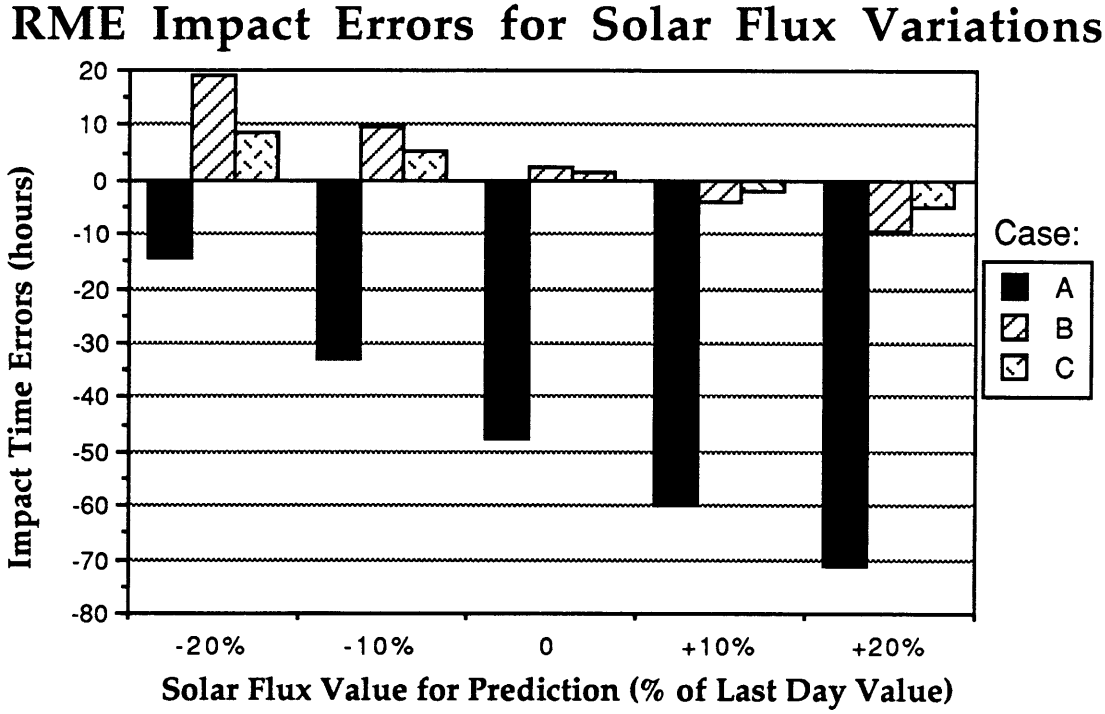

Figure 6-8 : RME F_{10} Sensitivity Results

The A cases show a markedly different pattern of results than cases B and C. For the original impact prediction with actual solar values (Table 5-1 and Figure 6-5) the A case had a significant time error compared to the B and C cases. For this sensitivity study, the A case showed an error minimum for the -20% solar value while cases B and C behaved similarly with a minimum error at the constant last day of data value. Examining the true solar data of Figure 6-9, below, provides some insight. The A span begins right before the sudden upward then downward solar flux fluctuations, while the other cases begin at a point where the constant last day value approximates the average of the remaining data fairly well. The data fluctuations could be the source of the results seen in Figure 6-8. Also evident in Figure 6-8 is that the longer prediction spans resulted in larger time errors for all flux estimates. This makes some sense, since a shorter prediction span means less time for the

accumulation of errors. Also, the greatest error ranges occurred for the longest prediction span cases.

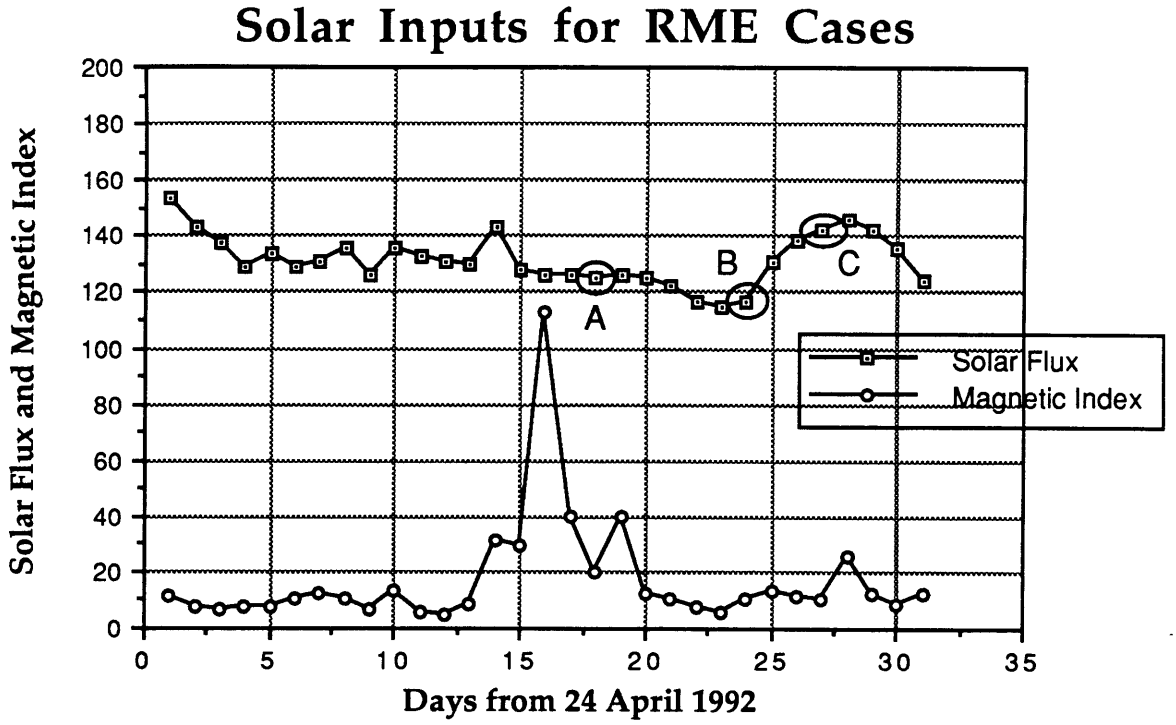

Figure 6-9 : RME Solar Inputs with Prediction Spans Noted

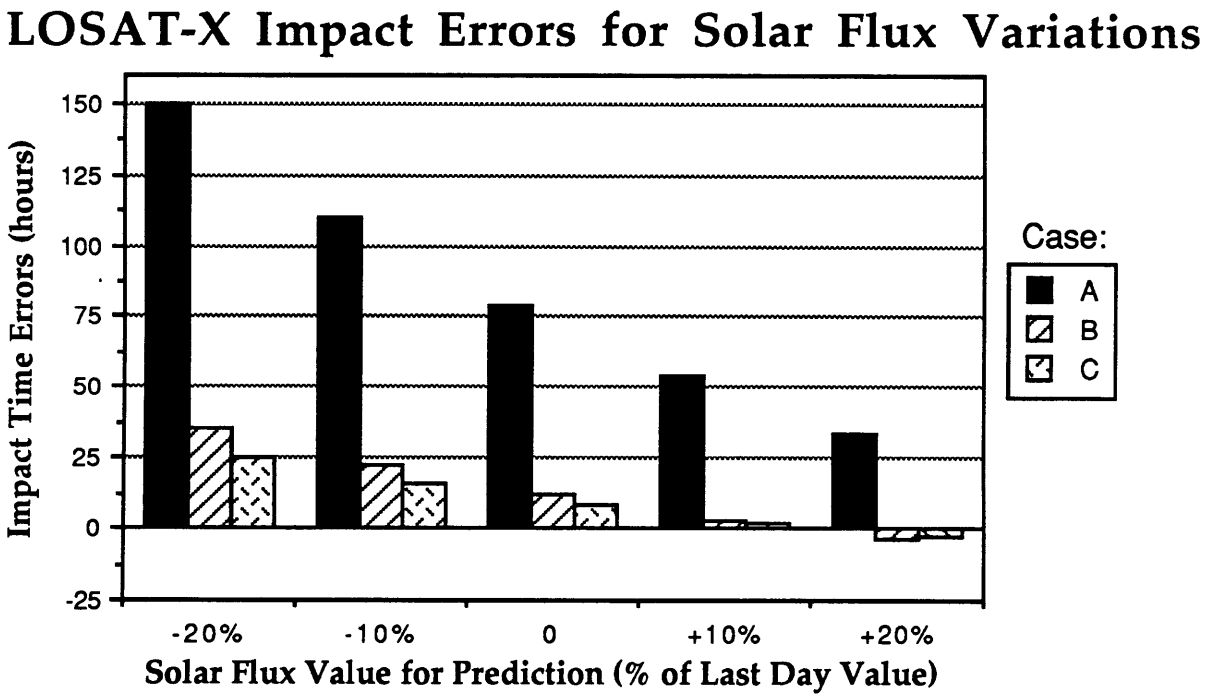

Figure 6-10 : LOSAT-X F_{10} Sensitivity Results

Figure 6-10 (previous page) shows the results for the LOSAT-X satellite. These results exhibit a general trend similar to the RME cases, with greater errors for the longer prediction spans. However, here the A cases have a minimum at the +20% flux value while the B and C cases show a minimum error at the +10% value (although the error is small for the unchanged last day of data value as well). Examining the true solar data in Figure 6-11 provides some clarity.

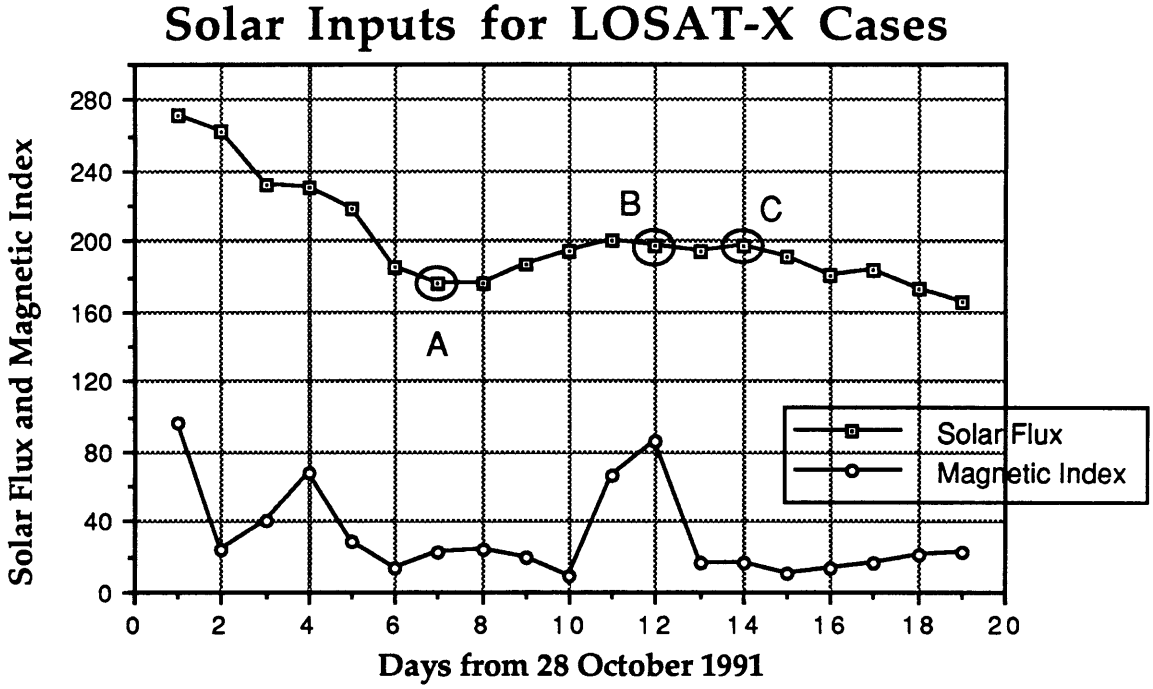

Figure 6-11 : LOSAT-X Solar Inputs with Prediction Spans Noted

For the A cases, a -20% or -10% flux value would yield a prediction much lower than the actual values, thus causing an erroneously long lifetime prediction for the satellite (Figure 6-10 supports this). A positive percentage of the flux of the last day of data should yield a more accurate impact prediction. Likewise, the B and C cases should have had their least error for a slightly negative percentage flux value. However, although the error was small for no percent change of the last day's flux value the minimum was for the +10% value.

It should be noted that the error ranges caused by the F10 sensitivity for the B and C cases are not large, while the range for the A case is quite big (about 125 hours of error).

Figure 6-12 shows the results for the NORAD-1 satellite cases.

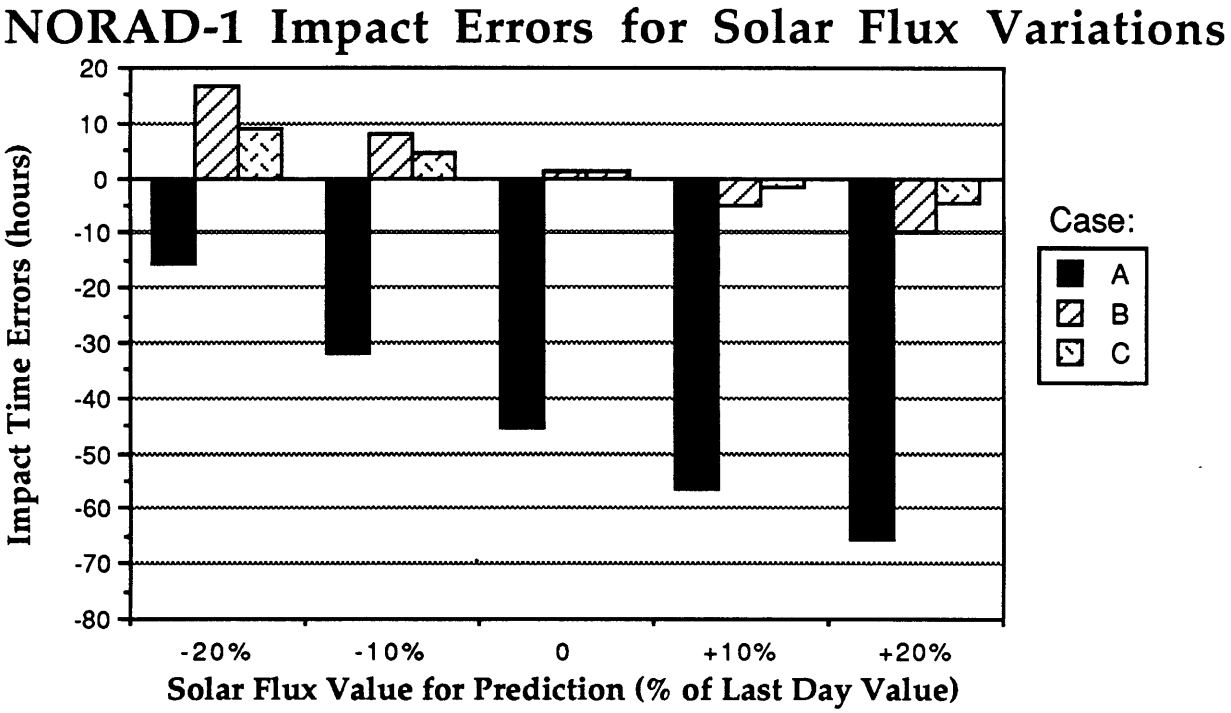

Figure 6-12 : NORAD-1 F_{10} Sensitivity Results

These results are extremely similar to those of the RME cases in Figure 6-8. Remarkably so, actually. Both satellites had similar NORAD data spans (18 and 20 days) and similar solar data profiles (see Figure 6-13). The same trends are evident, with the A cases having a minimum error for the -20% flux values with the B and C cases having a minimum error for the unchanged flux value of the last day of data.

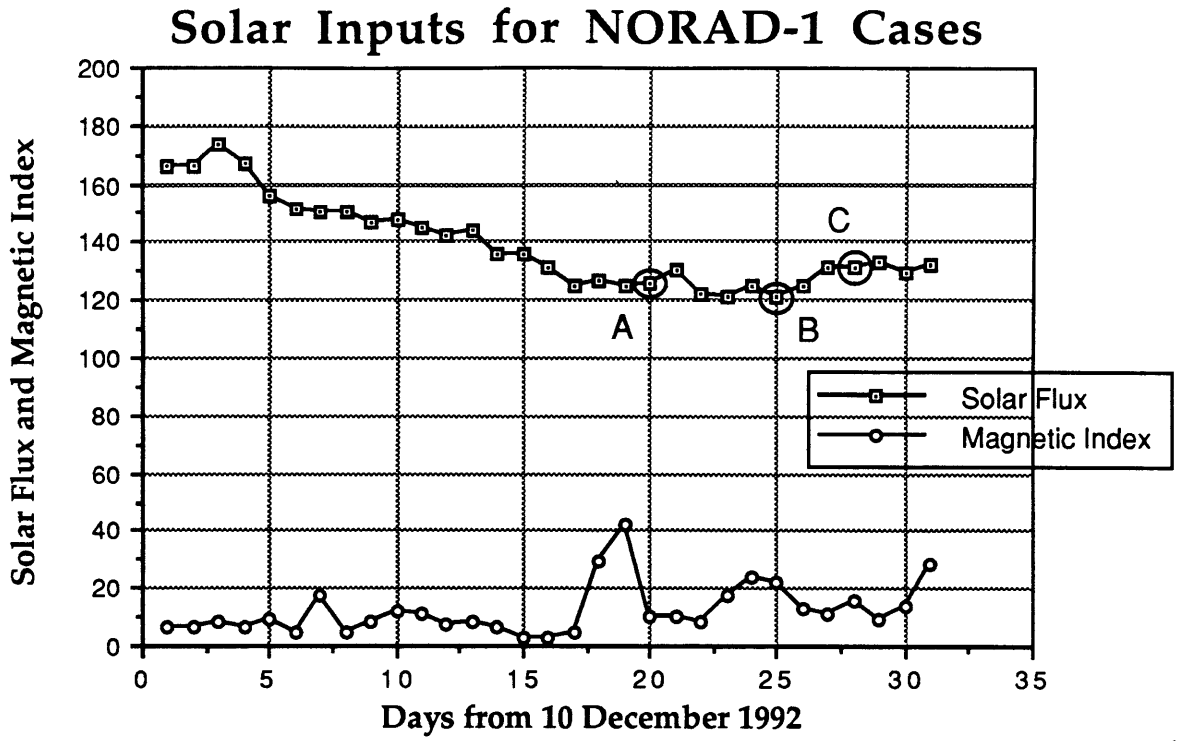

Figure 6-13 : NORAD-1 Solar Inputs with Prediction Spans Noted

Figure 6-14 shows the results for the NORAD-2 satellite cases.

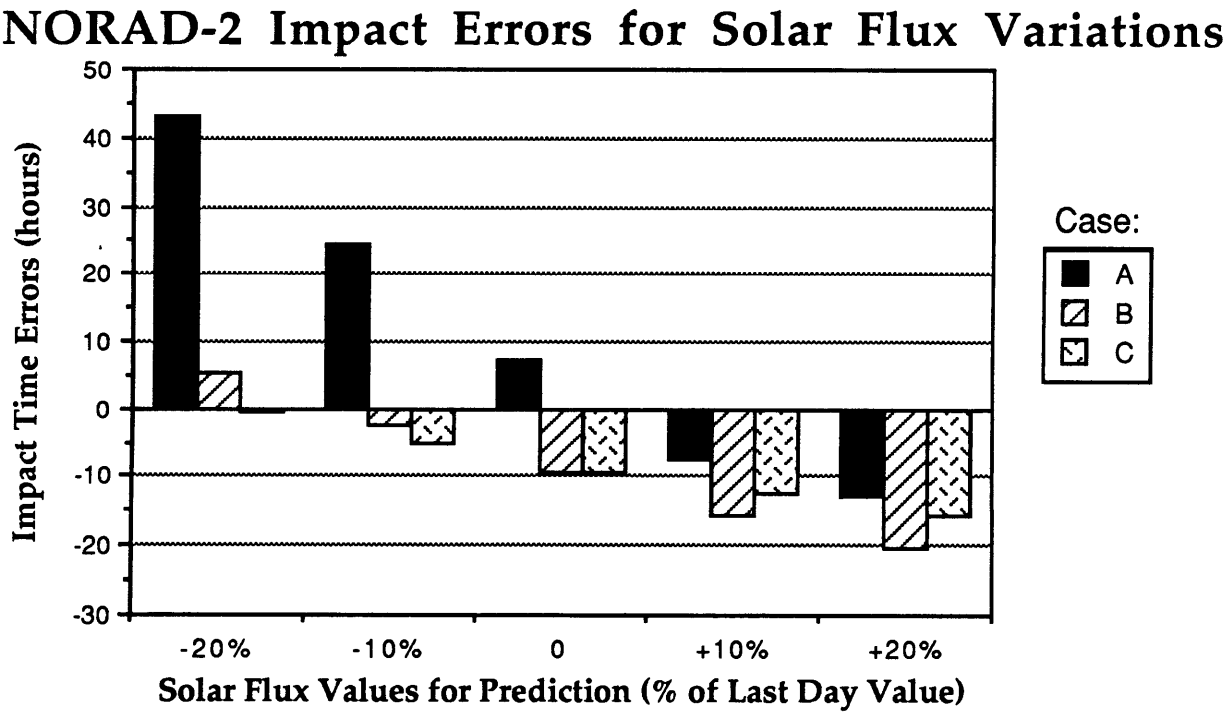

Figure 6-14 : NORAD-2 F_{10} Sensitivity Results

The general trend of less error for shorter prediction span is continued for these cases. Additionally, this plot is the first instance when the A cases have a minimum error for the unchanged flux value (with a similar opposite error for +10%). The minimum errors for the B and C cases come at -10% and -20%, respectively. The solar data with the prediction spans noted is presented in Figure 6-15.

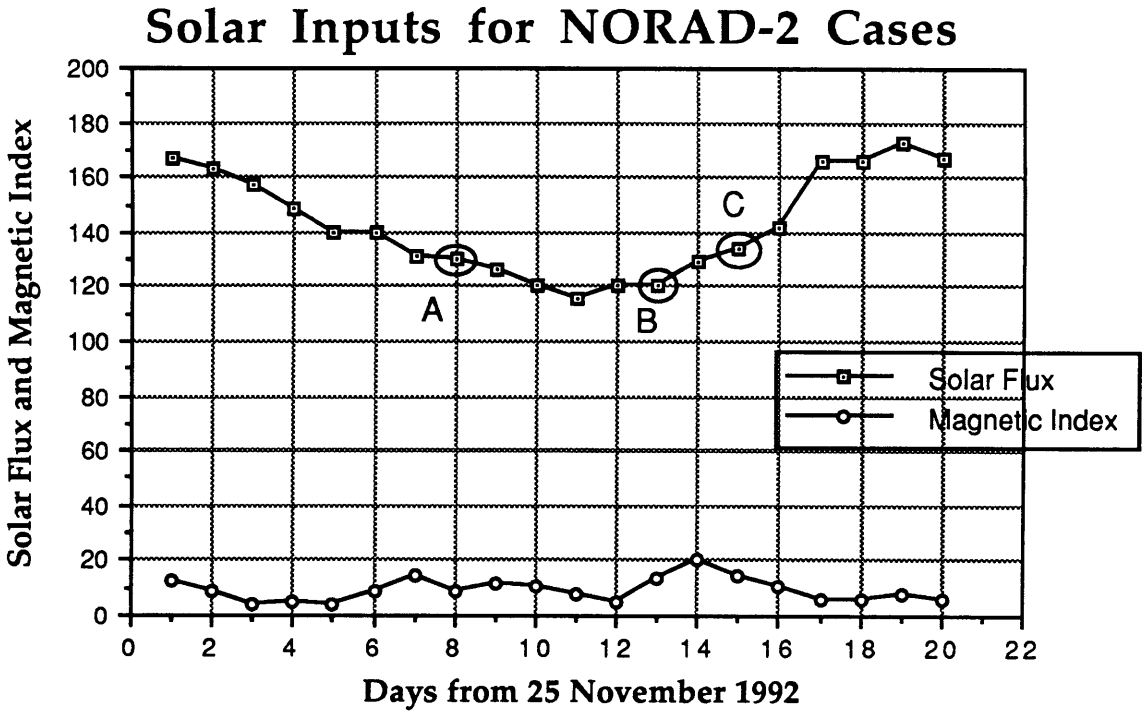

Figure 6-15 : NORAD-2 Solar Data with Prediction Spans Noted

From Figure 6-15 it can be seen that the unchanged flux value of the last day of data for the A case could give a fair approximation of the solar activity. The +10% value would also do well. However, it is not clear from Figure 6-15 that a -10% or -20% flux value for the B or C cases would be a good approximation of the actual solar activity. A direct relationship there is not clear.

6.4.3 Summary

The results presented thus far for the solar flux sensitivity do not clearly point to a simple relationship between estimated values and impact errors. A general trend that increased prediction length leads to increased errors is not a new finding and does not aid in clarifying the behavior of the errors to aid in making better solar flux estimates. What is evident is the complex relationship that exists between the differences in actual and predicted solar flux values, the prediction span, and the impact time errors. A case with a broad range of solar flux values to begin with, such as the LOSAT-X case, only adds to the uncertainty by causing large errors immediately. Fairly steady solar activity of a modest level, such as that for the RME and NORAD-1 satellites, seem to provide the conditions for best accuracy, especially when using a constant solar flux value that is the same as that of the last day of NORAD data.

Chapter 7

Conclusions and Recommendations

This chapter summarizes the results presented in this study and offers conclusions in light of the goal and objectives stated in Section 1.3. Recommendations on further research and development are also presented.

7.1 Summary and Conclusions

The original goals and objectives of the study are reprinted below.

(1) Improve upon the accuracy of the current LIFETIME algorithm, LIFETIME 3.0. The NORAD tracking data sets for decaying satellites contain intrack motion information that could aid in this improvement.

(2) Either adjust the current algorithm or develop a new one to decrease the uncertainty associated with the exact prediction of the impact time.

(3) Enhance the output capabilities of the program. Develop plots of the final revolution's altitude decay history and world-wide groundtrack with impact area.

(4) Package the completed software package as LIFETIME 4.0 for:

- IBM PC with NAMELIST input format
- IBM PC with a user-friendly menu-driven shell program to run it
- Macintosh version

(5) Initiate an accuracy sensitivity study, looking at the sensitivity of the program's impact prediction accuracy to:

- The amount of NORAD data used for the differential correction fit
- The length of prediction, from the last data point to actual impact
- The inputted solar flux (F_{10}) values used for the prediction

Chapter 2 introduced the satellite cases used in this study and presented the time errors that accumulated from the LIFETIME 3.0 algorithm. The NORAD tracking data required for the differential correction process was used to note the accumulation of errors with each orbital period computation. This indicated a potential algorithm deficiency and testing with the SPIN program confirmed that some error did exist.

Proposed algorithm improvements were presented in Chapter 3. These involved using an improved method of nodal period computation derived from Claus & Lubowe and developing a new method for NORAD 2-card element conversion using the actual NORAD propagator type used in forming the original element sets. These upgrades formed programs LIFETIME 4.0 and PRELIFE, which were tested with the same satellite cases used to identify the time errors in LIFETIME 3.0.

The results of the comparison between LIFETIME 3.0 and LIFETIME 4.0 as presented at the end of Chapter 3 indicated major improvements in period calculation for LIFETIME 4.0, indicated by a significant reduction in the time errors evident at the end of the differential correction process. A portion of goal (1) had been achieved at this point.

Chapter 4 addressed the issues of goals (2) and (3) by developing an innovative propagation method for the final stage of orbit decay that results in debris impact. A model for re-entry and breakup from Stern, et. al., was developed using a Runge-Kutta 7(8) integration scheme to propagate the satellite through its breakup altitude down to Earth impact. This would decrease the uncertainty in impact time determination that existed in LIFETIME 3.0, where the minimum propagation step size was one orbit revolution. The output capabilities of LIFETIME were enhanced to use the information from the integration propagation to plot the groundtrack and debris impact area on a world map and to produce an altitude decay history.

To finish the evaluation of how well goal (1) was achieved a complete impact accuracy comparison between LIFETIME 3.0 and LIFETIME 4.0 was conducted and the results presented in Chapter 5. The results indicated some notable improvement of LIFETIME 4.0 over LIFETIME 3.0, with 9 of 16 cases showing

a lower impact error (percent) for LIFETIME 4.0. The results are not definitive and a larger sample size is most likely necessary to establish a firm conclusion. However, the general improvement is noted. Overall, LIFETIME 4.0 contains a more comprehensive period calculation method and more definitive impact time estimation than LIFETIME 3.0. It's completion as an improved software package signifies a general increase in its usefulness as an orbit decay and impact prediction tool.

Goal (4) was completed with substantial input from C. Johnson of The Aerospace Corporation. The menu-driven software package was designed to meet the needs of the customer for efficiency and ease of use. A sample is presented in Appendix A.2.

Chapter 6 was comprised of the sensitivity studies needed to achieve goal (5). It was necessary to analyze the impact prediction results for all the LIFETIME 4.0 satellite cases, focusing separately on the three major sensitivities to be studied: NORAD data span, prediction span, and solar flux estimates for the prediction period.

The NORAD data span sensitivity was viewed in terms of period calculation accuracy and impact prediction accuracy. The period calculation accuracy analysis produced mixed results, with Category II data spans having the greatest averaged time errors at the end of the differential correction process. A strong trend for this sensitivity was not indicated. The impact prediction accuracy analysis indicated a general trend for less averaged impact time error for greater data spans. Thus, Category III cases had the smallest errors.

The prediction span sensitivity was analyzed in terms of the impact time errors for all the cases. A strong trend for increased accuracy with shorter prediction spans was established.

The solar flux estimate sensitivity analysis required additional testing using the methodology described in detail in Section 6.4. The results were analyzed for each satellite separately, since solar data is unique to the time frame in which it is recorded and used. The results indicated that quite a complex relationship exists between the estimated solar flux for the prediction period,

the actual values, the span of the prediction, and the resulting impact errors. A general observation and conclusion is that fairly steady solar activity of a modest level provides the solar conditions for the most accurate impact prediction, especially when using the solar flux value of the last day of NORAD data as the constant value during the prediction span. For cases of highly variable solar flux values assuming a constant value equal to that of the last day of data may not give the least error (that depends on the actual solar conditions that develop). However, this conservative assumption will not result in the maximum error, either (for the cases studied, with solar flux estimate ranges of ±20%).

In conclusion, this research resulted in the development of an improved algorithm for satellite orbit decay and re-entry prediction. Comparisons between the existing program version, LIFETIME 3.0, and the improved algorithm, LIFETIME 4.0, were made using four actual decayed objects. Results show that version 4.0 is significantly more accurate than version 3.0 during decay curve fitting. Comparison of impact prediction shows some increase in accuracy with version 4.0 for some cases. Generally, LIFETIME 4.0 is an improved algorithm with less uncertainty in impact prediction than LIFETIME 3.0, and it has enhanced output capabilities. The impact error sensitivity results indicate some improved accuracy by using long data spans, short prediction spans, and estimated solar flux values equal to the value on the last day of data. However, these results are not definitive and further research is recommended.

7.2 Recommendations on Research and Development

There are two main areas for continued research and development that come to light out of the results of this study: the accuracy of the LIFETIME impact prediction algorithms and the sensitivity of impact accuracy to estimated solar flux conditions.

Some inconsistency in the results between Chapter 3 and Chapter 5 exist. The Chapter 3 results indicated an order of magnitude reduction in time errors at the end of the differential correction process because of algorithm

improvements in LIFETIME. This same improvement was not readily apparent in the impact prediction comparisons of Chapter 5. It seems there are still dynamic aspects of the final orbit decay and re-entry process that warrant further study.

The generally high accuracy of LIFETIME 3.0 is a tribute to its computation method and its performance was better than LIFETIME 4.0 in a few cases. There is a chance that the correct combination of errors (period calculation, NORAD data conversion, and exact impact time uncertainty) could result in an accuracy not truly inherent in the algorithm. These issues could warrant further study, but it seems more practical to take LIFETIME 4.0 as the upgraded program and work within its algorithm and structure to resolve remaining issues concerning re-entry effects.

Since the improvement inconsistencies developed between the end of differential corrections and impact prediction, there is the possibility that an error enters the process near the area of propagation hand-off, from the LIFETIME propagation method to the Runge-Kutta 7(8) integration scheme. The integration algorithm itself has been comprehensively and successfully tested against other integration routines and other programs containing the same integration scheme. However, the conditions of the phase of re-entry during the propagation change may induce an error. A study evaluating different integration start altitudes may isolate some windows of maximum and minimum error and may reveal some additional information on the true motion of a re-entering satellite under those conditions. (The integration altitude (RKALT) for all cases in this study was 125 km, to give ample clearance above the 78 km breakup altitude.) Presently, research along these lines has been initiated at The Aerospace Corporation (Chao & Williams, 1993).

The second major area of interest is the estimation of solar activity, mainly solar flux, during the prediction span. Section 6.4 initiated a fairly comprehensive sensitivity study, the results of which led to a general conclusion that an assumed constant flux value of the last day of NORAD data will result in high accuracy impact predictions for fairly short prediction spans during smooth, moderate solar activity. This conclusion offers little in

the way of guidance for achieving accuracy in non-ideal solar conditions. Only an extensive, statistical study of estimated and actual solar activity can hope to provide a useful model for predicting solar flux values in a manner to minimize the impact prediction error.

It will be impossible to eliminate error entirely, or probably even come close to doing so. Yet further research could increase prediction accuracy overall. Of course, there has been full time research for years into predicting solar activity, most of it not very conclusive. Current neural networking attempts may prove fruitful; but a continued statistical sensitivity study could provide some useful prediction information.

Generally, it is this inability to predict future solar activity, and thus the atmosphere density, that limits the accuracy of any orbit decay and re-entry prediction program.

References

1. Lenorovitz, J.M., "Steady Growth Seen for Commercial Space," *Aviation Week and Space Technology*, 15 March 1993.

2. Stern, R., Refling, O., and Potz, C., "Review of Orbital Re-entry Risk Predictions," ATR-92(2835)-1, The Aerospace Corp., El Segundo, CA, July 1992.

3. Roy, A.E., *The Foundations of Astrodynamics*, The Macmillan Co., NY, 1965.

4. Lefebvre, S.V., "An Analysis of Tracking and Impact Predictions," AFIT/AU Master's Thesis, No. AFIT/GSO/ENS/91D-11, December 1991.

5. Battin, R.H., *An Introduction to the Mathematics and Methods of Astrodynamics*, AIAA, Inc., NY, 1987.

6. Liu, J.J.F., and Alford, R.L., "A Semi-Analytic Theory for the Motion of a Close-Earth Artificial Satellite with Drag," AIAA Paper 79-0123, 1979.

7. Chao, C.C., and M.H. Platt. "An Accurate and Efficient Tool for Orbit Lifetime Predictions," AAS Paper 91-134, AAS/AIAA Spaceflight Mechanics Meeting, Houston, TX, February 1991.

8. Williams, K.E., "Prediction of Solar Activity with a Neural Network and Its Effect on Orbit Prediction," *Johns Hopkins APL Technical Digest*, Vol. 12, No. 4, 1991.

9. Withbroe, G.L., "Expectations for Solar Activity in the 1990's," of the NASA Working Group on the Prediction of Solar Activity, July 1989.

10. Strizzi, J.D., "Updated FATABLE Values in 3272 MAD," ATM No. 91-(6464-03)-1, The Aerospace Corp., December 1990.

11. Marcos, F.A., "Accuracy of Satellite Drag Models," AAS Paper 87-552, AAS/AIAA Astrodynamics Specialist Conference, Kalispell, MT, August 1987.

12. Chao, C.C., "Program LIFETIME: Past, Present, and Future," Briefing, October, 1992.

13. Chao, C.C., "Procedure for Satellite Re-entry Prediction," ATM No. 92(2047-01)-4, The Aerospace Corp., July 1992.

14. Downs, W.D., et al, "TRACE - Trajectory Analysis and Orbit Determination Program, Vol. VII: User's Guide," SD-TR-82, Vol. VII, The Aerospace Corp., January 1982.

15. Chao, C.C., "LIFETIME Version 3.0," FORTRAN Source Code, The Aersospace Corp., 1992.

16. Claus, A.J., and Lubowe, A.G., "A High Accuracy Perturbation Method with Direct Application to Communication Satellite Orbit Prediction," *Astronaut. Acta.*, Vol. IX, Fasc. 5-6, September 1966.

Additional Readings

Baker, R.M.L., *Astrodynamics: Applications and Advanced Topics,* Academic Press, NY, 1967.

Herrero, F.A., "Satellite Drag Coefficients and Upper Atmosphere Densities: Present Status and Future Directions," AAS Paper 87-551, AAS/AIAA Astrodynamics Specialist Conference, Kalispell, MT, August 1987.

Hoots, F.R., and France, R.G., "Uncertainty Estimation for Satellite Lifetime Prediction," AAS Paper 91-431, *Advances in the Astronautical Sciences*, Vol. 76, Part II, 1991.

Jacchia, L.G., "Revised Static Models of the Thermosphere and Exosphere with Empirical Temperature Profiles," SAO Science Report No. 332, 1971.

King-Hele, D.W., *Theory of Satellite Orbits in an Atmosphere,* Butterworths, London, 1964.

Liu, J.J.F., and Alford, R.L., "Semianalytic Theory for a Close-Earth Artificial Satellite," *Journal of Guidance and Control*, Vol 3, No. 4, July-August 1980.

Liu, J.J.F., "Advances in Orbit Theory for an Artificial Satellite with Drag," AIAA Paper 82-1399, 1982.

Loboda, G. G., "Peformance Enhancement of Segmented Infared Reflectors via Quasistatic Shape Control," MIT Master's Thesis, 1992

Oltrogge, D.L., "User's Guide to the 6-D SPIN Program," TOR-92(9975)-1, The Aerospace Corp., November 1991.

Regan, F.J., *Re-Entry Vehicle Dynamics*, AIAA, Inc., NY, 1984.

Romer, R.W., Johnson, C.J., and Chao, C.C., "Program LIFETIME Upgrades and User's Manual," ATM No. 92(2047-01)-1, The Aerospace Corp., March 1992.

Runge-Kutta 7(8) Numerical Integration Scheme, JPL EM 312/85.140 (1985)

Space Track Report No. 3, December 1980.

Strizzi, J. D., and C.C. Chao., "An Improved Algorithm for Satellite Orbit Decay and Re-entry Prediction," Briefing, January 1993.

Strizzi, J. D., "Program LIFETIME: An Improved Algorithm for Satellite Orbit Decay and Re-entry Prediction," Briefing, March 1993.

Uphoff, C., (Orbital Element Conversion Algorithm Based on a Combination of Kozai's and Izsak's Theories), The Jet Propulsion Laboratory, JPL EM 312/87-153, April 1987.

Walker, J.C.G., "Analytical Representation of Upper Atmosphere Densities Based on Jacchia's Static Diffusion Models," *Journal of Atmosphere Sciences*, Vol. 22, July 1965.

Willson, R.C., Hudson, H., and Woodard, M., "The Inconstant Solar Constant," *Sky and Telescope*, June 1984.

Appendix

This appendix presents the LIFETIME 4.0 input variables. They are used in a NAMELIST format with the executable LIFETIME code on either a Macintosh or IBM PC. The menu-driven version of LIFETIME 4.0 guides the user to input the values that form the NAMELIST. This information is a copy of the file LIFEIN.DOC, which is part of the LIFETIME 4.0 software package.

Inputs for the Lifetime Program (Vers. 4.0)
15 January 1993

VARIABLE	DESCRIPTION	UNITS	DEFAULT
AREA1	AREA OF SOLAR PANELS (ISOLAR=1)	M^2	2.D0
AREA2	AREA OF S/C BODY (ISOLAR=1)	M^2	1.D0
ASUBP	DAILY GEOMAGNETIC PLANETARY INDEX	N.D.	10.D0
BIASDY	DAY BIAS TO F10.7 CURVE; A POSITIVE VALUE DENOTES A MORE ADVANCED CURVE	N.D.	0.D0
BIASUP	VERT. BIAS TO F10.7 CURVE; A POSITIVE VALUE YIELDS A HIGHER F10.7 VALUE	N.D.	0.D0
BRKALT	ALTITUDE OF S/C VEHICLE BREAK-UP	KM	77.784D0
CD	DRAG COEFFICIENT (ISOLAR=1)	N.D.	2.2D0
CDAM	INVERSE BALLISTIC COEFFICIENT: FOR IUNIT=0, CDAM=FT^2/LB FOR IUNIT=1, CDAM=CM^2/KG	 FT^2/LB CM^2/KG	50.D0
DCTOL	CONVERGENCE TOLERANCE FOR DIFFERENTIAL CORRECTION FOR BALLISTIC COEFFICIENT. CONVERGENCE IS INTERACTIVE IF DCTOL IS SET TO ZERO.	CM^2/KG	0.D0
DFDDAY	LINEAR RATE-OF-CHANGE TO F10.7	W/M^2/DAY	0.D0
DSMA	SEMI-MAJOR AXIS TOLERANCE (ISUST=1)	KM	1.D0
DSTK	IN-TRACK POSITION TOLERANCE, MEASURED IN TERMS OF THE EARTH ARC LENGTH OF THE GROUND TRACK'S LONGITUDINAL SHIFT	KM	1.D0

ENDALT	PERIGEE ALTITUDE LOWER LIMIT AT WHICH PROGRAM LIFETIME ENDS PROPAGATION	KM	10.D0
ERRTOL	ERROR TOLERANCE (BOTH RELATIVE AND ABSOLUTE) FOR RK78 INTEGRATOR		1.D-9
FTENI	THE F10.7 SOLAR FLUX INDEX (IFLUX=0)	W/M^2	150.D0
IATM	ATMOSPHERE MODEL SELECTION FLAG: 1: WALKER ANALYTICAL REPRESENTATION OF THE JACCHIA 1964 DYNAMIC MODEL 2: JACCHIA 1971 DYNAMIC MODEL FOR ALTITUDES ABOVE 90KM, STD ATM '62 STATIC MODEL FOR ALTITUDES BELOW	N.D.	2
IDC	DIFFERENTIAL CORRECTION OF CDAM FLAG: 0: OFF 1: ON IF IDC = 1: ** EITHER ** FILE "INAE" MUST BE CREATED, CONTAINING NAMELIST "INAE" WITH THE VARIABLES TAG (TIME IN DAYS), SMA (MEAN SEMI-MAJOR AXIS IN METERS), & ECC (MEAN ECCENTRICITY). ** OR ** "INAE." MUST CONTAIN A INTEGER IN ROW 1 (I12 FORMAT), FOLLOWED BY THREE COLUMNS: (1) DAYS FROM EPOCH, (2) MEAN SEMI-MAJOR AXIS (METERS), & (3) ECCENTRICITY; (E27.9,2E25.9)	N.D.	0
IFLUX	ASUBP, F10.7 PREDICTION MODE: 0: ASUBP=USER INPUT; F10.7 COMPUTED FROM FTENI+TDAYS*DFDDAY 1: ASUBP, F10.7 COMPUTED FROM BUILT-IN 11-YR SOLAR CYCLE, BIASUP, AND BIASDY 2: ASUBP, F10.7 COMPUTED FROM TVF10, TVAP VECTORS IN SPECIAL "FIND" FORMAT, E.G. TVF10(1) = 0.D0 TVF10(2,4,6,...) = MOD JUL DAY# TVF10(3,5,7,...) = F10.7 VALUES TVF10(LAST 2 ENTRIES)=-555.D0 3: ASUBP, F10.7 COMPUTED FROM TVF10, TVAP VECTORS DURING FIT AND BUILT-IN 11-YR SOLAR CYCLE AFTER.	N.D.	1
IOSC	OSCULATING ELEMENTS INPUT FLAG: 0=ORBIT(#S 1 THROUGH 6) ARE MEAN 1=ORBIT(#S 1 THROUGH 6) OSCULATING	N.D.	0

IPLOT	HPAOUT. AND OBSHPA. OUTPUT FLAG 0: OFF 1: ON	N.D.	1
IPRT	OUTPUT DEVICE SPECIFICATION FLAG: -1: SCREEN OUTPUT W/INTEG.STEPS,F10.7 0: SCREEN OUTPUT W/INTEG. STEPS 1: SCREEN OUTPUT W/0 INTEG. STEPS 2: LIFEOUT. OUTPUT W/INTEG. STEPS 3: LIFEOUT. OUTPUT W/O INTEG. STEPS	N.D.	0
ISOLAR	VARIABLE CDAM CAUSED BY SOLAR PANELS: 0: OFF 1: ON	N.D.	0
ISUST	ORBIT SUSTENANCE SPECIFICATION FLAG: 0: OFF 1: SEMI-MAJOR AXIS TO "DSMA" TOL. 2: GROUND TRACK SHIFT TO "DSTK" TOL.	N.D.	0
IUNIT	UNITS FLAG FOR CDAM I/O: 0 = CDAM IN UNITS OF FT^2/LB 1 = CDAM IN UNITS OF CM^2/KG	N.D.	1
J3FG	J3 PERTURBATIONS (0=OFF, 1=ON)	N.D.	0
NREVS	ORBIT INTEGRATION STEP SIZE	REVS	2
ORBIT(6)	ORBIT CLASSICAL ELEM (A,E,I,O,W,& TA) OF TYPE MEAN/OSC FOR IOSC=0/1	KM N.D. DEG. DEG. DEG. DEG.	6678.D0 .005D0 60.D0 0.D0 0.D0 0.D0
RKALT	ALTITUDE LOWER LIMIT AT WHICH PROGRAM LIFETIME TRANSITIONS TO CARTESIAN NUMERICAL INTEGRATION USING RK78	KM	0.D0
TMDY	LENGTH OF ORBIT PROPAGATION	DAYS	100.D0
TVAP	TIME (MODIFIED JULIAN DATE) VS ASUBP VECTOR IN "FIND" FORMAT (SEE IFLUX VARIABLE FOR FORMAT DESCRIPTION). DEFAULT VALUES SPAN PERIOD JAN.1 1990 TO JAN.1 2008, WITH DATA A PT EVERY TWO YEARS. THIS DATA WAS EXTRACTED FROM NASA/MARSHALL "SOLAR ACTIVITY INPUTS..." DOCUMENT DATED 11/05/91	N.D. MOD JUL DY N.D. MOD JUL DY N.D. MOD JUL DY N.D. MOD JUL DY N.D. MOD JUL DY N.D.	0.D0 47892.D0 14.0D0 48622.D0 20.5D0 49353.D0 18.1D0 50083.D0 13.9D0 50814.D0 9.4D0 51544.D0 12.6D0

		MOD JUL DY	52275.D0
		N.D.	12.5D0
		MOD JUL DY	53005.D0
		N.D.	14.2D0
		MOD JUL DY	53736.D0
		N.D.	13.2D0
		MOD JUL DY	54466.D0
		N.D.	11.5D0
		N.D.	-555.D0
		N.D.	-555.D0
TVF10	TIME (MODIFIED JULIAN DATE) VS F10.7 VECTOR IN "FIND" FORMAT (SEE IFLUX VARIABLE FOR FORMAT DESCRIPTION). DEFAULT VALUES SPAN PERIOD JAN.1 1990 TO JAN.1 2008, WITH DATA A PT EVERY TWO YEARS. THIS DATA WAS EXTRACTED FROM NASA/MARSHALL "SOLAR ACTIVITY INPUTS..." DOCUMENT DATED 11/05/91	N.D.	0.D0
		MOD JUL DY	47892.D0
		W/M^2	210.1D0
		MOD JUL DY	48622.D0
		W/M^2	195.1D0
		MOD JUL DY	49353.D0
		W/M^2	115.6D0
		MOD JUL DY	50083.D0
		W/M^2	82.9D0
		MOD JUL DY	50814.D0
		W/M^2	74.8D0
		MOD JUL DY	51544.D0
		W/M^2	191.0D0
		MOD JUL DY	52275.D0
		W/M^2	231.1D0
		MOD JUL DY	53005.D0
		W/M^2	154.3D0
		MOD JUL DY	53736.D0
		W/M^2	109.9D0
		MOD JUL DY	54466.D0
		W/M^2	89.0D0
		N.D.	-555.D0
		N.D.	-555.D0
UT(6)	EPOCH OF ORBIT(5) (YR,MO,DY,HR,MN,SC)	(TIME)	1992.D0
			3.D0
			1.D0
			0.D0
			0.D0
			0.D0
WGTKG	S/C MASS	KG	60.